Fouilles Massives d'Archives Spectroscopiques : L'Observatoire Virtuel, de la Vapeur d'Eau Atmosphérique au Carbone dans les Astéroïdes.

Alain Sarkissian

Dossier pour examen par les membres du jury

Soutenance d'Habilitation à diriger des Recherches

Université Versailles Saint-Quentin-en-Yvelines

Sciences Chimie-physique étendue aux Sciences de l'Environnement

Fouilles Massives d'Archives Spectroscopiques : L'Observatoire Virtuel, de la Vapeur d'Eau Atmosphérique au Carbone dans les Astéroïdes.

Alain Sarkissian

LATMOS / OVSQ

Le 18 Mars 2011 à 14h00

Membres du jury

Ralf TOUMI, Professeur, Imperial College of London - Rapporteur

William THUILLOT, Directeur de l'IMCCE (Institut de Mécanique céleste et de calcul des éphémérides) Observatoire de Paris - Rapporteur

Claude BOUTRON, Professeur à l'Université Joseph Fourier Grenoble 1 - Rapporteur

Maria-Teresa CAPRIA, Directeur de recherche, IASF Rome - Italie - Membre examinateur

Guy MOREELS, Professeur, Observatoire de Besançon - Membre examinateur

Pierre-Richard DAHOO, Professeur UVSQ, OVSQ - Membre examinateur

Slimane BEKKI, Directeur de Recherche, LATMOS - Membre examinateur

Table des Matières

Curriculum Vitae

SARKISSIAN Alain
LATMOS
11, boulevard d'Alembert
78280 GUYANCOURT
France
Physicien Adjoint
Institut Pierre-Simon LAPLACE (IPSL)
Tel.: +33 (0)1 802 85 265
E-mail : alain.sarkissian@latmos.ipsl.fr
Né à Issy-les-Moulineaux, le 31 Janvier 1960, nationalité française, marié, deux enfants.

Formation

- 1980 Bac, Orsay, France.
- 1988 Diplôme d'Etudes Approfondies (DEA) "Astronomie et Techniques spatiales" , Université Paris VI, France.
- Octobre 1988 à avril 1992 : Thèse au Service d'Aéronomie, (Directeur : J.-P. Pommereau) et enseignement à l'UVSQ (Monitorat en 1989-1990 et 1990-1991).

Carrière professionnelle

1992 - 1994: Post-doctorant au Service d'Aéronomie.
1994 - 1996: Post-doctorant au British Antarctic Survey, Cambridge, UK.
1996 - 1998: Post-doctorant au Service d'Aéronomie.
Depuis septembre 1998: Astronome Adjoint au LATMOS (fusion Service d'Aéronomie et CETP en 2008) .

Responsabilités

- CoI NDSC de 1996 à avril 2001 des instruments SAOZ à lOHP, Dumont D'Urville, Kerguelen, Réunion, Zhigansk (Sibérie), Tarawa (Kiribati), Sodankyla (Finlande), Bauru (Brésil).
- Coordinateur du projet "Nuages Stratosphériques Polaires " du PNCA de 1996 à 2000.
- Représentant des personnels chercheurs au Conseil Scientifique du Service d' Aéronomie de 1996 à 2000.
- Organisation de la campagne internationale NDSC/ SCUVS III d'intercomparaison de spectromètres UV-visibles, 43 participants, 15 laboratoires, 14 instruments participants + 7 instruments et météo en support, OHP, Juin 1996.

- Membre du comité d'organisation du symposium NDSC, Arcachon, 24-27 septembre 2001.
- Membre du Topical Team "Ices in Space" à l'ESA d'avril 2001 à Décembre 2005.
- Membre du groupe de travail "VO-Paris data Center " depuis Octobre 2004, (http://vo-web.obspm.fr/index.php).
- Membre du groupe de travail "VO-planeto-Ile de France" de l'OV-France depuis Octobre 2004, (http://www.france-ov.org/twiki/bin/view/GROUPEStravail/Planeto).
- Membre du groupe de travail "Base de Données Planétaires " du CNES depuis Novembre 2003.
- **Membre du "Steering Comittee" de l'International Planetary Data Alliance depuis Mars 2007**,(IPDA, http://planetarydata.org/).
- Membre du Conseil Scientifique de l'Observatoire de Haute-Provence (OHP) de Février 2007 à Janvier 2008.
- Membre du Comité de Pilotage du Centre de Données de l'IPSL depuis Septembre 2006.
- Membre du groupe de travail "OHP Avenir " de Novembre 2005 à Janvier 2008.
- Membre du groupe de travail FONDUE de l' International Space Science Institute (ISSI) depuis Juillet 2008, (http://bdap.ipsl.fr/fondue/).
- Membre du Conseil Scientifique de VO-Paris Data Centre depuis Janvier 2008.
- Membre du Centre Européen Arctique (CEARC) de l'UVSQ depuis Novembre 2009.
- Membre du SOERE (Systèmes d'observation et d'expérimentation au long terme pour la recherche en environnement de l'INSU) ROSEA (réseau d'Observatoires pour la Surveillance et l'exploration de l'Atmosphère) depuis juillet 2010.

Publications à comité de lecture

1- Sarkissian A., J.P. Pommereau and F. Goutail, Identification of polar stratospheric clouds from the ground by visible spectrometry, *Geophys. Res. Lett.*, **18**, 779-782, 1991.

2- Lee A. M., H.K. Roscoe, D.J. Oldham, J.A.C Squires, A. Sarkissian and J-P. Pommereau, Improvements to the accuracy of measurements of NO2 by zenith-sky visible spectrometers, J. Quant. Spectrosc. *Rad. Trans.*, **52**, 649-657, 1994.

3- Roscoe, H.K., J.A.C Squires, D.J. Oldham, A. Sarkissian, J-P. Pommereau and F. Goutail, Improvements to the accuracy of zenith-sky measurements of total ozone by visible spectrometers, *J. Quant. Spectrosc. Rad. Trans.*, **52**, 639-648, 1994.

4- Goutail F., J.P. Pommereau, A. Sarkissian, E. Kyro and V. Dhorokov, Total nitrogen dioxide at the Arctic polar circle since 1990, *Geophys. Res. Lett.*, **21**, 1323-1326, 1994.

5- Sarkissian A., J.P. Pommereau, F. Goutail and E. Kyro, PSC and volcanic aerosol observations during EASOE by UV-visible ground-based spectrometry, *Geophys. Res. Lett.*, **21**, 1319-1322, 1994.

6- Jones A. E., H.K. Roscoe, A. Sarkissian, J.D. Shanklin and E.W. Wolff, Year-round column ozone observations at 65 degree S: validation and polar winter data, *J. Quant.*

Spectrosc. Rad. Trans., **54**, 481-494, 1995.

7- Sarkissian A., H.K. Roscoe, D. Fish, Ozone measurements by zenith-sky spectrometers: an evaluation of errors in air-mass factors calculated by radiative transfer models, *J. Quant. Spectrosc. Rad. Trans.*, **54**, 471-480, 1995.

8- Sarkissian A., D. Fish, M. Van Roozendael, M. Gil, H.B. Chen, P. Wang, J.P. Pommereau and J. Lenoble, Ozone and NO2 air-mass factors for zenith-sky spectrometers: Intercomparison of calculations with different radiative transfer models, *Geophys. Res. Lett.*, **22**, 1113-1116, 1995.

9- Hoffman D.J., P. Bonasoni, M. de Mazière, F. Evangelisti, G. Giovanelli, A. Goldman, F. Goutail, J. Harder, R. Jakoubek, P. Johnston, J. Kerr, T. McElroy, R. McKenzie, G. Mount, U. Platt, J.P. Pommereau, A. Sarkissian, P. Simon, S. Solomon, J. Stutz, A. Thomas, M. Van Roozendael and E. Wu, Intercomparison of UV/visible spectrometers for measurements of stratospheric NO2 for the Network for the Detection of Stratospheric Changes, *J. Geoph. Res.*, **100**, 16765-16791, 1995.

10- Vaughan G., H.K. Roscoe, L. Bartlett, F.M. O'Connors, A. Sarkissian, M. Van Roozendael, J.-C. Lambert, P.C. Simon, K. Karlsen, B.A. Kastad Hoskar, D. J. Fish, R.L. Jones, R. Freshwater, J.-P. Pommereau, F. Goutail, S.B. Andersen, D.G. Drew, P.A. Hughes, D. Moore, J. Mellqvist, E. Hegels, T. Klupfel, F. Erle, K. Pfeilsticker, and U. Platt, An intercomparison of ground-based UV-visible sensors of ozone and NO2, *J. Geoph. Res.*, **102**, 1411-1422, 1997.

11- Sarkissian A., G. Vaughan, H.K. Roscoe, L. Bartlett, F. M. O'Connor, D. G. Drew, P. A. Hughes and D. M. Moore, Accuracy of measurements of total ozone by a SAOZ ground-based zenith-sky visible spectrometer, *J. Geoph. Res.*, **102**, 1379-1390, 1997.

12- Slusser J., D. Fish, E.K. Strong, R.L. Jones, H.K. Roscoe and A. Sarkissian, Five Years of NO2 Vertical Column Measurements at Faraday (65 S): Evidence for the Hydrolysis of BrONO2 on Pinatubo Aerosols, *J. Geoph. Res.*, **102** , No. D11 , p. 12,987, 1997.

13- Lambert J.C., Van Roozendael M., De Maziere M., Simon P.C., Pommereau J.P., Goutail F., Sarkissian A. and Gleason J.F., Investigation of pole-to-pole performances of space-borne atmospheric chemistry sensors with the NDSC, *J. Atmos. Sci.*, **56**, 176-193, 1999.

14- Pfeilsticker K., Arlander D. W., Burrows J. P., Erle F., Gil M., Goutail F., Hermans C., Lambert J.-C., Platt U., Pommereau J.-P., Richter A., Sarkissian A., Van Roozendael M.,Wagner T., Winterrath T., Intercomparison of the influence of tropospheric clouds on UV-visible absorptions detected during the NDSC intercomparison campaign at OHP in June 1996, *Geophys. Res. Lett.*, **26**, , p. 1169, 1999.

15- Goutail F., Pommereau J.P., Phillips C., Deniel C., Sarkissian A., Lefevre F., Kyro

E., Rummukainen M., Ericksen P., Andersen S.B., Kaastad-Hoiskar B.A., Braathen G., Dorokhov V. and Khattatov V.U., Depletion of column ozone in the Arctic during the winters of 1993-94 and 1994-95, *J. Atmos. Chem.*, **32**, 1-34, 1999.

16- Roscoe H.K., Johnston P.V., Van Roozendael M., Richter A., Roscoe J., Preston K.E., Lambert J.C., Hermans C., De Cuyper W., Dzienus S., Winterrath T., Burrows J., Sarkissian A., Goutail F., Pommereau J.P., d'Almeida E., Hottier J., Coureuil C., Ramon D., Pundt I., Bartlett L.M., Mc Elroy C.T., Kerr J.E., Elokhov A., Giovanelli G., Ravegnani F., Premuda M., Kostaadinov I., Erle F., Wagner T., Pfeilsticker K., Kenntner M., Marquard L.C., Gil M., Puentedura O., Arlander W., Kastad Hoishar B.A., Tellefsen C.W., Heese B., Jones R.L., Aliwell S.R. and Freshwater R.A., Slant column measurements of O3 and NO2 during the NDSC intercomparison of zenith-sky UV-visible spectrometers in june 1996, *J. Atmos. Chem.*, **32**, 281-314, 1999.

17- Lambert J.C., Van Roozendael M., Simon P.C., Pommereau J.P., Goutail F., Gleason J.F. Andersen S.B., Arlander D.W., Buivan N.A., Claude H., De la Noe J., De Maziere M., Dorokhov V., Eriksen P., Green A., Karlsen Tornqvist K., Kastad Hoiskar B.A., Kyro E., Leveau J. Merienne M.F., Milinevsky G., Roscoe H.K., Sarkissian A. , Shanklin J.D., Staehelin J., Wahlstrom Tellefsen C. and Vaughan G., Combined characterisation of GOME and TOMS total ozone measurements from space using ground-based observations from the NDSC, *Adv. Space Res.*, **26**, 1931-1940, 2000.

18- Roscoe H.K., J.G.T. Hill, A.E. Jones and A. Sarkissian, Improvements to the accuracy of zenith-sky measurements of total ozone by visible spectrometers II: use of daily air-mass factors, *J. Quant. Spectrosc. Rad. Trans.*, **68**, 327-336, 2001.

19- Ehrenfreund, P., Fraser, H.-J., Blum, J., Cartwright, J.-H.-E., Garcia-Ruiz, J.-M., Hadamcik, E., Levasseur-Regourd, A.C., Price, S., Prodi, F. and Sarkissian, A., Physics and chemistry of icy particles in the universe: answers from microgravity, *Planet. Space Sci.*, **51**, 473-494, 2003.

20- Yan N., E. Chassefière, F. Leblanc and A. Sarkissian, Thermal model of Mercury's surface and subsurface: Impact of subsurface physical heterogeneities on the surface temperature, *Advances in Space Research*, doi: 10.1016/j.asr.2005.11.010ASR, 2005.

21- Hoareau C., Keckhut P., Sarkissian A., Baray J.-L., Durry G., Methodology for Water monitoring in Upper Troposphere with Raman Lidar at Observatory of Haute-Provence, *Journal of Atm. and Ocean Tech.*, **26**, 2149-2160, 2009.

22- Gigoyan K.S., Russeil D., Sarkissian A., Sargsyan L.A., FBS 2213+421, an extremely red object with C-rich characteristics, *Astrophys.*, **52**, pp493-497, 2009.

23- Sarkissian A. and J. Slusser, Water Vapour Total Column Measured on Elodie Spectra at Observatoire de Haute Provence between 1994 and 2004, *Atmos. Meas. Tech.* , **2**,

319-326, 2009.

24- Sarkissian A., Brightness temperature of synchronic exoplanets measured by infrared photometry: Method and perspective, *Infrar. Phys. and Tech.*, **53**, 186-192, 2010.

25- Russeil D., Gigoyan K. S., Sarkissian A. and Avtandilyan M. G.,Search for new N-Type Carbon stars in the Digitized First Byurakan Survey, *Astrophys.*, **in press**.

Autres publications (62)

- Sarkissian A., J.P. Pommereau and F. Goutail, Identification of Polar Stratospheric Clouds from the ground by visible spectrometry, First European Workshop on Polar Stratospheric Ozone Research, 193-196, Pyle, Harris Ed, 1991.
- Pommereau J.P., F. Goutail, M. Pinharanda, J. Piquard and A. Sarkissian, Ground-based total ozone measurements in the visible Chapuis bands, First European Workshop on Polar Stratospheric Ozone Research, 41-44, Pyle J., Harris Ed, 1991.
- Van Roozendael M., Hermans C., de Mazière M., Simon P., A. Sarkissian, J. Piquard, F. Goutail and Pommereau J.P., UV-visible measurements of stratospheric trace species at the Jungfraujoch, First European Workshop on Polar Stratospheric Ozone Research, 85-89, Pyle, Harris Ed, 1991.
- Pommereau J.P., F. Goutail and A. Sarkissian, Ground-based detection of polar stratospheric clouds by visible spectrometry (abstract), Annales Geophysicae, Supplement III, volume 9,1991.
- Sarkissian A., Thèse de Doctorat en avril 1992: "Observation depuis le sol des nuages et poussières dans l'atmosphère: Applications à la stratosphère polaire et à l'atmosphère de Mars " sous la direction de J.P. Pommereau; President du Jury: J.E. Blamont; rapporteurs: C. Camy-Peyret et J. Lenoble; Examinateur: G. Mégie, 1992.
- Goutail F., J.P. Pommereau and A. Sarkissian, V. Dorokhov, E. Kyro and P. Eriksen, Stratospheric NO2 and ozone at the Arctic polar circle from 1990 to 1993 from ground-based UV-visible spectrometers (abstract), Annales Geophysicae, Supplement III, volume 11,1993.
- Sarkissian A. and J.P. Pommereau, Volcanic aerosol and PSC optical properties from simultaneous measurements of optical thickness and backscattering ratio (abstract), Annales Geophysicae, Supplement III, volume 11,1993.
- Goutail F., J.P. Pommereau and A. Sarkissian, Stratospheric ozone and NO2 monitoring with SAOZ ground-based UV-visible spectrometer, Proc. 1993 Atmospheric spectroscopy applications, A. Barbe and L. Rothman, 59-62, 1993.
- Sarkissian A., M. Van Roozendael, D. Fish, M. Gil and J. Lenoble, Ozone and NO2 air-mass factors for zenith-sky spectrometers: Intercomparison of calculations with different radiative transfer models (abstract), Annales Geophysicae, Supplement III volume 12, C602,1994.
- Sarkissian A. and H.K. Roscoe, Ozone and NO2 air-mass factors for zenith-sky spectrometers: Numerical integration of the first and the second orders of scattering (abstract), Annales Geophysicae, Supplement III volume 12, C602,1994.

- Sarkissian A., J.P. Pommereau and F. Goutail, PSC and Volcanic Aerosol routine observations in Antarctica by UV-visible ground-based spectrometry, Proc. 1992 Quadriennal Ozone Symposium, 586-589,1994.
- Roscoe H. K., Oldham D.J., Squires J., J.P. Pommereau, F. Goutail and A. Sarkissian, Year-round measurements of ozone at 66 ∘ S with a visible spectrometer, Proc. 1992 Quadriennal Ozone Symposium, 569-572, 1994.
- Godin S., A. Sarkissian, C. David, G. Megie, J.P. Pommereau, F. Goutail, P. Aimedieu, J. Piquard, E. Le Bouar, L. Stefanutti, M. Morandi and M. del Guasta, Systematic stratospheric observations on the Antarctic continent at Dumont d'Urville, Proc. 1992 Quadriennal Ozone Symposium, 561-564, 1994.
- Goutail F., Pommereau J. P.and Sarkissian A., Four years of ground-based total ozone measurements by visible spectrometry in Antarctica, Proc. 1992 Quadriennal Ozone Symposium, 602-605, 1994.
- Vaughan G., H.K. Roscoe, L. Bartlett, F.M. O'Connors, A. Sarkissian, M. Van Roozendael, J.-C. Lambert, P.C. Simon, K. Karlsen, B.A. Kastad Hoskar, D. J. Fish, R.L. Jones, R. Freshwater, J.-P. Pommereau, F. Goutail, S.B. Andersen, D.G. Drew, P.A. Hughes, D. Moore, J. Mellqvist, E. Hegels, T. Klupfel, F. Erle, K. Pfeilsticker, and U. Platt, An intercomparison of ground-based UV-visible sensors of ozone and NO2, European Workshop on Polar Stratospheric Ozone Research, Pyle J.and N. Harris Ed, 1995.
- Sarkissian A., H.K. Roscoe, D. Fish, L. Bartlett and G. Vaughan, Vertical resolution of stratospheric aerosol by ground-based zenith-sky UV-visible spectrometers (abstract), Annales Geophysicae, Supplement III volume 13, C721, 1995.
- Sarkissian A., H.K. Roscoe, L. Bartlett, G. Vaughan, F. O'Connor, P. Hughes, D. Moore, and D. Drew, Ozone air-mass factors for ground-based zenith-sky spectrometers: Validation at mid-latitudes (abstract), Annales Geophysicae, Supplement III volume 13, C722, 1995.
- Sarkissian A., F. Goutail, J.-P. Pommereau, H.K. Roscoe and J. Slusser, Stratospheric Aerosol measured by SAOZ UV-visible ground-based Spectrometer (extended Abstract) , Colloq. Atmospheric Applications (ASA), Reims, France, 4-6 Septembre 1996, Université de Reims, p 52, 1996.
- Pommereau J.P., F. Goutail and A. Sarkissian, SAOZ total ozone measurements in Antarctica: Comparisons with TOMS versions 6 and 7, European Workshop on Polar Stratospheric Ozone Research, Pyle J.and N. Harris Ed, Air Pollution Report, pp 516-520, 1996.
- Denis L., J.P. Pommereau, F. Goutail, T. Portafaix, A. Sarkissian, M. Bessafi, S. Baldy, J. Leveau, P. Johnston and A.W. Mathews, SAOZ total ozone and NO2 at the Southern Tropics and Equator, European Workshop on Polar Stratospheric Ozone Research, Pyle J.and N. Harris Ed, Air Pollution Report, pp 458-462, 1996.
- Lambert J.C., Van Roozendael M., M., Simon P.C., De Maziere, Pommereau J.P., Goutail F. and Sarkissian A., Pole-to-pole validation of GOME level-2 products with ground-based networks, ESA Earth Observation Quarterly, 58, 6-8, 1998.
- Lambert J.C., Van Roozendael M., M., Simon P.C., Pommereau J.P., Goutail F. Andersen S.B., Arlander D.W., Buivan N.A., Claude H., De La Noe J., De Maziere M., Dorokhov V., Eriksen P., Gleason J.F., Karlsen Tornqvist K., Kastad Hoiskar B.A., Kyro E., Leveau

J., Merienne M.F., Milinevsky G., Roscoe H., Sarkissian A.,., Sanklin J.D., Staehelin J., Tellefsen C.W. and Vaughan G., Combined characterisation of GOME and TOMS total ozone using ground-based observations from NDSC, in: Proceedings of the 32nd COSPAR Scientific Assembly, 12-19 July 1998, Nagoya, Japan, 1998.

- Sarkissian A., F. Fierli, F. Goutail, J-P. Pommereau, E. Kyro and M. Rummukainen, Frequency of occurrence of PSC above Northern Scandinavia from 1990 to 1997 from SAOZ zenith sky colour index, Proceedings of the 4th European Symposium on Polar Stratospheric Ozone, Schliersee, Germany, 22-26 September 1997. Air Pollution Research Report 66, Harris, N.R.P., Kilbane-Dawe, I. and Amanatidis, G.T. (ed.), European Commission, 163-166, 1998.
- Fierli F., Cairo F., Pulvirenti L., Nardi B., Mandolini S., Di Donfrancesco G., Adriani A., Hauchecorne A., Goutail F., Sarkissian A., Deshler T., Rizi V., Redaelli G., Visconti G., Knudsen B., Hansen G. and Hoppe U.P., 1998, January 23rd PSC above Andoya: different aerosol characteristics retrieval from backscatter data, comparison with Optical Particle Counter measurements and interpretation by Lagrangian box modelling, in: Proceedings of the 4th European Symposium on Polar Stratospheric Ozone, Schliersee, Germany, 22-26 September 1997. Air Pollution Research Report 66, Harris, N.R.P., Kilbane-Dawe, I. and Amanatidis, G.T. (ed.), European Commision, 119-122, 1998.
- Lambert J.C., Van Roozendael M., M., Simon P.C., De Maziere M., Pommereau J.P., Goutail F., Sarkissian A. , Andersen S.B., Eriksen P., Kastad Hoiskar B.A., Arlander W., Karlsen Tornqvist K., Dorokhov V., Kyro E., GOME and TOMS total ozone in northern winter 1996/97: comparison with SAOZ/UV-visible ground-based measurements in the Arctic and at middle latitude, in: Proceedings of the 4th European Symposium on Polar Stratospheric Ozone, Schliersee, Germany, 22-26 September 1997. Air Pollution Research Report 66, Harris, N.R.P., Kilbane-Dawe, I. and Amanatidis, G.T. (ed.), European Commission, 696-699, 1998.
- Sarkissian A., F. Goutail, F. Fierli and J-P. Pommereau E. Kyro and M. Rummukainen V. Dorokhov and V.U. Khattatov Frequency of PSCs observed at Arctic SAOZ stations compared to that simulated from ECMWF: Distribution in and out vortex, European Workshop on Mesoscale Processes in the Stratosphere, Bad Tolz, Germany, 9-11 November, 1998.
- Keckhut P., Godin, S., Goutail F., Sarkissian A., Hauchecorne A., Souprayen C., Vialle C., David C., Bergeret V., Hertzog A., Marchand M., Pommereau J.-P., Chanin M.-L., Mégie G., Guirlet M., de la Noé J., Ricaud P., Lezeaux O., Bencherif H., Portafaix T., Posny F., Mérienne M.-F., Barbe A. and Leblanc T., Détection des changements de la stratosphère, in: Rapport Quadriennal 1995-1998 du Comité National Franais de Géodésie et de Géophysique. XXIIème Assemnlée Générale de l'Union Géodésique et Géophysique Internationale, Birmingham (Angleterre), 18-30 Juillet 1999, CNFGG (ed.), 199-218, 1999.
- Lambert J.-C., J. Granville, M. Van Roozendael, J.-F. Mller, J.-P. Pommereau, F. Goutail, and A. Sarkissian, A pseudo-global correlative study of ERS-2 GOME NO2 data with ground-, balloon-, and space-based observations, in Proc. European Symposium on Atmospheric Measurements from Space (ESAMS), ESA/ESTEC, Noordwijk, The Netherlands, 18-21 January 1999, ESA WPP-161, Vol. 1, 217-224, 1999.

- Lambert J.-C., M. Van Roozendael, J. Granville, P. Gerard, P.C. Simon, J.-P. Pommereau, F. Goutail, and A. Sarkissian, Geophysical validation of ERS-2 GOME ozone products by means of correlative observations from the NDSC, in Proc. European Symposium on Atmospheric Measurements from Space (ESAMS), ESA/ESTEC, Noordwijk, The Netherlands, 18-21 January 1999, ESA WPP-161, Vol. 2, 595-601, 1999.
- Sarkissian A., F. Goutail, P. Keckhut and J.-P. Pommereau, H. K. Roscoe and J. Slusser, Long Series of Total Ozone Measured by SAOZ Network at Polar Circle, Mid-latitude and Tropics, proc. SPARC meeting, 2000.
- Sarkissian A., Monitoring Stratospheric Constituents by Ground-based UV-visible Dobson and SAOZ spectrometers, European Research Courses on Atmosphere Volumn 4, C. Boutron, Chapter X, pp 179-194, 2000.
- Lambert J.-C. , J. Granville, M. Van Roozendael, and J.-F. Mller, F. Goutail, J.-P. Pommereau, and A. Sarkissian, P. V. Johnston and J. M. Russell III, Global Behavior of Atmospheric NO2 as Derived from the Integrated Use of Satellite, Ground-based Network and Balloon Observations, Proc. 2000 Quadriennal Ozone Symposium, 2000.
- Sarkissian A. , A. Richter, M. Van Roozendael, J.-C. Lambert, J. Granville, J.-M. Vandenberghe, M. Buchwitz, B. A. K. H øiskar, I. Flisand, K. T ørnkvist, H.K. Roscoe, F. Goutail and J.-P. Pommereau, Improved Air-Mass Factors for Ground-Based Total NO2 Measurements: A Sensitivity Study, Proc. 5th European Workshop on Stratospheric Ozone, Saint-Jean-de-Luz, France, 27 September - 1 October 1999, 730-733, 2000.
- Lambert J.-C. , J. Granville, M. Van Roozendael, A. Sarkissian, F. Goutail, J.-F. Mller, J.-P. Pommereau, and J.M. Russell III, A climatology of NO2 profile for improved Air Mass Factors for ground-based vertical column measurements, Proc. 5th European Workshop on Stratospheric Ozone, Saint-Jean-de-Luz, France, 27 September - 1 October 1999, 703 706, 2000.
- Sarkissian Alain, Florence Goutail et Jean-Pierre Pommereau, Surveillance de la Stratosphère depuis le sol à l'aide du réseau de spectromètres SAOZ, Atelier Experimentation et Instrumentation, Toulouse, 9-10 Decembre 1999, CNES, 2000.
- Yan N., E. Chassefière, F. Leblanc, M. Meftha, J. Porteneuve and A. Sarkissian, Desorption laser coupled to mass spectrometer for the analysis of regoliths (abstract) , EGS, General Assembly, Nice, 2003.
- Fraser, H.-J., Ehrenfreund, P., Blum, J., Cartwright, J.-H.-E., Hadamcik, E., Levasseur-Regourd, A.C., Price, S., Prodi, F., Sarkissian A. and R. Seurig, Physics and Chemistry of Ices in the Universe: Answers from Microgravity, ESA Topical Team: Physico-Chemistry of Ices in Space, ESTEC Contract No: 15266/01/NL/JS, ESA SP, 2004.
- Dubernet M.L., J. Aboudarham, C. Barache, J. Berthier, F. Boone, J. Crovisier, J.M. Desert, D. Egret, A.M. Gontier, J. Guibert, R. Haigron, P. Hennebelle, I. Jegouzo, J. Le Bourlot, F. Le Petit, P. Le Sidaner, E. Lesquoy, J.B. Marquette, N. Moreau, J.M. Martin, D. Pelat, M. Perault, P. Prugniel, F. Roques, F. Royer, A. Sarkissian, J. Schneider, G. Simon, F. Tajahmadi, G. Theureau, W. Thuillot, F. Tran-Minh, J. Vetois, F. Viallefond, VO Paris Federation between Paris Observatory, IAP and IPSL, ADASS 15, Madrid, 2005.
- Fraser, H.-J., Ehrenfreund, P., Blum, J., Cartwright, J.-H.-E., Hadamcik, E., Levasseur-Regourd, A.C., Price, S., Prodi, F., Sarkissian A. and R. Seurig, Ices in the Universe:

Answers from Microgravity, ESA Topical Team in Physical Sciences, ESTEC, 2005.
- Sarkissian A., Brightness temperature of synchronic exoplanets measured by infrared photometry: Method and perspective, Abstract, Geophysical Reserach Abstract, Vol. 7, 2005, EGU 2005.
- Sarkissian A.,J.E. Arlot, Y. Benilan, J.-L. Bertaux,J. Berthier, N. Biver, C. Boone, A. Brahic,G. Chanteur, E. Chassefière,L. Chevallier, I. Chilingarian, J.M. Desert, P. Didelon, P. Drossart, C. Ferrari, F. Forget, T. Fouchet,F. Genova,V. Lainey, F. Leblanc, F. Lefevre,P. Lesidaner, S. Lebonnois, P. Lognonné, D. Le Quéau, S. Maurice,V. Maigne, F. Montmessin, R. Moreno,J.-L. Orcesi, P. Pinet, F. Poulet, G. Poulleau, F. Raulin, F. Rocard, W. Thuillot, and F. Vachier, Planetology in the Virtual Observatory and connection to Europlanet Network, Poster Europlanet, Vienna, EGU 2005.
- Sarkissian A., Brightness temperature of synchronic exoplanets measured by infrared photometry: Method and perspective, Notes du Pole de Planétologie de l'IPSL, Vol 9, 2005.
- Thuillot W., J. Berthier, A. Sarkissian, A. Mickaelian, L. Sargsyan, J. Iglesias, V. Lainey, M. Birlan, G. Simon, First step to Massive physical and dynamical characterization of asteroids, IAU XXVIth General Assembly, Prague, 2006.
- Sarkissian A., Workflow for fast and simple analysis of Elodie spectra, invited paper at EPSC 1, Berlin, Germany, 18-22 Septembre 2006.
- Le Sidaner, P. et al., Latest VO developments at Paris VO Data Centre, Poster session ASOV, Paris, 26-30 Juin 2006.
- Sarkissian A., Workflow for fast and simple analysis of Elodie spectra, Poster session ASOV, Paris, 26-30 Juin 2006.
- Sarkissian A., Data Base for planetary Atmospheres, Semaine de la Société Franaise d'Astronophysique et d'Astronomie, Poster session PNP, Paris, 26-30 Juin 2006.
- Patris, J. and Sarkissian, A., Astronomical observations with OHP telescopes, European Research Courses on Atmosphere Volumn 4, C. Boutron, Journal de Physique IV - Proceedings, 139, 373-390, Doi :10.1051/jp4:2006139024, 2006.
- Gasq C., D.Sourgen, G.Bannerot, A.Guilbaud, O. Bousquet et A.Sarkissian, DEPIR : Détecteur pour Exoplanètes par Photométrie Infra-Rouge: Mise en oeuvre d'un détecteur infra-rouge HgCdTe sur un télescope, Rencontres Electroniques, Poster, Annecy, Mai 2006.
- Berthier J., Thuillot W., Mickaelian A., Sarkissian A., et al. Asteroid Search with the DFBS // Science with Virtual Observatories: JENAM-2007, Special Session #8, Yerevan 2007.
- Mickaelian A., Sarkissian A., Dubernet M.-L., Le Sidaner P., Prugniel P., Nesci R., et al. Simple Spectral Access VO Application on the Digitized First Byurakan Survey // Science with Virtual Observatories: JENAM-2007, Special Session #8, Yerevan 2007.
- Sarkissian A., Détection de planètes extrasolaires par la méthode des vitesses radiales, Les Cahiers Clairaut, n 117, , G. Paturel, Printemps 2007.
- Thuillot W., Berthier J., Sarkissian A., Mickaelian A., Sargsyan L., Iglesias J., Vachier F., Birlan M., Simon, G. Massive Physical and Dynamical Characterization of Asteroids // The Virtual Observatory in Action: New Science, New Technology, and Next Generation Facilities, 26th meeting of the IAU, Special Session 3, 17-18, 21-22 August, 2006 in Prague, Czech Republic, SPS3, 2007.

- Sarkissian A. and Chassefière E., VO activities at the french data base for planetary atmospheres, the BDAP, EPSC 2007, Posdam, August 2007.
- Sarkissian A., Water Vapour Total Column Measurements with Elodie at Observatoire de Haute Provence from 1994 to 2005, Virtual Observatories in Geosciences, Denver, June 2007.
- Le Sidaner, P. et al., Paris VO Data Centre : Une fédération de laboratoires et de projets autour de l'Observatoire Virtuel, Observatoire de Paris, IPSL et CEA, Poster session ASOV, Grenoble, June 2007.
- Mickaelian A.M. , L.A. Sargsyan , R. Nesci, G. Cirimele, A. Sarkissian , "Spectra extraction and analysis software for the Digitized First Byurakan Survey (DFBS) and research projects ", XXVII IAU General Assembly, Rio de Janeiro, Brazil, August 2009.
- Berthier J., Sarkissian A. and Thuillot W., Asteroids in DFBS, DFBS book, DFBS book, Universita di Roma "La Sapienza ", Massaro, Mickaelian, Nesci and Weedman editors, p57, 2009.
- Mickaelian A and Sarkissian A., DFBS and the Virtual Observatory, DFBS book, DFBS book, Universita di Roma "La Sapienza ", Massaro, Mickaelian, Nesci and Weedman editors, p59, 2009.
- Sarkissian A., Planetary Atmospheres: Developments of Data Archiving, tools and Services in France, XXVII IAU General Assembly, Rio de Janeiro, Brazil, August 2009.
- Alkasm S. and Sarkissian A., Sensitivity study of water vapor total column measurements using the Elodie Archive at Observatoire de Haute-Provence from 1994 to 2004, International Conference on Comparative Planetology: Venus - Earth - Mars, 11-15 May 2009.
- Kasaba Y., Capria M. T., Crichton D., Zender, J., Beebe, R. and the IPDA, , The International Planetary Data Alliance (IPDA): Activities in 2008-2010, Space Research Today, 176, 40-45, Dec. 2009.

Développement de sites web à rapporteurs

Sarkissian A. et al., idis.ipsl.jussieu.fr, le site web de l' "Integrated and Distributed Information Service " d'Europlanet, depuis 2008, rapports NASA et ESA.

Autres sites et services web

- Sarkissian et al., http://bdap.ipsl.fr/ : Le site web des bases de données et d'information pour l'étude des atmosphères planétaires initié par le pôle Système Solaire de l'IPSL, depuis 2002.
- Sarkissian et al., http://bdap.ipsl.fr/fondue/ : Projet ISSI de bases de données de mesure du fond UV interplanétaire, depuis 2008.
- Sarkissian et al., http://bdap.ipsl.fr/voscat/ : Base de données sur les relations Soleil-Climat, depuis janvier 2010.
- Sarkissian et al., http://bdap.ipsl.fr/tellodie/ : web service de la mesure de la vapeur d'eau atmosphérique dans les spectres d'Elodie de l'OHP, depuis 2007.
- Sarkissian et al., http://bdap.ipsl.fr , portail des activités bases de données du pôle Système Solaire de l'IPSL, depuis 2009.

Participation à l'encadrement du travail de thèse

(Nom du directeur de thèse, % de ma participation)

- Thierry Carpentier 1992-1996 (J.-P. Pommereau, 20%), développement d'un capteur pour l'étude de l'atmosphère de Mars ODS.
- Céline Philips 1993-1997 (J. -P. Pommereau, 20 %), Développement d'un spectromètre embarqué en ballon pour l'étude des composants minoritaires de l'atmosphère terrestre, une publication [15].
- Vanessa Sherlock 1995-1998 (A. Hauchecorne, 10 %) étude des nuages dans l'atmosphère de la Terre.
- Fédérico Fierli 1998-2000 (A. Hauchecorne, 20 %), étude des nuages dans l'atmosphère de la Terre.
- Nicolas Yan 2003-2006 (E. Chassefière, 20%), étude des propriétés thermiques du sol de Mercure, une publication [20].
- Younes Gabsi 2004- 2008 (A. Hauchecorne, 10%), étude des vents dans l'atmosphère de Vénus.
- Christophe Hoareau 2008- (P. Keckhut, 20 %), mesure de la vapeur d'eau par Lidar, une publication [21].
- Sulaf Alkasm 2008- (P. Keckhut, 90 % en attente HDR), étude des composants minoritaires de l'atmosphère de la Terre mesurés dans les spectres d'Elodie à l'OHP.

Développement d'instruments

2004 - 2007: Détecteur d'Exoplanètes par Photométrie Infra-Rouge (DEPIR) en collaboration avec le Laboratoire de Météorologie Dynamique (LMD), 2 fois une semaine d'observation à l'OHP, les hivers 2005 et 2006, une publication [24].

Tâches de service

- Responsable dans le cadre des Services d'Observation de l'IPSL (i) des spectromètres Dobson de l'OHP et de Bordeaux, (ii) de la station NDSC Alomar en Norvège; et (iii) du réseau SAOZ de 1996 à Décembre 2001.
- Responsable de la coordination des activités denseignement à l'OHP dans le cadre des Services dObservation de lIPSL depuis Janvier 2002.
- Responsable et fondateur de base de Données sur les Atmosphères Planétaires (BDAP, http://bdap.ipsl.fr/).
- **Responsable et fondateur du noeud Atmosphères d'IDIS du programme européen Europlanet (FP6 et FP7)** (http://bdap.ipsl.fr/idis/).
- Responsable et fondateur du centre de Données thématique FONDUE depuis janvier 2008 (Fully On-line Data center for Ultraviolet Emissions, http://bdap.ipsl.fr/fondue/).
- **Responsable et fondateur du centre de Données thématique VO-SCAT depuis Janvier 2010** (Observatoire Virtuel Soleil-Climat-Atmosphère de la Terre, http://bdap.ipsl.fr/voscat/).

Enseignement

- Co-responsable du M2 international "Arctic Studies" à l'UVSQ, ouverture rentrée 2010 (http://www.uvsq.fr/formations-et-inscriptions/master-professionnel-arctic-studies-63103.kjsp?RH=ACCUEIL-FR).

- 34 participations (dont 24 avec l'organisation de la formation) de 1996 à 2010 à des formations et écoles doctorales (dont 14 ERCA, 12 SIMO et 7 DEA Astro, 1 ENS) sur site instrumental à l'OHP avec séminaires, présentation instrumentale et TP sur instruments, pour des étudiants de DEA ou en Thèse, de niveau national et international.

ERCA: European Research Courses on Atmospheres, 50 à 60 étudiants, international, (http://www-lgge.ujf-grenoble.fr/enseignement/erca/).

SIMO: Stage d'Initiation aux méthodes d'Observation, 20 à 50 étudiants, (http://simo.ipsl.jussieu.fr/).

- Responsable pour le réseau SAOZ de la formation des hivernants de l'IFRTP (maintenant Institut Paul-Emile Victor, IPEV) de 1996 à 2000.
- TP en 1998-1999 et 1999-2000, "Pollution Urbaine l'Instrument SANOA " pour le DESS de l'UVSQ "Qualité de l'Air et Lutte contre le Bruit ".

A. Synthèse des travaux scientifiques

I. Introduction

C'est à l'intersection des domaines de recherches qu'il y a aujourd'hui le plus de chance de participer à une découverte majeure. Les domaines eux-même sont très bien couverts et c'est vrai qu'il faut parfois tant se spécialiser que les aspects marginaux nous échappent. Voila une motivation qui sort des motivations scientifiques actuelles telles que la compréhention de la destruction de l'ozone polaire, l'évolution de notre climat, ou la recherche d'une vie en dehors de notre planète. C'est pourtant également une motivation qui permet d'être simultanément sur plusieurs sujets brûlants du moment. Ainsi, mon travail passé, actuel et probablement futur sur les atmosphères et les climats de la Terre en particulier et en planétologie en général montrent bien le fil conducteur de mes recherches. La spectroscopie et la modélisation radiative étaient mes outils qui jusqu'à présent marquaient les limites de ces recherches.

Mon investissement récent aux techniques de l'observatoire virtuel orienté vers la fouille et le traitement massifs d'archives ou de données est mon troisième outil. C'était déjà mon outil (plus primitif, car la notion d'interopérabilité n'y était pas associée) lorsque je faisais ma thèse sur le SAOZ (Système d'Analyse par Observation au Zénith). C'est encore plus le cas maintenant puisque j'exploite le DFBS (Digitized First Byurakan Survey) ou l'Archive Elodie de l'OHP (Observatoire de Haute-Provence) avec les standards de l'Observatoire Virtuel (VO, pour Virtual Observatory en anglais). C'est la raison pour laquelle je me suis orienté dès sa création vers l'Observatoire Virtuel qui, grâce au concept d'interopérabilité, pouvait faciliter mes recherches mais aussi leur permettre de se développer en utilisant ce troisième outil qui est issu d'un domaine que vous pourrez appeller la recherche informatique appliquée.

J'ai divisé ce document en deux parties principales pour séparer mes activités passées de mes projets à venir. Je présenterai dans cette section les quatres grands thèmes scientifiques auxquels j'ai participé au cours de mes activités, sur l'ozone polaire, la détection d'exoplanètes par photométrie infrarouge, la vapeur d'eau atmosphérique, et l'Observatoire Virtuel. Ces activités ont été accompagnées de nombreuses campagnes d'observation sur le terrain et d'ateliers de travail que je ne pourrai pas énumérer ici, mais je pense qu'il faut bien insister sur le fait que j'ai un profil instrumentaliste de terrain et que la partie Observatoire Virtuel que je vais présenter est un complément indissociable de l'expérimentation car elle permet la valorisation de ces activités.

II. L'ozone polaire

La destruction de l'ozone polaire avec ses effets sur l'environnement polaire ou à moyennes latitudes, et ceux sur l'augmentation du rayonnement UV qu'elle entraine a été l'un des éléments moteur depuis plus d'une vingtaine d'année de l'activité de toute une communauté dont je fais partie. L'importance de son étude à court et long termes et de sa surveillance journalière a entrainé des développements instrumentaux et de modélisation qui ont permis de bien comprendre les causes et les effets de ce phénomène qui résulte principalement de l'activité humaine, sans négliger le rôle également important du Soleil en particulier et d'autres phénomènes naturels en général (volcanisme, inclinaison de l'orbite de la Terre, etc...). Dans cette partie, ma contribution porte surtout sur la possibilité d'étudier l'impact des nuages stratosphériques polaires sur la destruction de l'ozone [1,5] et l'évaluation annuelle de cette destruction [15]. Je vais présenter ici ma contribution à ces activités.

Mon travail de thèse puis mon expérience de post-doctorant au British Antartic Survey m'ont permis de me spécialiser dans l'étude des atmosphères des planètes, principalement de la Terre, avec comme principales applications:
- Mise au point d'une méthode de détection des nuages et des poussières dans les atmosphères des planètes, c'est mon sujet de thèse [1,5];
- Etude du rôle du facteur de masse d'air dans les mesures crépusculaires de l'ozone par spectrométrie UV-visible du ciel au zénith [3];
- Participation à la validation des données du réseau SAOZ sol pour mise à disposition dans les banques de données internationales et européennes (NDSC-Network for Detection of Stratospheric Changes, maintenant NDACC- Network for Detection of Atmospheric and Climates Changes, NILU Data Centre (Centre de Données des campagnes Arctiques KEOPS en 1991, EASOE en 1993 et SESAME en 1995) et en libre accès au Service d'Aéronomie (Base de données SAOZ);
- Participation à l'amélioration de l'analyse spectrale des données du réseau SAOZ sol [2,3,4,6];

Si ce dernier point est plus technique que scientifique (ou plus "service d'observation"), c'est bien sûr en affinant celui-ci que nous avons pu avancer sur les trois premiers points tant pour la Terre et le réseau SAOZ que pour la planétologie. A noter également les débuts de mes implications dans le principe d'Observatoire Virtuel (qui n'existait pas encore à l'époque) avec la mise en ligne en temps réel des données du réseau SAOZ sur internet dès 1994 à mon retour du British Antarctic Survey.

Mon programme de recherche a ensuite été orienté vers la compréhension du rôle du rayonnement UV et visible dans l'atmosphère de la Terre comme suite logique à mon travail de thèse puis de post doc au British Antartic Survey, en ne négligeant pas l'influence des aérosols, la diffusion multiple et la polarisation de la lumière diffusée. J'ai ainsi participé à:
- L'étude des variations saisonnières de l'apparition des nuages polaires stratosphériques

en Arctique [5];
- La poursuite de l'amélioration de l'analyse spectrale des données du réseau SAOZ sol [9,10,12,14,16];
- L'étude du rôle du facteur de masse d'air dans les mesures crépusculaires de l'ozone et du NO_2 par spectrométrie UV-visible au zénith [7,8,11,18];
- La validation des données du réseau SAOZ sol pour mise à disposition dans les banques de données (NDSC, NILU, SAOZ) [13];
- La quantification de la destruction d'ozone dans le vortex polaire arctique [15];
- La validation des données GOME (Global Ozone Monitoring Experiment, expérience embarquée sur satellite) à l'aide des données du réseau SAOZ sol [13,17].

L'affinement de nos connaissances sur l'étude de la destruction de l'ozone polaire et ma participation à ces progrès dans le cadre de collaborations internationales ont été mis en évidence par ma participation active aux principales campagnes d'observations en régions polaires, ainsi qu'à l'interprétation des observations obtenues durant ces campagnes. Des études de tendances, possibles dès les années 2000 grâce aux longues séries de données (plus de 11 ans, le cycle solaire) accessibles dans les bases de données mises en route à cette époque, telles que le NDSC que nous avions également très largement alimenté.

C'est à partir de ces données que j'ai pu mettre en évidence la fréquence d'apparition des nuages stratosphériques polaires et montrer que ceux ci étaient de plus en plus fréquents depuis les années quatre-vingt dix au dessus de l'Arctique principalement en janvier et février, qu'ils pouvaient toutefois apparaitre également de façon plus ponctuelle quelquefois en décembre ou en mars, avec tout ce que cela implique dans les taux de destructions de l'ozone dans ces régions [5, 15]. En fait, il est clairement apparu que les nuages formés au printemps avaient un effet sur l'ozone beaucoup plus prononcé que ceux qui apparaissent en hiver car ce n'est pas la formation, mais plutôt leur évaporation qui affecte l'équilibre de l'ozone stratosphérique en libérant les produits azotés piégés dans les cristaux de ces particules pendant leur formation.

En ce qui concerne les mesures de l'ozone avec le réseau SAOZ, il est toujours complètement opérationel avec plus d'une vingtaine d'instruments répartis tout autour du globe et ce réseau est particulièrement utilisé lors des validations satellitaires, des campagnes thématiques, de l'étude des tendances et de la surveillance d'évènements particuliers tels qu'une éruption volcanique. Nous avons ainsi montré et évalué l'amplitude de la destruction de l'ozone stratosphérique dans l'hémisphère Nord au printemps en comparant nos observations aux sorties de modèles dans lesquels nous n'avions laissé que la dynamique pour évaluer la fraction due à la chimie stratosphérique dans cette destruction. Cette méthode d'évaluation est toujours exploitée aujourd'hui car elle permet d'identifier clairement l'origine de la destruction d'ozone en régions polaires en hiver et au printemps (Figure 1). A noter également que cette étude a donnée lieu à la publication la plus citée de mes travaux [15].

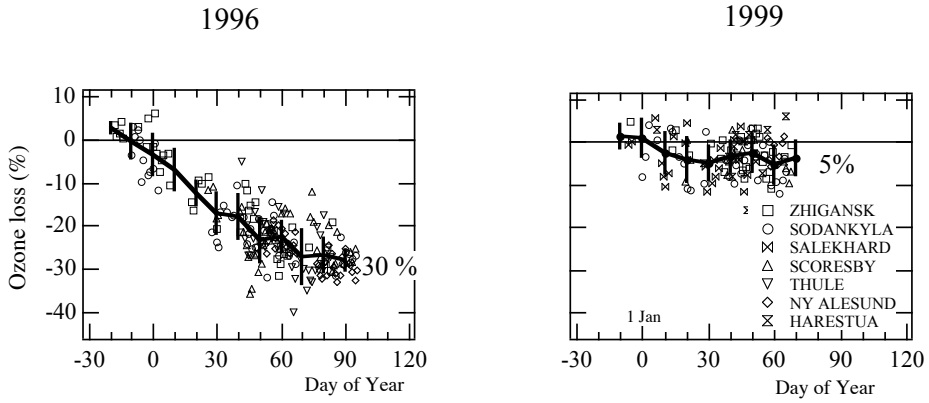

Figure 1: Destruction de l'ozone Arctique observée par le réseau SAOZ, d'après [15].

III. Mise au point d'un instrument infrarouge pour la mesure de la température à la surface des exoplanètes

La découverte vers les années 1995 puis l'étude des exoplanètes par la méthode des vitesses radiales a une importance primordiale tant sur la compréhension de la formation des systèmes stellaires, et en particulier du Système Solaire, que sur la démonstration que des situations similaires à celles rencontrées sur Terre peuvent exister en dehors du système solaire. En effectuant des recherches dans l'infrarouge, nous avons accès à la température des exoplanètes et donc aux conditions à leur surface. Ceci est d'une importance capitale car il est maintenant clair pour toute la communauté scientifique concernée que l'étape à venir concerne la découverte d'une planète sur laquelle la vie est possible ou au moins envisageable. De plus, cette température donne également accès à la présence ou non d'atmosphère (après la taille et la masse qui sont les paramètres déterminants) et à toutes les implications que cela entraîne, en dynamique de l'atmosphère dans des cas extrêmes par exemple avec un gradient de température important entre les faces éclairées et celles à l'ombre pour les planètes synchrones. Les récentes possibilités d'observations depuis l'espace en infrarouge ont favorisé ce type d'études qui étaient à leurs début dans les années 2000 à 2003. La recherche de méthodes autres que celle des vitesses radiales est justifiée par l'accès à de nouveaux paramètres, un challenge pour la discipline. Notez que la mesure de la température par observation en infrarouge pendant le passage de la planète devant le disque de l'étoile ou pendant l'éclipse de la planète a, depuis le développement de cette expérience, déjà été réalisée depuis l'espace.

Il faut noter également que pour faire de telles études, il fallait que je développe des modèles thermiques et radiatifs pour les solides et pour les atmosphères, et qu'ils m'ont servi d'outils dans ce chapitre.

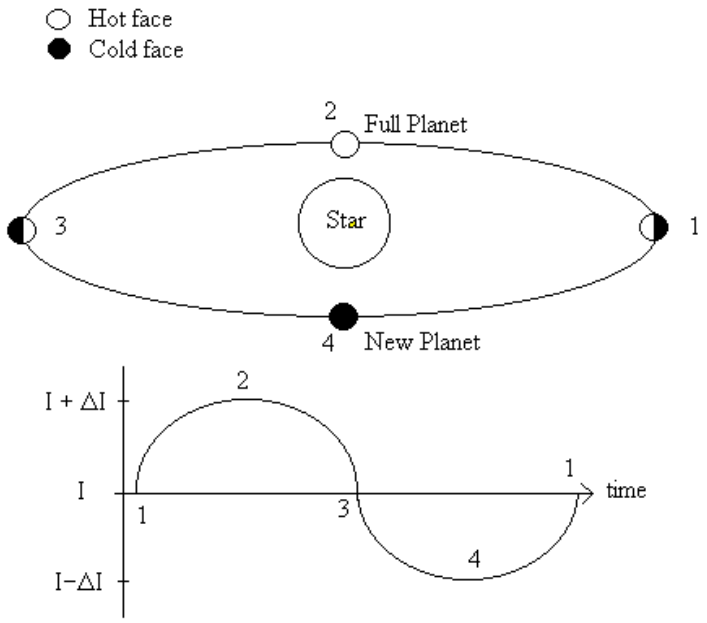

Figure 2: Principe de la méthode de détection.

Cette expérience correspond à ma prise d'autonomie scientifique, période de recherche d'un sujet exotique et d'actualité dans le domaine de mon expertise. C'est pour cela que l'on verra apparaitre des recherches brèves ou longues, pas toujours concluantes, variées, mais très gourmandes en temps de travail: développement d'instrument, domaine de recherche original et travail scientifique complètement indépendant, sans quitter toutefois mes activités engagées par ailleurs.

Dans ce cadre, j'ai été amené à étudier plus en détail tous les facteurs importants pour l'observation de sources lumineuses dans l'infrarouge thermique. Pour cela, j'ai développé un modèle de transfert de rayonnement thermique dans les solides et dans les atmosphères ce qui m'a permis de:

- Contribuer à l'étude de l'inertie thermique à la surface des planètes, principalement Mercure, pour inversion des propriétés thermiques du sol sous la couche du régolithe [20];

- Etudier l'impact des Cirrus sur le rayonnement UV au niveau du sol et sur le budget radiatif de l'atmosphère de la Terre [19];

- Etudier des propriétés optiques et de la formation des particules qui contiennent de l'eau sous forme liquide ou solide dans les atmosphères planétaires [19].

Bien évidemment, le point le plus important de cette section reste le développement

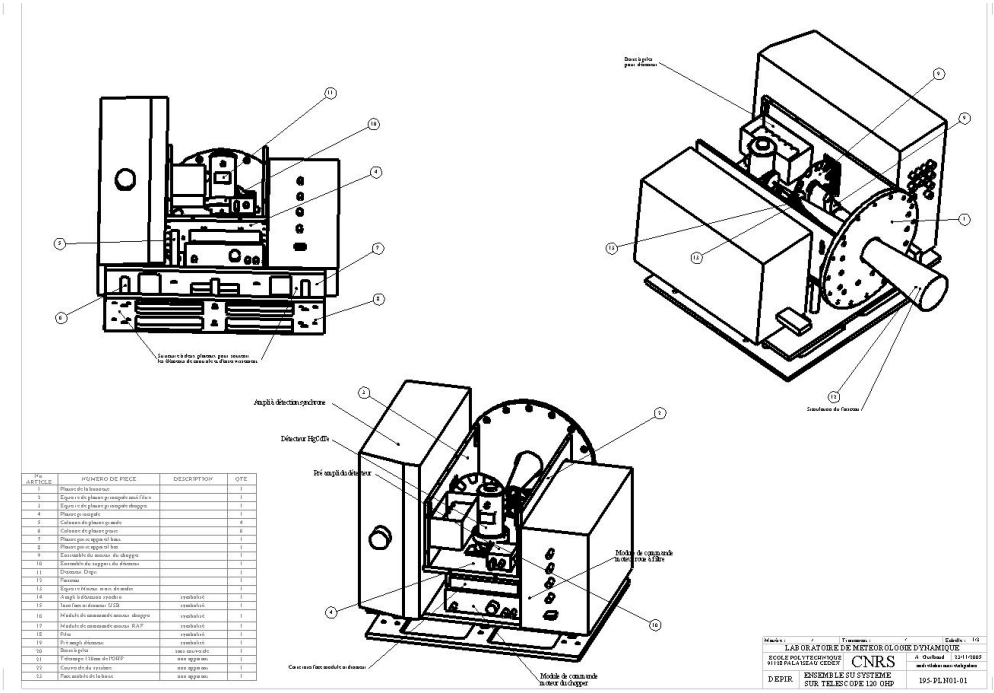

Figure 3: Schéma de l'instrument Depir.

instrumental basé sur une idée originale que je vais présenter maintenant et qui concerne l'étude des exoplanètes. J'ai ainsi proposé et mis au point une méthode de détection des exoplanètes par photométrie différentielle infrarouge afin de déterminer leur température de brillance.

Une exoplanète géante et synchrone montre alternativement, pendant son orbite autour de son étoile mère, les parties de sa surface éclairées et à l'ombre. Observée à distance, l'étoile montrerait ainsi une signature variable de même périodicité mais d'amplitude bien plus faible comparée à la luminosité de l'étoile mère (Figure 2), mais détectable grâce aux techniques différentielles maintenant utilisées en géophysique. A l'aide de nos simulations nous avons évalué ces rapports qui peuvent descendre jusqu'à 100 seulement dans certains cas, des valeurs que l'on pourrait observer depuis le sol avec un instrument dédié [24].

J'ai développé un détecteur (bande N autour de 10 μm, quatre canaux) dédié à cette technique d'observation en collaboration avec nos collègues du Laboratoire de Météorologie Dynamique (LMD) à Palaiseau (Figures 3 et 4). Nos collègues du LMD ont entièrement conçu et fabriqué l'instrument DEPIR (Détecteur d'exoplanètes par photométrie infrarouge) avec les moyens du bord et de la récupération, un temps de travail limité par d'autres contraintes (une semaine/an seulement pour chacun des cinq membres de l'équipe: chef d'équipe, conception mécanique, mécanique, électronicien, banc de test corp noir) et un budget très réduit puisqu'à peine suffisant pour acheter le détecteur infrarouge du commerce (photoconducteur une cellule HgCdTe de chez Judson, en rouge sur la figure 4).

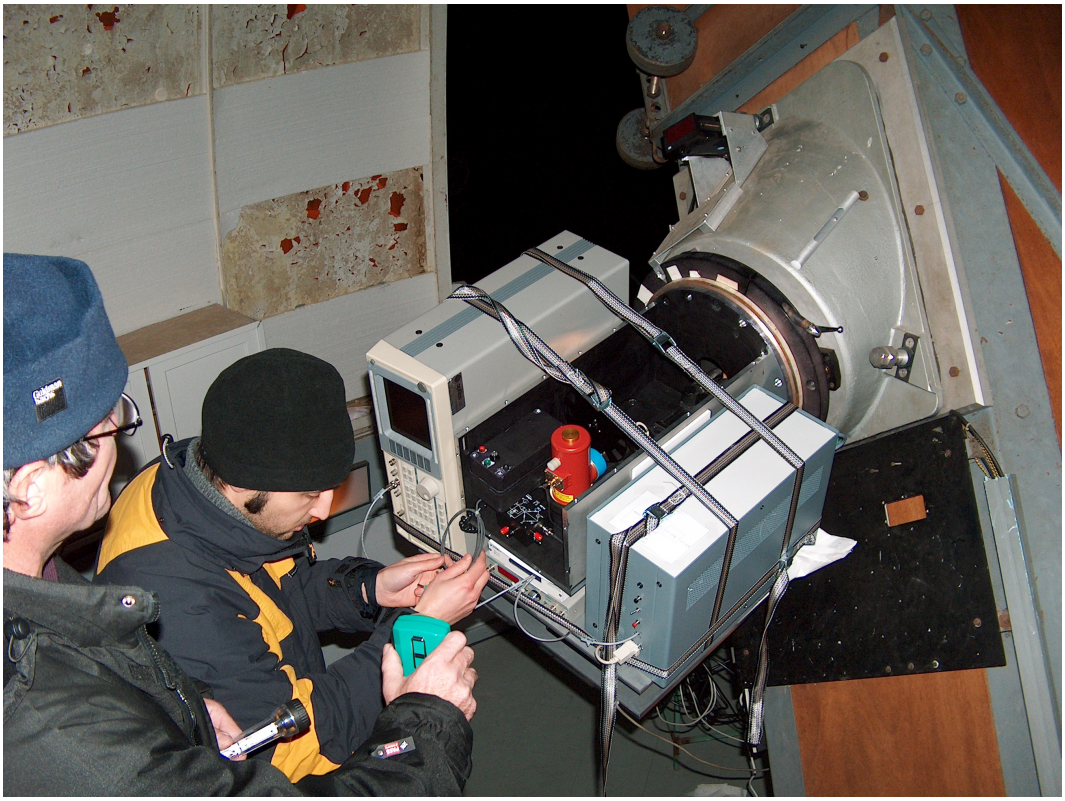

Figure 4: L'instrument Depir au centre installé au foyer Newton du télescope de 120 cm de l'OHP à droite. Le détecteur Judson HgCdTe est en rouge, refroidit à l'azote liquide. La détection synchrone est le boitier à gauche avec l'écran, alors que le module de commande de la roue à filtre est le boitier bleu à droite. Le module de commande de l'obturateur (1000 Hertz pour notre expérience), plus moderne, est le boitier sous le détecteur.

Une première série d'observations a été obtenue sur le télescope de 120 cm de l'OHP en janvier 2006 avec un instrument préliminaire. Nous avons obtenu de bons résultats sur la Lune pour tester l'instrument, et des résultats moins satisfaisants sur les étoiles brillantes en IR mais avec des difficultés de pointage du télescope, en aveugle puisque la poursuite était défaillante lors de notre mission. Nos observations ont montré une très forte variabilité de l'atmosphère terrestre à l'OHP et les simulations préliminaires ont été publiées [24]. La deuxième série d'observations est en cours de dépouillement, activité ralentie par manque de moyens. Il faut indiquer ici qu'un développement instrumental demande du temps et des recherches techniques et de financement, un autre justificatif du manque de publication dans les activités entre 2004 et 2008.

IV. La vapeur d'eau atmosphérique dans les spectres d'Elodie à l'OHP

La vapeur d'eau atmosphérique joue un rôle crucial car elle interagit avec le rayonnement infrarouge émis par la surface de la Terre. La quantité de vapeur d'eau atmosphérique est supposée augmenter avec la température (équation de Clausius-Clapeyron) et donc amplifier le réchauffement climatique dû à l'émission de gaz à effet de serre enthropogéniques. Une série de mesures assez longue, supérieure à dix ans, permet une étude de tendances, et des mesures multiples et régulières dans le temps permettent une étude comparative avec d'autres instruments et des études de budget [21].

Aujourd'hui, la vapeur d'eau atmosphérique est mesurée avec différents instruments sur différents sites (voir les listes sur le NDACC) et ce présent travail n'est pas censé entrer en compétition avec les nombreux instruments dédiés, mais de revenir quelques années en arrière avec un jeu de données homogène et calibré. La base de données d'Elodie contient 34 992 spectres dont plus de la moitié est accessible dans le cadre de l'Observatoire Virtuel Astronomique. Le spectromètre Elodie ayant commencé à fonctionner en juillet 1994 sur le télescope de 193 cm de l'Observatoire de Haute-Provence et étant suivi en 2005 par Sophie sur le même télescope, nous disposons ainsi d'un potentiel de 15 années de mesure de la colonne totale de la vapeur d'eau au dessus de l'OHP. Les spectres sont mis en ligne à la disposition des scientifiques régulièrement, après que les équipes scientifiques qui ont observé ces objets aient livré leurs nouveaux spectres à la base de données.

La description de la méthode de mesure et d'interprétation des données est indiquée dans [23]. Elle consiste à aller chercher dans tous les spectres observés par Elodie, donc des spectres très variés allant de l'étoile à la galaxie, une signature spectrale d'absortion de la vapeur d'eau et d'y appliquer la loi de Beer-Lambert. Nous avons effectué une première évaluation de la qualité de ces mesures, sous forme de leur utilisation afin de calibrer les profils de vapeur d'eau mesurés par lidar à l'OHP [21]. Par rapport à d'autres mesures effectuées à proximité à moins de 200 km de distance (GPS, micro-ondes, sondes sous

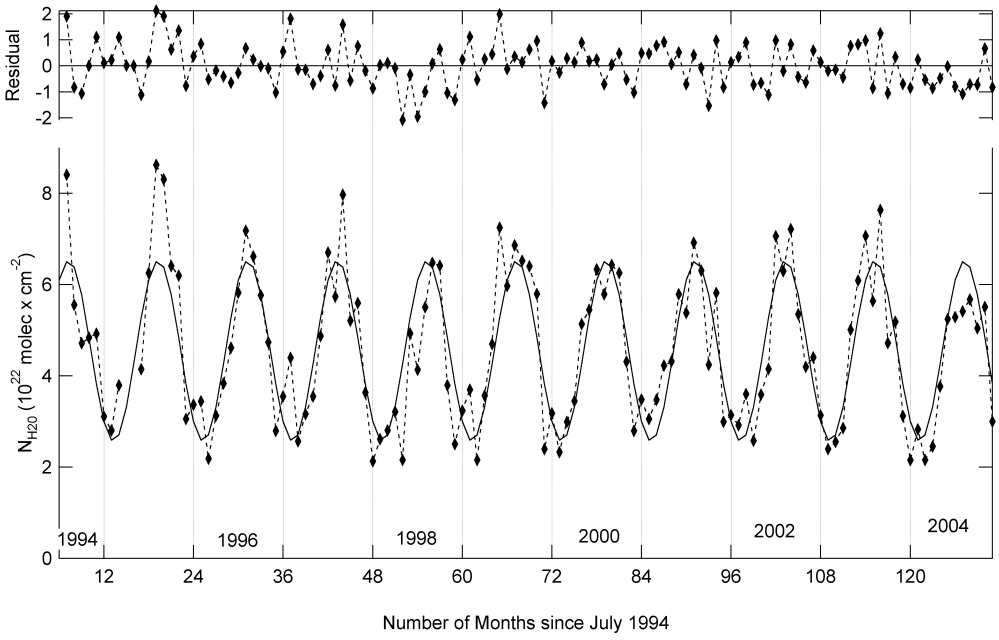

Figure 5: Moyennes mensuelles de la vapeur d'eau au dessus de l'OHP de 1994 à 2004 qui montre une tendance de $-0.44 \pm 0.72 \times 10^{22} molécule \times cm^{-2}$ par 10 ans.

ballon, etc...), les mesures co-localisées et simultanées sont plus adaptées aux exercices de comparaisons car la vapeur d'eau atmosphérique a des variabilités géographiques et temporelles importantes. Les résultats de cette étude sont présentés dans la figure 5 qui montre les moyennes mensuelles de la colonne totale de la vapeur d'eau sur 10 ans et la tendance obtenue, dans notre cas pas de tendance significative car proche du nul et inférieure à la barre d'erreur correspondante à trois sigma.

Ce résultat est important car il faut préciser que la probabilité d'avoir un saut instrumental due à une re-calibration ou à un changement partiel de l'instrument est ici quasi nul grâce à la méthode utilisée, et à l'inverse d'autres méthodes plus connues de mesure de la vapeur d'eau atmosphérique. Nous sommes donc en présence d'une série temporelle homogène et régulière puisque les interruptions dans la série, dues au temps couvert (nuageux ou pluvieux) ou à l'arrêt de l'instrument pour entretien ne dépasse pas le mois.

L'exploitation des archives Elodie de l'OHP pour la mesure de la vapeur d'eau dans les spectres existants se poursuit encore aujourd'hui grâce au spectromètre Sophie qui a remplacé Elodie en 1995 et qui fonctionne encore parfaitement et régulièrement maintenant, avec une plus grande résolution spectrale encore qu'Elodie.

A noter également que ces résultats sont en libre accès dans le cadre des Observatoires Virtuels Astronomique et en Planétologie à l'IPSL (Tellodie, Telluric Lines in Elodie

Spectra, http://bdap.ipsl.fr/tellodie/, Sarkissian A., 2009). Cela me permet d'introduire la section suivante, l'Observatoire Virtuel, qui m'a donné les bases pour développer mes outils, mais auquel je participe également très fortement dans la définition des standards et dans l'exploitation de celui-ci, comme nous allons le voir maintenant.

V. L'Observatoire Virtuel en Planétologie

Je vais montrer ici comment j'ai été l'un des initiateurs, dès 2004, dans le cadre de mes activités de Service, de la mise en place de l'Observatoire Virtuel en Planétologie dans le cadre de collaborations nationales et internationales. L'objectif étant ici de trouver un moyen ou une méthode pour exploiter pleinement les ressources existantes (et localisées sur différents sites et accessibles de manière non homogènes) et à venir dans notre domaine scientifique. Cet objectif ne peut être atteint que si, à l'exemple de l'Observatoire Virtuel Astronomique, nous proposons des protocoles et des modèles d'architectures ou de types de données acceptés par toute la communauté. Le résultat attendu de tels efforts sera l'utilisation large de l'Observatoire Virtuel en Planétologie par notre communauté sous forme de recherche d'évènements observés par différents systèmes d'observation par exemple, ou bien des recherches massives nécessitant des outils performants et ayant accès à de multiples sources. C'est ma contribution à cet effort que je vais présenter dans cette section. Je vais également montrer en fin de cette partie comment l' Observatoire virtuel a été utilisé pour la recherche avec la description d'un exemple d'utilisation que j'ai développé.

Bien qu'étant une activité de service, la mise en place de l' Observatoire Virtuel en Planétologie contient une activité scientifique qu'il ne faut absolument pas négliger sous peine de voir se dé-engager les acteurs potentiels de cette activité, pas très porteuse en terme de publication scientifique (d'òu un manque de publication dans mes activités entre 2004 et 2008). Il n'est pas question ici de site web ou de service web pour la communauté (bien que je considère pour ma part qu'un service web soumis à un comité d'évaluation ou de labellisation soit l'équivalent d'une publication à rapporteurs), mais bien de la définition des standards pour l'Observatoire Virtuel en Planétologie.

Dans ce sens, mes participations actives à: l'IVOA (http://www.ivoa.net/), l'International Virtual Observatory Alliance pour laquelle j'ai participé à la définition du STC, le "Space Time Coordinates" (les standards pour identifier la localisation et l'orientation d'un objet dans l'espace et le temps) et les Workflows (des suites de tâches dans l'Observatoire Virtuel); à VO-France (http://www.france-ov.org/) dont principalement VO-planéto dont je suis l'un des initiateurs et VO Gaff (l'Observatoire Virtuel en Géodésie et Astronomie Fondamentale); à VO-Paris (http://vo-web.obspm.fr/) comme membre du Conseil Scientifique; à l'International Planetary Data Alliance (http://planetarydata.org/),

l'IPDA comme Membre du Conseil Scientifique, assesseur du PDS4 (le nouveau format VO du PDS, Planetary Data System de la Nasa, http://pds.nasa.gov/), le "data model" (les standards pour décrire un modèle de données), le "data dictionary model" (les standards pour le dictionnaire), le "registry" (les standards pour les registres) ainsi qu' au "technical expert group" (groupe pour validation des documents de l'IPDA); et enfin à Europlanet (http://www.europlanet-ri.eu/), projet européen dans lequel je porte le noeud Atmosphères d' IDIS (http://idis.ipsl.jussieu.fr/), le système d'intégration et de distribution des données en planétologie (Integration and Distribution Information Service, Europlanet FP6 puis Europlanet RI FP7) porteront à court terme maintenant la mise en place de l' Observatoire Virtuel en Planétologie.

Notez que la terminologie que je viens d'utiliser est assez complexe à décrire et qu'elle est souvent légèrement différente d'une communauté à l'autre et je demanderai donc au lecteur de se rendre sur les pages web des organisations citées pour plus de détails. Je vais décrire ici seulement les éléments les plus importants de mes contributions en ne présentant pas mes contributions dans les définitions des standards.

Tout d'abord, il faut préciser que les développements récents et originaux en planétologie proviennent de l'accès à l'espace (expériences spatiales) et que la planétologie depuis le sol reste très proche de l'astronomie traditionnelle: imagerie, spectrométrie. Avec l'arrivée des expériences embarquées en planétologie, nous nous sommes rendu compte que l'approche "plate-forme instrumentale uniquement" pour mettre à disposition des jeux de données n'était pas le plus judicieux, et c'est pour cette raison que très tôt, le PDS puis le PSA (Planetary Science Archives de l'ESA, http://www.rssd.esa.int/index.php?project=PSA) ont séparé leurs services (communautés) en plusieurs parties, notamment: Atmosphère, petits corps, milieu inter-planétaire, etc... Ainsi, l'approche imagerie-spectrométrie n'étant plus valable pour les mesures in-situ des aérosols atmosphériques de Titan par exemple, il fallait améliorer nos systèmes de mises à disposition des données et l'Observatoire Virtuel est le cadre idéal pour cette activité car une grosse partie du travail est chez eux déjà bien avancée. C'est ainsi qu'a été développé dans le cadre d'Europlanet, en plus de l'approche thématique dont nous avons parlé, une approche par cas scientifique pour IDIS, moi-même étant en charge de la partie Atmosphère d'IDIS (http://idis.ipsl.jussieu.fr/). L'idée est de proposer un service qui donne accès à beaucoup plus d'information qu'auparavant, avec en plus, les laboratoires impliqués dans les cas scientifiques, les personnels et leurs bibliographies, et les références des experts concernés. Cette approche, évaluée par nos collègues du PDS et du PSA dans le cadre de l'évaluation du projet européen a été particulièrement bien évaluée puisque recommandée aux autres systèmes similaires.

C'est cette approche que j'ai étendue à différents cas scientifiques par la suite, dans et hors noeud Atmosphères d'IDIS tels que FONDUE (Fully On-line Data Center for Ultraviolet Emissions, http://bdap.ipsl.fr/fondue/) ou le DFBS (Digitized First Byurakan Survey, http://bdap.ipsl.fr/dfbs/) que je ne vais pas décrire ici, mais dont je suis l'initiateur et le responsable dans le cadre de coopérations internationales.

Je vais par contre présenter les outils qui permettent d'utiliser l'Observatoire Virtuel, qu'il soit Astronomique ou pour la Planétologie. Bien sûr, ces outils ont besoin d'avoir des bases de données ouvertes et accessibles ("harvestable" en anglais). Je ne parle pas ici d'un mot de passe pour accéder à cette base, mais d'une base accessible par une machine extérieure avec qui elle peut discuter et échanger des informations. Pour cela, l'Observatoire Virtuel a défini les langages, formats et protocoles nécessaires et la planétologie utilise (pour l'instant et probablement dans le futur également) des standards pour la plupart existants ou basés sur des protocoles existants (par exemple PDAP, Planetary Data Access Protocol). A ce niveau, les outils que je vais présenter maintenant ont utilisé les standards de l'IVOA, ceux de l'IPDA n'étant pas encore pleinement exploitables.

Partons d'un exemple courant de fouille d'archives et qui va nous faire utiliser plusieurs outils développés (et donc la définition des standards) par l'Observatoire Virtuel: chercher dans des banques d'images du ciel en astronomie des traces d'astéroïdes. Dans les années 1960, nous ne connaissions que quelques 100 000 astéroïdes, alors qu'on en connait plus de 400 000 maintenant, et ce nombre ne cesse d'augmenter. L'importance de ces études sur les astéroïdes tient en deux mots: géocroiseurs et système solaire. La découverte récente d'un nombre important de ces objets du système solaire leur donne un rôle de plus en plus important dans la compréhension de la formation du Soleil et de notre système solaire. Leurs formation, classification, évolution, composition, surface, forme, etc.. restent des questions encore bien ouvertes aujourd'hui et c'est en cherchant leurs traces dans les archives anciennes que l'on peut apporter des réponses à certaines questions telles que leur évolution, leur composition, et affiner nos connaissances sur leurs orbites.

Le DFBS est la version digitalisée du fameux First Byurakan Survey ou Markarian survey, à l'aide duquel Markarian a découvert les galaxies actives qui portent son nom avec excès d'UV. Le DFBS couvre $17000^{\circ 2}$ du ciel de l'hémisphère nord en grande partie, mais aussi de l'hémisphère sud. Ces images du ciel ont été obtenues sur un télescope de type Schmidt (donc à grand champ, $2^\circ \times 2^\circ$) muni d'un prisme objectif de 1.5° d'angle qui permet d'obtenir sur l'image les spectres des objets plutôt que les images des sources, qu'elles soient ponctuelles ou diffuses. La figure 6 montre un morceau de la plaque 0125. Les spectres sont les trainées verticales et le rouge (700 nm) est en haut. Lorsqu'un astéroïde est présent dans l'image, il se remarque par son déplacement par rapport aux étoiles du fond du ciel s'il a une vitesse propre importante. Il se confond aux étoiles du champ stellaire dans les autres cas et il faut donc comparer notre champ à un catalogue de sources, par exemple l'USNO (US Naval Observatory Catalogue), ou bien à d'autres images du ciel, par exemple le SkyView de la Nasa. La figure 6 montre un exemple d'utilisation d'EXATODS et des outils de l'Observatoire Virtuel que j'ai utilisés pour cette étude.

La recherche d'astéroïdes avec EXATODS consiste donc à analyser les 1700 plaques disponibles du DFBS pour y identifier les astéroïdes connus, pour éventuellement y détecter les astéroïdes inconnus et pour analyser les spectres de ces astéroïdes. La description de ce "workflow ", ou suite de tâches faisant appel à des bases de données dy-

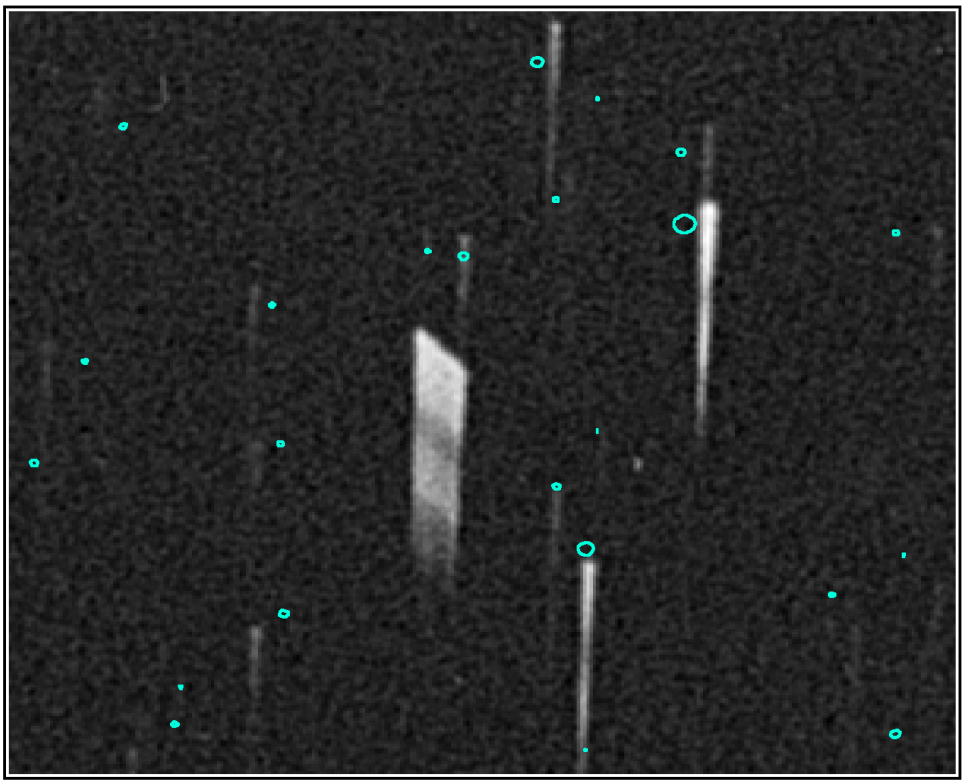

Figure 6: Outils utilisés pour la recherche d'astéroïdes projetés sur une partie de la plaque 0125 du DFBS. Les spectres des sources lumineuses s'étendent du haut (670 nm) vers le bas (340 nm), avec un creux de sensibilité vers 530 nm. Les cercles en vert montrent les étoiles du champ dans le catalogue SkyView. L'astéroïde Arethusa repéré à l'aide de Skybot a laissé sa trace qui est différente de celles des étoiles voisines par son déplacement.

namiques et éventuellement interactives est présentée en Annexe B. L'expression "fouille massive" prend ici tout son sens puisque chercher 400 000 objets dans $17000^{\circ 2}$ du ciel relève effectivement d'une analyse massive et par conséquent longue (un mois complet) et délicate puisque les interruptions du réseau par exemple sont importantes à gérer. Une première analyse a pu détecter plus de 200 astéroïdes connus qu'il faut maintenant cataloguer et analyser, cette étude est en cours. Etant donnée la complexité de recherche, sans l'Observatoire Virtuel il aurait fallu faire tout le travail manuellement, ce qui aurait nécessité un temps considérable, et donc une étude non réalisable rapidement.

B. Projets

I. Introduction

Je compte poursuivre mes activités scientifiques dans les équipes IMPEC (Instrumentation et Modélisations en Planétologie, Exobiologie et Comètes) et SHTI (Stratosphere, Haute Troposphere, Interfaces) au LATMOS et dans le cadre du Pôle Système Solaire de l'IPSL. Mes activités restent orientées principalement vers:

- la compréhension du rôle de la vapeur d'eau dans les atmosphères de la Terre et des autres planètes,

- l'étude de la place du carbone dans notre système solaire et dans les autres systèmes stellaires, dans les astéroïdes et des étoiles carbonées,

- la finalisation à court terme de l'Observatoire Virtuel en Planétologie avec mes collègues européens et internationaux (Europlanet, IPDA, IVOA), qui sera suivi par son exploitation, et

- la mise en place de l'Observatoire Virtuel pour les relations Soleil - Climat avec le nouveau SOERE (Service d'Observation de l'INSU section OA) VO-SCAT (Observatoire Virtuel Soleil-Climat-Atmosphère de la Terre) proposé à l'INSU en collaboration avec de nombreux laboratoires français et internationaux (http://bdap.ipsl.fr/VOSCAT/).

Les deux premiers thèmes sont exploratoires avec des résultats attendus très dépendants de l'effort qu'il faudra produire pour arriver à nos fins, les deux derniers se profilent dans des projets soutenus et donneront des résultats y compris en dehors de notre participation, ce qui est bien l'objectif et le fondement de l'Observatoire Virtuel: mettre en place un service pour la communauté.

II. La vapeur d'eau dans l'atmosphère de la Terre.

Dans le contexte actuel du changement climatique, le cycle de l'eau du bassin Méditerranéen est au coeur des questions scientifiques, économiques et environnementales pour toute une

région du globe incluant l'Europe du sud, l'Afrique du nord et le Moyen-Orient. Le projet HyMeX (HYdrological cycle in the Mediterranean Experiment) en cours d'élaboration a pour objectifs d'améliorer la caractérisation et la compréhension du cycle de l'eau sur le bassin Méditerranéen, en considérant les différents compartiments (océan, atmosphère, surface et hydrosystèmes continentaux, biogéochimie) et leurs couplages aux différentes échelles de temps. Le bilan hydrologique du bassin versant est étudié à la fois sous l'angle des événements intenses et de celui de la régionalisation climatique, incluant leurs impacts sur les écosystèmes marins et terrestres.

La région méditerranéenne est amenée à être soumise à un fort stress environnemental. L'amélioration des prévisions climatiques, l'identification des zones à risques, la mise en place d'alertes plus précises dans la gestion des risques, ou encore le développement d'expertise et de systèmes intégrés de gestion de l'environnement dans les domaines de l'aménagement du territoire et du développement durable, font partie des enjeux scientifiques importants pour cette région.

Progresser dans la compréhension du cycle de l'eau en Méditerranée est par conséquent essentiel pour répondre à ces attentes. Dans ce cadre, nos recherches en cours sur le bassin hydrologique autour de la Syrie avec Sulaf Alkasm, étudiante en thèse à l'UVSQ sous ma direction avec une bourse du gouvernement syrien montrent une variation saisonnière proche des prédictions des modèles pour cette région. La possibilité d'extraire les observations satellitales pour cette région permet une étude détaillée qui n'aurait pas été possible depuis la Syrie car ce pays ne développe pas d'instrument pour ce type de recherche. Les archives GOME et SCHIAMACHI sont ainsi exploitées massivement pour l'extraction régionale et spectrale de l'information.

Mon programme de recherche consistera à poursuivre l'étude des propriétés optiques et de la formation des particules contenant de l'eau sous forme gazeuse, liquide ou solide dans les atmosphères des planètes du système solaire (y compris notre Terre). Ce programme commencé par l'étude de la vapeur d'eau atmosphérique terrestre à partir de la banque de données Elodie de l'OHP sera étendu aux planètes du système solaire et aux exoplanètes dans l'infrarouge thermique et dans le visible. Cest un projet fédérateur Astronomie - Géophysique qui indique bien mon appartenance aux deux domaines. J'ai déjà mis en évidence la variabilité annuelle de la vapeur d'eau atmosphérique et il reste dans les données le potentiel pour affiner la mesure de H_2O et en extraire ainsi la température de l'atmosphère basse (1000 m à 3000 m) avec le décalage spectral des raies d'absorption du à l'effet de la réfraction.

Nous allons également étendre l'exploitation de ces spectres à la recherche du HDO, NO_3 et du NO_2 de nuit, permettant ainsi l'accès aux isotopes de l'hydrogène et aux composés azotés de l'atmosphère. Ce travail me permettra également de développer l'outil EXATODS (voir l'Annexe B) orienté vers la fouille massive d'archives spectroscopiques, ici les bases de données Elodie puis Sophie de l'OHP.

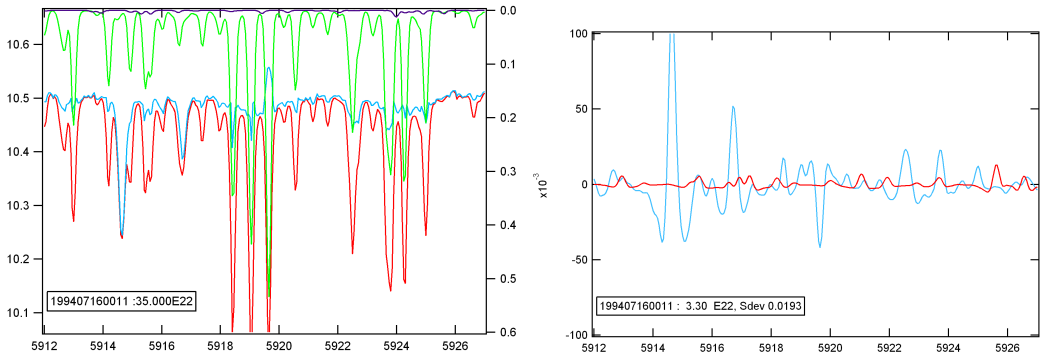

Figure 7: Recherche du HDO dans les spectres de SOPHIE autour de 592 nm (échelles du bas, la longueur d'onde, échelles de gauche et de droite, épaisseurs optique). Figure de gauche, soustraction de la vapeur d'eau, en rouge le spectre initial, en vert échelle de droite, la section efficace de $H2O$, en bleu, le spectre corrigé de la vapeur d'eau. Figure de droite, le résidu en rouge est comparé à la section efficace de HDO en différentiel. La corrélation est trop faible pour indiquer la présence d'HDO, de toute façon d'une quantité 20 fois supérieure ici à ce qu'on devrait théoriquement voir.

La recherche du HDO dans les spectres d'Elodie et de Sophie a des implications importantes car le rapport $H2O/HDO$ donne des informations pour étudier le cycle de l'eau car les propriétés physiques de ces deux molécules sont différentes (évaporation, sublimation, condensation, etc...). Ce rapport, déjà mesuré par des instruments depuis l'espace à faible résolution spatiale, doit être confirmé par des observations depuis le sol dans des conditions multiples (couverture nuageuse, température de l'atmosphère, etc...).

De plus, la possibilité d'avoir des séries temporelles longues et passées permettrait d'étudier l'évolution de ce rapport dans le temps, en liaison avec les effets climatiques récents dus au réchauffement climatique. La figure 7 montre une première tentative de mesure du HDO atmosphérique dans le visible depuis le sol avec Sophie sur le télescope de 193 cm l'OHP. Les interférences avec la vapeur d'eau (figure de gauche) complique la détection du HDO mais la méthode reste exploitable et nécessiterait plus d'investissement en temps ou un soutien supplémentaire. La méthode de mesure, basée sur une combinaison de mesure optique différentielle et de mesure absolue est originale et pas encore validée. Dans la figure de droite, la mesure en bleu devrait être corrélée avec la section efficace du HDO en rouge, ce qui n'est pas le cas et des efforts sont encore nécessaire pour rendre la mesure réalisable. Il faut cependant ajouter qu'une fois la méthode mise au point, l'exploitation des données en utilisant les outils de l'Observatoire Virtuel permettra une analyse massive des séries de spectres à haute résolution disponibles dans la communauté, ce qui donne à cette étude des perspectives intéressantes pour le futur.

III. Le carbone dans les astéroïdes et dans les étoiles carbonées.

La présence de carbone dans des objets tels que les astéroïdes indique une composition chimique proche de celle du Soleil, excepté pour l'hydrogène, l'hélium et d'autres gaz volatils. Ce type d'astéroïde représente environ les trois quarts de la population totale et ils sont supposés être des objets primitifs formés lors de la formation du Système Solaire. Si on veut comprendre les différents stades de l'évolution de notre Système Solaire, il faut étudier tous les objets représentatifs des étapes successives de cette évolution, et ces astéroïdes en sont une partie non négligeable puisque présents dans plusieurs parties du Système Solaire, du plus proche au plus lointain. Si, de plus nous avons des informations espacées dans le temps, nous avons accès à des informations sur leur variabilité qui peut avoir des sources et des apparences différentes, rotation et variabilité cyclique, érosion dynamique et modification irréversible, etc...

Nous avons vu dans le chapitre précédent que la fouille massive d'archives spectroscopiques est un processus long car les traitements d'images nécessitent des machines puissantes et du temps d'exploitation non négligeable (un mois pour chercher les astéroïdes dans tout le DFBS). Pour poursuivre l'étude des propriétés spectrales des astéroïdes du DFBS, mon programme EXATOD a été étendu pour permettre l'extraction et l'analyse des spectres dans un premier temps, et pour permettre la calibration spectrale (longueur d'onde et photométrique) dans un deuxième temps. A noter que EXATODS permet de mettre en évidence à faible résolution les bandes d'absorption du carbone ou du silicate dans ces spectres ce qui représente un apport considérable par rapport aux méthodes photométriques utilisées jusqu'à présent pour les études massives. Ici, le résultat final (mise en évidence de la classification spectrale et recherche de variabilité éventuelle) n'est pas encore obtenu et l'effort à apporter reste raisonnable pour un apport scientifique important puisque concernant des objets qui peuvent être des géocroiseurs ou qui ont des propriétés spectrales pas toujours bien exploitées. De plus, l'option de détection de nouveaux objets (ou anciens et disparus) n'a pas été encore exploitée à ce stade et c'est une direction que je compte étudier plus en détail.

La présence de carbone dans des objets tels que les étoiles froides carbonées indique soit une étoile en fin dévolution, soit une étoile ayant connu un évènement cataclismique. Ce type d'étoile est rare et très mal connu. Pour comprendre les différents stades de l'évolution stellaire, l'étude d'objets qui sortent du parcours majoritaire permet d'identifier les sources d'inhomogénéité dans ces formations.

L'exploitation d'EXATODS pour l'extraction des étoiles froides carbonées (leurs propriétés spectrales sont identifiables avec un faible taux d'échec) m'a permis d'améliorer EXATODS et il est prévu d'améliorer encore plus cet outil en y ajoutant des fonctionalitées, voir l'Annexe B. L'importance de découvrir des étoiles de type carbonées est ici primordiale car nous ne connaissons que très peu d'exemples de ce type, et tant leur étude statistique que leurs études physique et dynamique (cause de variabilité lumineuse, répartition dans la galaxie, etc...) est une information riche en conséquences sur les for-

mations des galaxies, les formations et les évolutions stellaires. Mon investissement sur ce thème, bien que réduit à la fourniture de l'outil de découverte pourrait ainsi apporter des résultats importants.

IV. L'Observatoire Virtuel en Planétologie.

Je vais montrer ici comment je vais poursuivre mes activités dans le cadre de ma participation à la mise en place de l'Observatoire Virtuel en Planétologie.

La mise en place de l'Observatoire Virtuel en Planétologie n'est pas à ce jour considérée comme une activité scientifique dans notre communauté, alors que les astronomes et les astrophysiciens l'ont fait depuis quelques années déjà lorsqu'ils ont fondé en 2001 l'Observatoire Virtuel Astronomique. Mon objectif sera ici de poursuivre le développement de cette activité dans notre communauté et de montrer qu'il est primordial de le mettre en place pour une exploitation optimale de nos données existantes avant que celles-ci ne disparaissent, et pour la préparation de nos futures bases.

Je compte poursuivre cette activité à travers trois champs d'application que je vais décrire ici.

Le premier consiste à participer à la rédaction des standards et protocoles que nous allons exploiter par la suite. Cette étape, longue et délicate car ce sont des activitées affectés à des groupes de travail plutôt qu'à des individus, car la plupart des domaines de la planétologie doivent être représentés. Un exemple concret, je suis membre du groupe de travail technique de l'IPDA qui évalue les protocoles proposés par des groupes (dont je fais aussi éventuellement partie) et nous mettons en place la distribution et la procédure d'évaluation de ces nouveaux protocoles (ou d'une version plus récente). J'ai également validé (donc testé par des applications concrètes) par exemple le PDS4 qui contient les bases du modèle de données pour la planétologie et qui est simultanément testé également par des équipes japonaises et indiennes. Le résultat attendu d'une telle activité consistera à fournir à la communauté les documents qui lui permettront de faire partie de l'Observatoire Virtuel.

Le second champ d'application est d'ordre organisationnel puisqu'il m'a été proposé par le président actuel de devenir en 2011 le vice président (vice-chair) de l'IPDA (qui je le rappelle représente toutes les agences spatiales des pays impliqués dans la recherche spatiale) pour devenir en 2013 le président (chairman) comme pour les précédentes nominations. Cette mission, que j'ai acceptée (validée par le CNES, le CNAP et l'INSU), est une mission à l'échelle internationale et consolidera la place de la France dans cette activité. Les objectifs à atteindre seront d'élargir la participation d'un plus grand nombre de

pays, notamment les ex-pays de l'est encore peu impliqués et les pays d'Europe du Nord, d'encourager les initiatives de développement de nouveaux outils ou d'adaptation d'outils existants, et de finaliser les deux actions prioritaires que sont la définition des protocoles pour les modèles de donnée et du dictionnaire, en supposant que le protocole d'accès et le registre seront finalisés avant 2013 et que l'Observatoire Virtuel en Planétologie pourra commencer à fonctionner dès 2011.

Le troisième champ d'application est l'utilisation des protocoles et standards que je viens de décrire puisqu'il concerne les outils que je compte développer dans ce cadre. Il existe plusieurs type d'outils que la planétologie peut élargir en partant du VO astronomique: les outils de recherche, de visualisation et d'analyse de données tels que Simbad, Vizier et Aladin (au Centre de Données de Strasbourg), mais également les outils multidisciplinaires que la planétologie doit produire elle même, en s'inspirant bien entendu des "Workflow" tels que celui décrit dans ce manuscrit, Tellodie. Le type d'outil auquel je pense devrait permettre de corréler des phénomènes observés dans l'atmosphère de Mars par exemple, avec le vent solaire. dans cet exemple, l'approche multidisciplinaire est essentielle mais inexistante à l'heure actuelle, sauf au cas par cas, d'un évènement majeur connu et observé par plusieurs communautés simultanément. Or, dans les archives existantes en planétologie de nombreux cas peuvent être détectés et l'Observatoire Virtuel doit être le support de telles études.

Les résultats attendus sont bien sûr scientifiques et exploratoire, dépendant surtout de la communauté qui désire s'impliquer. L'exemple de l'Observatoire Virtuel Astronomique, avec quelques dizaines de publications sur la découverte dans les archives de galaxies particulières ou de radio émissions corrélées avec des sources optiques sont maintenant données régulièrement comme références à l'intérêt de l'Observatoire Virtuel.

Il devient donc urgent de proposer des solutions identiques dans les domaines voisins à la planétologie, ce que je vais proposer dans la partie qui suit.

V. L'Observatoire Virtuel pour les relations Soleil-Terre.

Je vais montrer ici comment je vais poursuivre mes activités de Service dans le cadre de la mise en place de l'Observatoire Virtuel VO-SCAT en montant des collaborations nationales et internationales reconnues.

Je suis en train d'utiliser mes connaissances dans le domaine de l'Observatoire Virtuel pour développer l'Observatoire Virtuel des Relations Soleil-Climat-Atmosphère de la Terre pour répondre à une demande nationale et internationale de coordination de nos efforts. Ce travail a déjà commencé grâce au projet VOSCAT dont je suis l'un des initiateurs

avec mes collègues (http://bdap.ipsl.fr/VOSCAT) et qui regroupe maintenant plus d'une vingtaine de collaborateurs en France et dans le Monde. L'objectif est de mettre à disposition des chercheurs au moins, et éventuellement à un plus large public les données observationnelles et les sorties de modèles climatiques pour permettre une meilleure interprétation des phénomènes que nous observons actuellement, ou qui ont été observés par le passé. L'investissement ici en temps et en moyens demande bien sûr des efforts de la part de la communauté.

Au moment ou l'ensemble de la planète s'interroge sur les conséquences de l'augmentation des gaz à effet de serre sur le climat, il devient de plus en plus nécessaire de distinguer les modifications d'origine anthropique de la variabilité naturelle de l'atmosphère et de l'océan. La qualité des prévisions de l'évolution future du climat en dépend. Parmi les causes naturelles qui peuvent avoir un effet sur le climat, la variabilité solaire est probablement une des plus importantes.

L'influence du soleil sur l'atmosphère et le climat peut se manifester de différentes manières:

- La variation de l'irradiance solaire totale (constante solaire) modifie la quantité d'énergie absorbée par l'atmosphère et la surface terrestres et peut influencer la température moyenne au sol. La variation de la constante solaire est limitée à 0.1% sur un cycle solaire de 11 ans et donc l'effet attendu sur le climat est probablement faible. Il existe par contre de grosses incertitudes sur la variation de la constante solaire sur de plus grandes périodes et sur la plus grande variabilité des maxima.

- La variabilité du flux solaire au cours d'un cycle de 11 ans se manifeste principalement dans le domaine ultraviolet (UV) du spectre et principalement aux longueurs d'ondes inférieures à 250 nm où elle peut dépasser 3%, et de 20% à 50% dans l'UV lointain. Cette partie du spectre n'atteint pas la surface parce qu'elle est complètement absorbée par l'ozone ou l'oxygène stratosphériques. Le rayonnement solaire UV joue par contre un rôle important dans la stratosphère où il modifie les champs de température, de pression et de vent et donc les conditions de propagation des ondes atmosphériques qui couplent les basses et les hautes couches de l'atmosphère.

- Les précipitations de particules solaires dans les régions polaires modifient la composition chimique de la stratosphère en produisant entre autres des oxydes d'azote qui détruisent partiellement la couche d'ozone et donc modifient son bilan radiatif.

- Les rayons cosmiques galactiques ionisent l'atmosphère et jouent ainsi un rôle dans le circuit électrique global. Ils peuvent favoriser la formation de noyaux de condensation et donc influer sur la formation et la durée de vie des nuages. Le flux de rayons cosmiques est modulé par le vent solaire qui varie avec l'activité solaire de 11 ans.

- L'activité géomagnétique, très liée à l'activité solaire, module le flux de particules

énergétiques entrant dans la haute atmosphère. L'interaction avec la plus basse atmosphère pourrait passer par différents processus faisant intervenir le rayonnement UV, la chimie atmosphérique et le circuit électrique atmosphérique.

Les mécanismes susceptibles d'intervenir dans les relations Soleil-climat sont donc complexes et pour avancer dans leur compréhension il est nécessaire d'une part de bien documenter les paramètres caractérisant l'activité solaire, d'en comprendre l'origine, et d'autre part de représenter correctement ces mécanismes dans les modèles de climat.

Le VO-SCAT a pour objectif scientifique l'étude des relations Soleil-chimie atmosphérique-climat. Pour cela il donnera accès à l'ensemble des indices solaires et géomagnétiques permettant de caractériser l'influence de la variabilité solaire et géomagnétique sur l'atmosphère et le climat. Cet accès peut se faire suivant les cas grâce à une base de données locale ou par des liens vers les centres d'archivage existants sur le principe d'interopérabilité des bases dans le cadre de l'Observatoire Virtuel. Il ne s'agit pas de remplacer ni de dupliquer les bases de données existantes mais de les exploiter et de les compléter avec des données pertinentes pour les objectifs du VO-SCAT . La mise en place d'une telle base de donnée thématiques (fondées sur des questions ou cas scientifiques) viennent ainsi compléter et valoriser les bases de données classiques organisées par expérience, au sol ou spatiales. Les données accessibles à travers ce service servent à alimenter les études sur les relations Soleil-atmosphère-climat à partir d'observations atmosphériques à partir du sol, en particulier celles du Service dObservation NDACC, à partir d'observation et d'intégration des contraintes paléoclimatiques en Amérique latine, dans l'Atlantique Nord et en Europe, de l'échelle millénaire jusqu'aux résolutions annuelle à pluri-annuelle, et depuis l'espace, des modèles de chimie-climat comme par exemple LMDZ-Reprobus.

VI. Conclusion

Ces études intègrent l'interopérabilité des bases de données, tant pour la planétologie que la géophysique, une spécificité dans laquelle je me suis engagé depuis 2002 et pour laquelle je considère avoir œuvré avec l'organisation de réunions VO-planéto au niveau européen, mes participations à l'IVOA, l'IPDA et à VO-France, mon engagement dans VO-Paris data Center et mes responsabilités dans Europlanet FP7. L'approche que nous avons développée dans le cadre d'IDIS FP6 et que nous appliquons maintenant dans d'autres études telles que FONDUE et le DFBS est originale puisqu'elle regroupe les données non pas par instrument ou par site, mais par problème scientifique à étudier à l'aide des outils interopérables que nous mettons à disposition. Je suis convaincu qu'une telle approche peut- être très fructueuse, tant pour l'étudiant qui cherche à comprendre le mode de construction d'une étude scientifique que pour le scientifique qui veut avoir

facilement à sa disposition les éléments et les outils pour effectuer sa recherche sur un sujet.

Mais bien sûr, ce n'est pas l'outil qui fait le travail scientifique tout seul, mais bien le chercheur. Les thèmes que j'ai choisis jusqu'à présent et pour la suite de mes activités reflètent bien mon intérêt vers les sciences de l'environnement, étendues à la planétologie et à la recherche de territoires ou espaces inconnus. Et comme je considère que c'est en connaissant le passé que l'on pourra bien préparer ou prévoir l'avenir (c'est aussi à cela que servent les modèles), mon intérêt vers la fouille d'archive est justifié par le fait qu'il existe beaucoup d'informations dans nos données et que nous devons les exploiter au maximum. De plus, la recherche de tendances dans des signatures atmosphériques justifie autant de nouvelles surveillances que l'exploitation d'anciennes observations, ce que je m'efforce de faire.

C'est dans cette optique que je suis co-responsable depuis son existence en Septembre 2010 du master 2 international "Arctic Studies" à l'Université Versaille - Saint-Quentin-en-Yvelines qui a accueilli 25 étudiants pour sa première année, dont une quinzaine d'étrangers. Cette responsabilité, vue comme un challenge au départ et que j'ai réussi à finaliser montre bien ma détermination à aboutir, même dans les cas les plus aléatoires.

VII. Annexe A: TELLODIE

Tellodie est un outil ou un service web qui permet l'analyse massive de grandes bases de données spectroscopiques telles que les Archives Elodie de l'OHP. Bien qu'utilisant en grande partie des éléments développés dans le cadre de l'Observatoire virtuel Astronomique l'association de ces briques, complété par des éléments propres à Tellodie. Appelé workflow en language de l'Observatoire Virtuel Astronomique, un tel outil met en série des briques individuelles existantes localement ou accessibles en ligne et en temps réel via le réseau. Un schéma de Tellodie est présenté dans la figure 8. En plus des briques locales, Tellodie fait appel à des briques extérieures telles que Aladin. Il apparait également que l'ajout de nouvelles briques ou la modification d'une brique existante est simplifié et ne modifie en rien la suite des taches de Tellodie.

Le programme local (colonne centrale), en fonction des paramètres demandés en local (colonne de gauche) va chercher en local (colonne de gauche) ou à l'extérieur (colonne de droite) les informations dont il a besoin pour répondre aux requêtes. Composé de plusieurs éléments que j'ai moi-même développés ou que j'ai trouvés dans l'Observatoire Virtuel Astronomique, Tellodie s'adapte aux autres bases de données du même genre (Sophie, Harps, etc...). La page web d'accueil de ce service est présenté en figure 9. Il faut remarquer que les recommandations de l'Observatoire Virtuel Astronomique sont suivies puisque les résultats de Tellodie peuvent être "moissonnés" à la main ou par une machine par des requêtes de type php telles que celle indiquée ci dessous:

"http://bdap.ipsl.fr/tellodie/results.php?function=results&output=votable
&startDate=yyyymmdd&endDate=yyyymmdd"

Le nombre de paramètres, ici réduit au minimum pour simplicité peut être étendu à une dizaine environ, avec des critères de minima, de conditions sur l'erreur ou de conditions plus techniques comme la température de l'instrument par exemple.

Tellodie se met à jour régulièrement en fonction i) de la disponibilité de nouveaux spectres sur Elodie et ii) de la mise à jour des sections efficaces de la vapeur d'eau dans le visible par requête automatique sur les bases de données correspondantes. Ainsi, une machine qui de manière automatique envoie des requêtes à Tellodie aura le jeu de données le plus récent, c'est la particularité de ce que peut faire l'Observatoire Virtuel.

Le travail sur Tellodie n'est pas encore terminé car de nombreuses sources de données s'ouvrent régulièrement chaque jour dans l'Observatoire Virtuel et sont donc des sources potentielles également pour Tellodie: c'est le principe de base de l'Observatoire Virtuel.

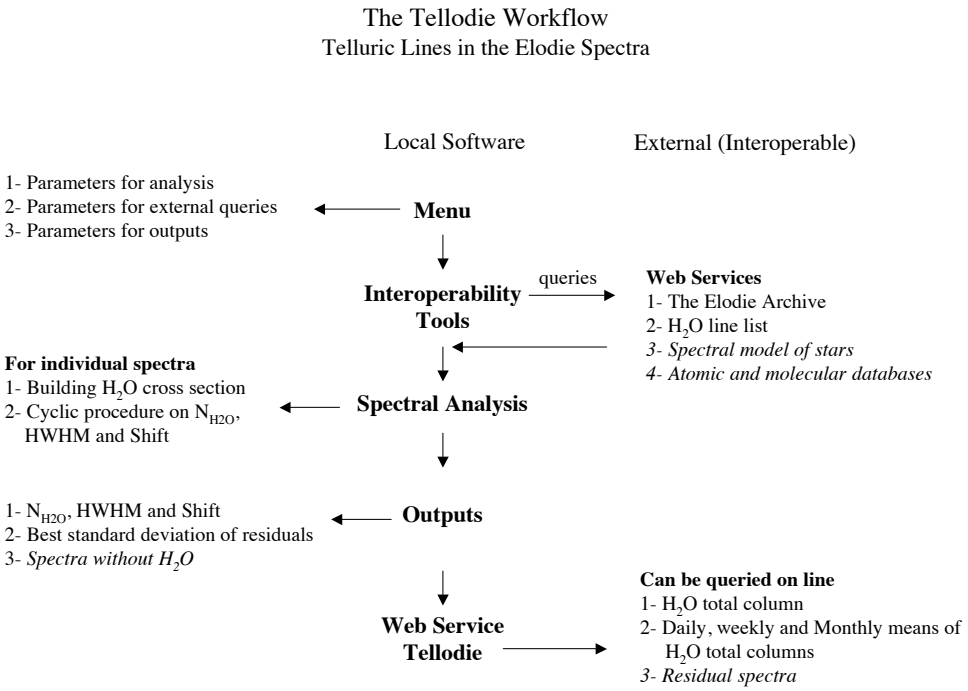

Figure 8: Diagramme du workflow pour la mesure de la vapeur d'eau atmosphérique dans les spectres d'Elodie. Les options en italique ne sont pas utilisées pour ce workflow mais pourraient l'être dans d'autres cas d'utilisation.

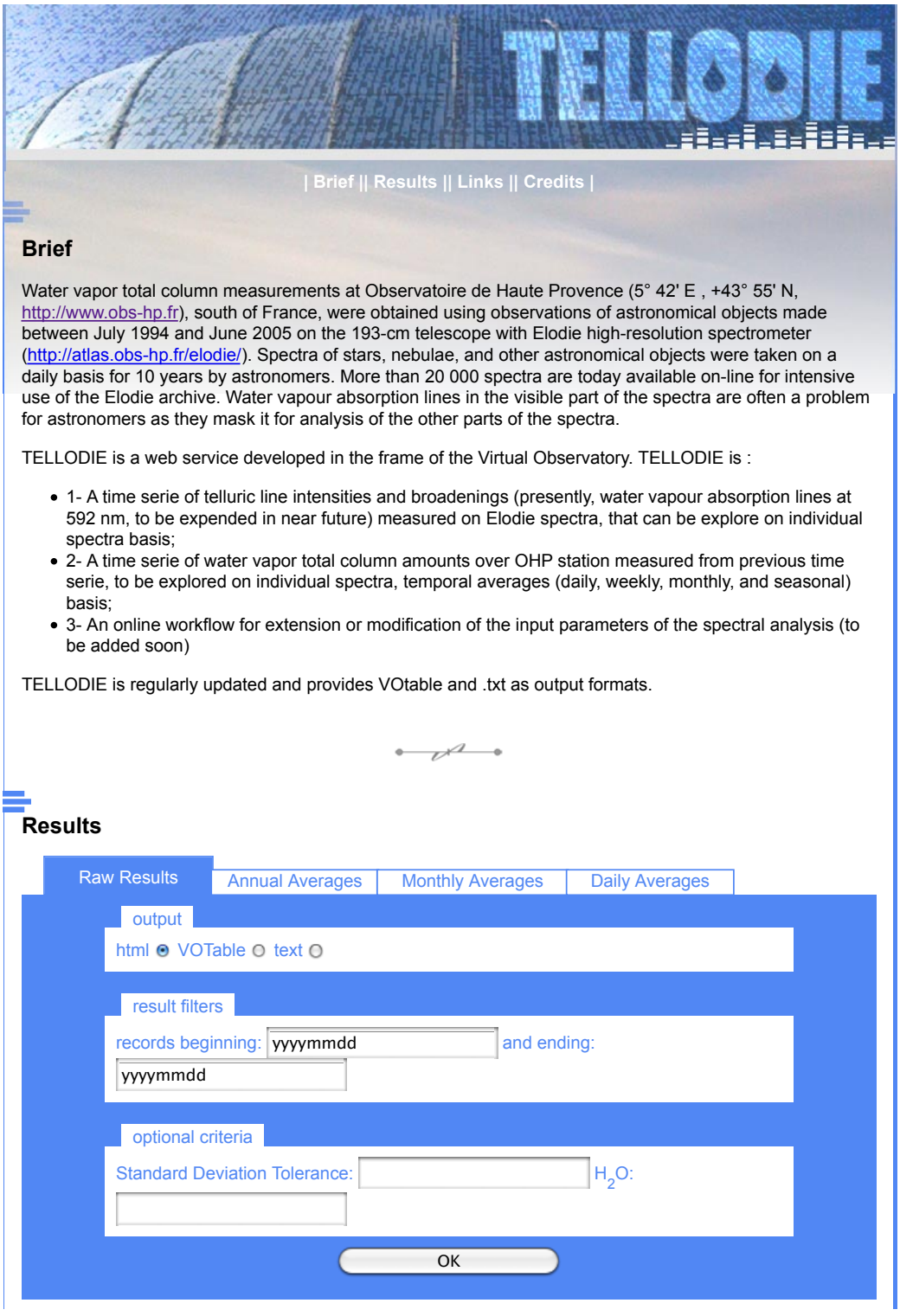

Figure 9: Page web du Service Tellodie.

VIII Annexe B: EXATODS

Exatods est un outil ou un service web qui permet l'analyse massive de grandes bases d'images astronomiques telles que le DFBS de l'Observatoire de Byurakan, les plaques digitalisées du SkyView de la NASA ou celles de l'ESO. Bien qu'utilisant en grande partie des éléments développés dans le cadre de l'Observatoire Virtuel Astronomique l'association de ces briques est complétée par des éléments propres à Exatods, notamment une brique d'analyse spectrale, une brique d'identification photométrique ou spectrale de l'indice de couleur des sources (étoiles, galaxies, nébuleuses, astéroïdes, etc...).

En fait, le principe d'EXATODS est assez simple: il faut lui donner en entrée un catatogue d'objets particuliers, par exemple un catalogue d'étoiles carbonées ainsi qu'un catalogue de clichés astronomiques dans lequel on désire effectuer la recherche, par exemple le Sky View de la NASA. L'outil EXATODS permettra en plus de fournir l'extraction des images Sky View dans lesquelles apparaissent les étoiles recherchées, mais également d'effectuer des analyses types photométrie, astrométrie etc... dans ces images. Des outils de "recherche de formes" pour des objets diffus et de recherche d'information spectroscopique via l'OV sont en cours d'implémentation.

Les utilisations d'EXATODS sont aujourd'hui principalement orientés vers la recherche d'astéroïdes et d'étoiles carbonées avec des résultats assez impressionnants puisqu'une vingtaine de nouvelles étoiles carbonées ont été découvertes et quelques 230 astéroïdes connus ont été retrouvés dans des clichés obtenus dans les années soixante. La figure 10 montre comment EXATODS est utilisé pour chercher des étoiles carbonées dans le DFBS [22,25]).

A noter également qu'EXATODS est la base, sous la forme présentée ci-dessus, d'un nouveau TD original mis en place pour l'Observatoire Virtuel présenté à l' International School for Young Astronomer (ISYA) en 2010.

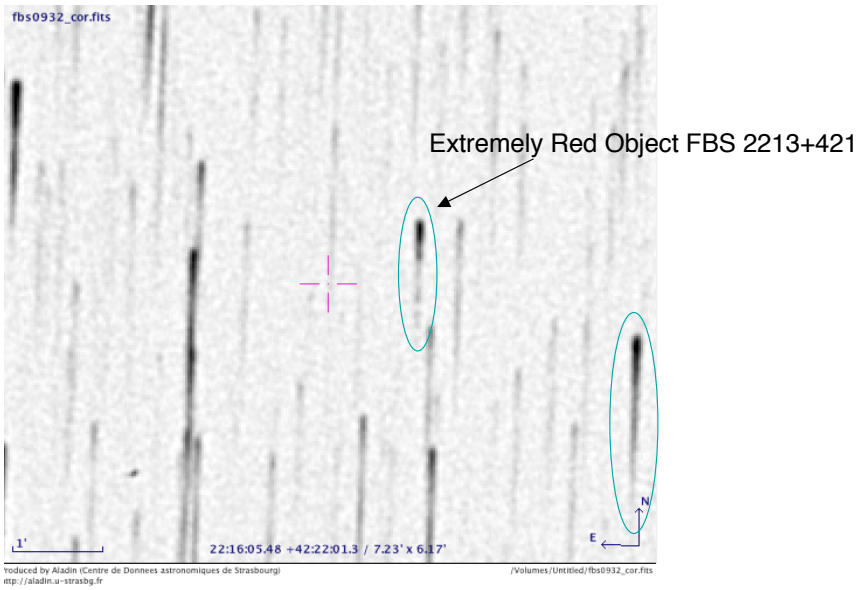

Aladin + DFBS + usno + Plastic = VO Workflow

Figure 10: EXATODS permet d'identifier des étoiles carbonées dans le DFBS grâce à ce workflow ou suite d'outils du VO dont il est composé.

Remerciements

Je tiens tout particulièrement à remercier mes rapporteurs, mes collègues de travail, le LATMOS, le LMD, le CNES, Europlanet FP6 et Europlanet RI FP7, l'IPSL, l'UVSQ, l'OVSQ, l'UPMC, l'INSU, VO-France, VO-Paris, et bien d'autres encore.

Pergamon

0022-4073(95)00085-2

J. Quant. Spectrosc. Radiat. Transfer Vol. 54, No. 3, pp. 471–480, 1995

0022-4073/95 $9.50 + 0.00

OZONE MEASUREMENTS BY ZENITH-SKY SPECTROMETERS: AN EVALUATION OF ERRORS IN AIR-MASS FACTORS CALCULATED BY RADIATIVE TRANSFER MODELS

A. SARKISSIAN,†‡ H. K. ROSCOE,‡ and D. J. FISH§

‡British Antarctic Survey, NERC, Madingley Road, Cambridge CB3 0ET, and §CCAS, Department of Chemistry, Lensfield Road, Cambridge CB2 1EP, U.K.

(Received 12 October 1994)

Abstract—Calculations of air-mass factors (AMFs) for ground-based zenith-sky UV-visible spectrometers are presented and discussed. Causes and size of errors in AMFs of ozone in the visible are evaluated. Errors can be caused by approximations in the calculation (intensity-weight approximation, ignoring the finite field of view of the instrument); by approximation in the scheme of the calculation (single scattering, ignoring refraction); or by variable geophysical parameters (vertical profile of constituents). These relative errors in AMF cause identical relative errors in vertical columns of ozone deduced from measurements by zenith-sky spectrometers. The mean of the relative errors of ozone AMFs due to using one set of AMFs for all seasons and locations is ±2.4% when averaged over the commonly used range of solar zenith angles.

1. INTRODUCTION

Zenith-sky UV-visible ground-based spectrometers have been used to measure stratospheric constituents important in ozone depletion since 1973 (e.g., Noxon et al[1]) and more recently by SAOZ instruments (Système d'Analyse par Observations Zénithales: Pommereau and Goutail[2]. From these instruments, the number of molecules in a vertical column per unit cross-sectional area (Y_{ver}) of an absorber Y is deduced by dividing the number of molecules per unit cross-sectional are in the line-of-sight of the observation (Y_{loss}) by an air-mass factor (AMF) calculated by a radiative transfer model. Hence by definition

$$\mathrm{AMF}_Y = \frac{Y^{\mathrm{los}}}{Y_{\mathrm{ver}}} \tag{1}$$

Y_{los} is measured by fitting laboratory cross-sections to the observed optical depth. Optical depth is determined from the ratio of the measured spectrum to a reference spectrum. Hence the measured amount (Y_{mes}) is the difference between amounts in the line-of-sight and in the reference spectrum (Y_{ref}):

$$Y_{\mathrm{mes}} = Y_{\mathrm{los}} - Y_{\mathrm{ref}}$$

and vertical amount is deduced from the measurement by:

$$Y_{\mathrm{ver}} = \frac{Y_{\mathrm{mes}} + Y_{\mathrm{ref}}}{\mathrm{A,F}_Y} \tag{2}$$

Errors can be calculated using the standard formula for independent errors (e.g. Topping[3]):

$$(\delta Y_{\mathrm{ver}})^2 = \left(\frac{\partial Y_{\mathrm{ver}}}{\partial Y_{\mathrm{mes}}}\delta Y_{\mathrm{mes}}\right)^2 + \left(\frac{\partial Y_{\mathrm{ver}}}{\partial Y_{\mathrm{ref}}}\delta Y_{\mathrm{ref}}\right)^2 + \left(\frac{\partial Y_{\mathrm{ver}}}{\partial \mathrm{AMF}_Y}\delta \mathrm{AMF}_Y\right)^2$$

†To whom all correspondence should be addressed.

Evaluating the differentials gives

$$(\delta Y_{ver})^2 = \left(\frac{1}{AMF_Y}\delta Y_{mes}\right)^2 + \left(\frac{1}{AMF_Y}\delta Y_{ref}\right)^2 + \left(Y_{ver}\frac{\delta AMF_Y}{AMF_Y}\right)^2 \quad (3)$$

δY_{mes} depends on the details of the instrument (resolution, sampling, aperture, sensitivity), on the illumination of the sky, and of the spectral fitting scheme (wavelength interval, interpolation error, accuracy of wavelengths, accuracy of laboratory cross-sections). The first term on right-hand side of Eq. (3) is minimised approaching twilight, where it is approximately $(4\,DU)^2$ (Dobson Unit) for SAOZ (Sarkissian[4]). The second term of the right-hand side of the equation depends on δY_{ref}, which is constant, so that it is also minimised after twilight where AMF_Y is maximum. For SAOZ, the second term is approximately $(0.2DU)^2$ at twilight (Jones et al[5]). Note that Y_{ref} is commonly calculated from Langley–Bouger plots so that systematic and pseudo-random errors in Y_{ref} depend on the errors in AMF_Y, pseudo-random errors being those which are uncorrelated from spectrum to spectrum or day to day. The third term on the right-hand side of the equation depends on the relative error of the AMF. Hence when errors in AMF are significantly greater than 1%, the relative error in Y_{ver} equals the relative error in AMF.

The sensitivity of AMFs of ozone to the computational scheme and model has recently been studied by Sarkissian et al,[6] who compared AMFs calculated by different radiative transfer models with the same specified vertical profiles. The sources of differences between results came from differences in computational parameters such as optical and geometrical path calculations, and from the use by some workers of the intensity-weighted approximation. Variations in model scheme (Monte-Carlo or standard) or complexity (e.g., introduction of multiple scattering) introduced smaller differences. The sensitivity of AMFs of ozone or NO_2 to atmospheric parameters had already been studied in some specific cases: Perliski,[7] Dahlback et al[8] and Lenoble and Chen[9] introduced polar stratospheric clouds and volcanic aerosol in their computations, which include multiple scattering; Sarkissian[4] and Friedler et al[10] made a similar study using a single-scattering model; Sarkissian[4] studied the effect of vertical profiles of air density, temperature and ozone; Van Roozendael et al[11] studied the perturbations due to surface pollution in the presence of thick tropospheric clouds.

The goal of this paper is to discuss the relative accuracy of ozone AMFs in the visible. A complete validation of AMF calculations can be made only by comparison with observations, which is beyond the scope of this paper. Here, calculations are made at 510 nm by a single-scattering radiative transfer model. The sensitivity of the AMF is studied by making changes in computational parameters and schemes. The effect of each change is calculated on its own. If the effects of the changes are independent, then the total error in AMF is the root-sum-square of all the individual changes in AMF.

2. FORMULATION OF AMF

Beer-Lambert's law gives the relation between measurements and Y_{los} for observations of atmospheric absorbers

$$I = I^* \exp(-\sigma_Y Y_{los}) \quad (4)$$

where I is the flux (W m^{-2}) received by the instrument at a given wavelength and solar zenith angle (SZA) with Y in the atmosphere, I^* is the flux received without Y in the atmosphere, and σ_Y is the absorption cross-section of Y. From Eq. (1), the AMF of the observation is then

$$AMF_Y = \frac{1}{Y_{ver}\sigma_Y}\left[-\ln\left(\frac{I}{I^*}\right)\right] \quad (5)$$

The calculation of AMF in the case of direct solar, lunar or stellar observations is simple: it is a ratio of geometrical path lengths because there is only one path. By contrast, in the case of zenith sky observation, the calculation of AMF needs models to integrate the light scattered by different air parcels seen by the instrument. These models must simulate radiative transfer of the sunlight in the atmosphere to calculate I and I^*, which involves running the model twice. Many earlier calculations used the intensity-weighted approximation (see Appendix 1), which only needs one model run. This approximation only agrees with the more exact Eq. (5) in the limit of weak

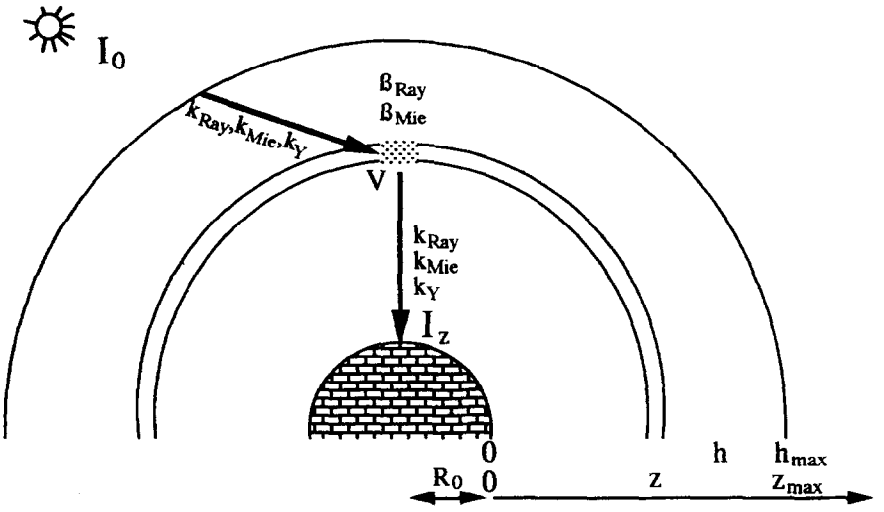

Fig. 1. AMF for zenith-sky ground-based observations are calculated by models which simulate the radiative transfer of sunlight as it traverses the atmosphere of the Earth and is scattered vertically downward into the field-of-view of the spectrometer.

absorption and give rise to a significant error in ozone AMF at SZA greater than 90° (typically 3% at 92°).

3. MODELS OF GROUND-BASED ZENITH-SKY OBSERVATIONS

Figure 1 shows sunlight as it traverses the atmosphere from its top (z_{max}) to the air volume V located at altitude z km. The radiation is scattered in this volume. This scattering is Rayleigh scattering by molecules $\beta_{Ray}(V)$ and Mie scattering by particles $\beta_{Mie}(V)$. Light is scattered in all directions, including toward the ground. On its path from outside the atmosphere to the ground, the radiation is attenuated by molecular scattering $k_{Ray}(h)$ and particulate scattering $k_{Mie}(h)$, and is absorbed by molecules $k_Y(h)$. β are the scattering coefficients, k the extinction or absorption coefficients, and h is the height of the current position along the path from the top of the atmosphere to V. Models must integrate this radiation reaching the instrument by varying the location of V in the field of view of the instrument.

The flux I received by an instrument is then

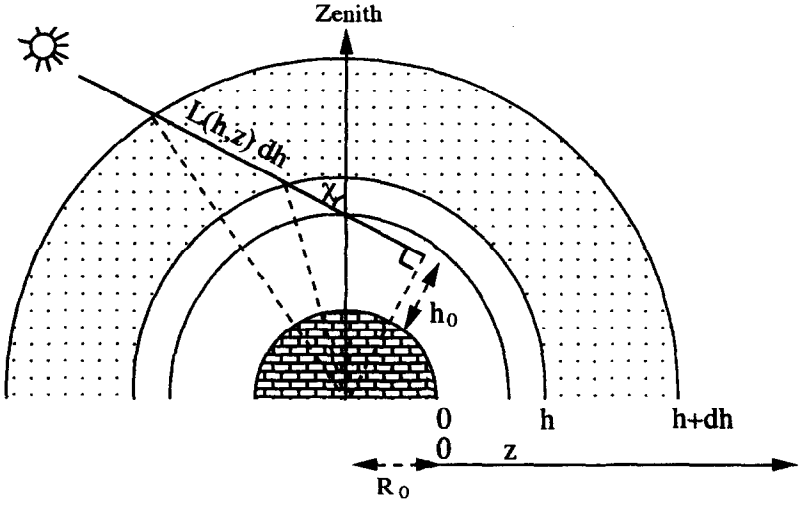

Fig. 2. In the common approximation whereby refraction is neglected, the geometric enhancement factor of the path in a spherical shell can be deduced from simple geometry. The formula, given in Eq. (11) is simple to derive once the tangent altitude h_0 is introduced.

$$I = \int dI_V \tag{6}$$

When treating single scattering only (see Appendix 2 for the treatment of double scattering), the individual contribution dI_V from volume element dV can be calculated from

$$\frac{dI_V}{I_0} = \frac{dV}{4\pi r(V)^2} \cos[\alpha(V)][\beta_{Ray}(V) + \beta_{Mie}(V)]\exp[-\tau(V)] \tag{7}$$

where I_0 is the solar flux outside the atmosphere, $r(V)$ is the distance between V and the instrument, (V) is the angle of incidence of the radiation at the instrument, and $\tau(V)$ is the optical thickness of the atmosphere traversed:

$$\tau(V) = \int_V^{top} \left[\sum_Y k_Y(h) + k_{Ray}(h) + k_{Mie}(h)\right] L(h, V)\, dh + \int_0^V \left[\sum_Y k_Y(h) + k_{Ray}(h) + k_{Mie}(h)\right] dh \tag{8}$$

where $Y = O_3, NO_2$, etc., $k(h) = \sigma n(h)$ except k_{Mie}, σ is the cross-section (cm^2), $n(h)$ is the density (molec cm^{-3}) at h, and $L(h, V)$ is the geometrical enhancement factor of the path when the ray is crossing dh. $L(h, V)$ must be calculated taking into account the refraction and the sphericity of the atmosphere.

When using the exact as opposed to intensity-weighted formulation of AMF, Eqs. (7) and (8) must be calculated for both I and I^*. Because the AMF depends on the ratio of I to I^* [Eq. (5)], all constants (e.g., I_0) cancel and can be removed from computations.

Most of the differences between models are caused by approximation in these formulae. A common approximation is to assume an infinitely narrow field of view and replace the integration in Eq. (6) by summation of contributions from homogeneous layers (e.g., Solomon et al[12]). Then dV depends on $r(V)^2$, and dI_V depends only on the altitude z, so that (6) and (7) give:

$$I = \text{Const} \sum_{z=0}^{top} \left[\beta_{Ray}(z) + \beta_{Mie}(z)\right] \exp\left[-\tau(z)\right] \Delta z \tag{9}$$

and (8) becomes

$$\tau(z) = \sum_{h=z}^{top} \left[\sum_Y k_Y(h) + k_{Ray}(h) + k_{Mie}(h)\right] L(h, z)\Delta h + \sum_{h=0}^{V} \left[\sum_Y k_Y(h) + k_{Ray}(h) + k_{Mie}(h)\right] \Delta h \tag{10}$$

Here, $L(h, V)$ becomes $L(h, z)$. In another common approximation, neglecting refraction, it is shown by Fig. 2 to be:

$$L(h, z)\Delta h = \sqrt{(h + \Delta h + R_0)^2 - (h_0 + R_0)^2} - \sqrt{(h + R_0)^2 - (h_0 + R_0)^2} \tag{11}$$

where R_0 is the radius of the Earth and h_0 the altitude of the tangent point:

$$h_0 = (z + R_0)\sin(\chi) - R_0$$

The default computation in this paper uses Eqs. (9) to (11) as approximations, with $\Delta h = \Delta z = 1$ km from the bottom of the atmosphere to 90 km altitude. Multiple scattering, ground albedo, Raman scattering, and refraction were excluded from this default because of their longer computation time, although the effects of adding each in turn were evaluated in Sec. 4.

In this default calculation, vertical profiles are the same as those used in the intercomparison of AMF calculations described by Sarkissan et al:[5] the air density is subarctic winter (*Handbook of Geophysics*[13]); the ozone profile is from the *Handbook of Geophysics*;[13] the background aerosol

Table 1—*Footnotes continued*

(r) Volcanic aerosol is taken from observations in winter 1991/92 in Northern polar regions by Pommereau and Piquard[23] after the eruption of Mt Pinatubo in June 1991: the optical thickness of the cloud is 0.05 at 550 nm, its geometrical thickness is 7 km, and the altitude of its base is 12 km.

(s) Calculations concerning changes of the vertical profile of the Mie scattering include double scattering, and values are given relative to the default computation but including double scattering. The phase function corresponds to a Henyey–Greenstein phase function with an asymmetry factor $g = 0.6715$.

Table 1. Relative percentage differences $\{100x[\mathrm{AMF}(x) - \mathrm{AMF(Default\ computation)}]/\mathrm{AMF(Default\ computation)}\}$ in ozone AMFs due to changing computational and geophysical parameters.

Change in parameter (footnote)	Change (%) in AMF at given SZA				
	86°	88°	90°	92°	94°
σ_{O3} + (-) 10% (a)	0.0	- (+) 0.1	- (+) 0.1	- (+) 0.3	- (+) 0.5
σ_{Ray} + (-) 1% (b)	0.0	- (+) 0.1	- (+) 0.1	- (+) 0.1	- (+) 0.2
Z_{max} = 80 km (c)	0.0	0.0	0.0	0.0	0.1
Z_{max} = 60 km (SAOZ)	0.0	0.1	0.1	0.4	2.8
Z_{max} = 50 km	0.1	0.2	0.5	1.4	10.4
Length of indiv. shell + (-) 1% (d)	+ (-) 0.9	+ (-) 0.9	+ (-) 0.9	+ (-) 0.8	+ (-) 0.7
Densities taken at shell base (e)	-0.3	-0.4	-0.4	-0.4	-0.4
Refraction (f)	0.0	0.1	0.2	0.4	3.0
Double scattering (g)	1.4	1.3	1.2	0.7	1.2
Adding ground albedo (0.5)	0.0	0.0	0.0	0.0	0.0
Adding Raman scattering (f)	0.9	0.9	0.7	0.6	0.2
Intensity-weighted approximation (h)	-0.3	-0.6	-1.2	-2.8	-5.1
Altitude of the instrument = 1 km (i)	0.6	0.7	0.8	0.8	0.8
Ozone hole 12-17 km (j)	-1.0	-1.8	-2.9	-0.1	9.1
Ozone hole 17-22 km	-4.0	-5.6	-8.7	-15.1	-10.8
Ozone layer - 3 km (k)	-3.2	-3.6	-4.6	-8.4	-13.4
Ozone layer + 3 km	0.8	0.3	0.0	2.2	8.4
Warm strat. (230 K at 10 mb) (l)	-0.4	-0.7	-1.2	-2.1	-2.5
Cold strat. (200 K at 10 mb)	0.2	0.3	0.6	1.5	3.2
No aerosol (m)	1.1	1.2	1.0	3.8	9.5
Cloud at ground level (n) (s)	-0.3	-0.2	-0.2	-0.2	0.0
Cirrus cloud at 8 km (o) (s)	-6.8	-4.5	-0.5	0.3	-0.4
Reduced stratospheric aerosol (p) (s)	0.6	0.7	1.0	3.3	6.3
Polar stratospheric cloud (q) (s)	-1.6	-2.6	-5.1	-12.3	-22.7
Volcanic aerosol (r) (s)	-9.6	-10.9	-13.0	-21.8	-41.5

(a) $\pm 10\%$ is the accuracy of σ_{03} (Johnston, private communication).
(b) $\pm 1\%$ is the accuracy of σ_{Ray} given by Bates[15] from which our formula and the formula by Nicolet[16] are derived (Farman, private communication).
(c) z_{max} is 50 km in Solomon et al,[12] 60 km in Sarkissian.[4]
(d) $\pm 1\%$ on $L(h, z)$ simulates systematic differences ($R_0 = 6378$ km at the equator and 6357 km at the pole) and systematic errors in computation (Sarkissian et al[6]).
(e) Some workers have taken values of densities in Eq. (9) at the bottom of the shells instead of at the middle (Sarkissian et al[6]).
(f) Raman scattering and refraction effects are calculated using the model of Fish.[17]
(g) Schemes of double scattering and of including albedo are similar to single scattering and contributions are added by numerical integration over all the spherical atmosphere (see Appendix 2). Sarkissian et al[6] showed that the standard scheme with only double scattering agrees well with a Monte-Carlo scheme with all orders of scattering (Lenoble and Chen[9]).
(h) see Appendix 1.
(i) z_{obs} is the altitude of the instrument.
(j) Altitudes of zero ozone in ozone holes are taken from Gardiner and Farman.[18]
(k) Changes in the altitude of the ozone layer are taken from observations over all latitudes and seasons (Komhyr et al[19]).
(l) Cold and warm stratospheric temperatures are taken at 60° N in January from *Handbook of Geophysics*.[13]
(m) A pure Rayleigh atmosphere assumes $\beta_{Mie}(z) = 0$ and $k_{Mie}(h) = 0$.
(n) The optical thickness of the cloud at ground level is 1.
(o) The optical thickness of the cirrus cloud is 0.1.
(p) A reduced stratospheric aerosol in the Antarctic vortex in winter (stratospheric cleaning) is taken from observations in spring by SAGE II (McCormick et al[20]).
(q) The optical thickness of the polar stratospheric clouds is 0.01 at 1 μm, its geometrical thickness is 7 km, and the altitude of its base is 14 km, as frequently observed in Northern and Southern polar regions (Sarkissian et al;[21] Sarkissian *et al*;[22] McCormick et al[20]).

(Footnotes continued on opposite page.)

Table 2. Relative percentage differences in ozone AMFs at 88° and 90° SZA due to changing seasons and locations. The fifth column is the mean value of the relative difference of 5 observations during twilight from 87° to 91° SZA, the range commonly averaged to give the daily vertical amount (Sarkissian[4]). Columns six and seven indicate respectively seasonal (for one location) and global means with their standard deviations. The last line is the relative differences from the SAOZ standard software AMFs (Sarkissian[4]).

Change from default computation		Change (%) in AMF at given SZA		Change (%) in AMF averaging from 87° to 91° SZA		
Location	Months	88°	90°		Annual	Global
15°N	DJF	-3.2	-4.7	-3.7	-2.9±0.9	
15°N	JJA	-1.7	-2.7	-2.0		
45°N	DJF	-1.1	-0.8	-0.9	-2.7±1.9	
45°N	MAM	-3.1	-3.4	-3.1		
45°N	JJA	-5.2	-6.4	-5.6		
45°N	SON	-1.5	-1.7	-1.3		
						-1.2±2.4
60°N	DJF	0.4	0.5	0.5	-1.7±2.1	
60°N	MAM	-1.1	-1.2	-1.2		
60°N	JJA	-4.6	-5.5	-5.1		
60°N	SON	-1.0	-0.8	-0.9		
60°S	DJF	1.6	1.7	1.7	1.6±0.2	
60°S	MAM	1.0	1.6	1.3		
60°S	JJA	1.2	2.1	1.7		
60°S	SON	1.3	1.6	1.6		
SAOZ		-0.7	-1.1	-1.0		

Profiles of temperature, and so air density, are taken at 15°, 45° and 60° N for July and January (*Handbook of Geophysics*[13]). Ozone vertical profiles are taken from ECC ozonesonde observations in 1985–1987 from Komhyr et al[19] for December–January–February (DJF), March–Airil–May (MAM), June–July–August (JJA) and September–October–November (SON) at Point Barrow, Alaska (71° N, 156° W) for the profile 60° N; at Boulder, Colorado (40° N, 105° W) for 45° N; at Hilo, Hawaii (19° N, 155° W) for 15° N; and at Syowa, Antartica (69° S, 39° E) for 60° S. To compute March–April–May and September–October–November AMFs, the winter vertical profiles of air densities are assumed.

extinction coefficient is from the *Handbook of Geophysics*[13] in the troposphere and from SAGE II observations in April 1988 at 65°N for the stratosphere. Background aerosol phase function corresponds to a Henyey–Greenstein phase function with an asymmetry factor $g = 0.6715$ (Lenoble, private communication). Individual shells are supposed homogeneous, and values of densities and Mie extinction are taken at the middle of the shell.

4. RESULTS OF AMF CALCULATIONS

AMFs for ozone were calculated with the default calculation and by changing each parameter and element of the scheme in turn. The default computation gives 12.071 at 88° SZA, and 16.778 at 90° SZA (respectively 11.99 and 16.59 for SAOZ standard software). Table 1 lists the relative differences from the default calculation, at several SZA. The chosen increment in each parameter and element of the scheme is representative of the typical error in the parameter or of the commonly used approximation in the scheme. The footnotes list the reasons for the chosen increments, and justify this assertion.

Ozone AMFs are calculated for different seasons and latitudes (profiles of air and ozone densities together) and results are presented in Table 2.

5. DISCUSSION

The results in Table 1 show that:

(a) Errors in ozone and Rayleigh-scattering cross-sections, have a small effect on the AMF computation and can be ignored at all SZA. The same is true of including ground albedo.

(b) Limiting the top of the model atmosphere to 50 km generates errors larger than 0.5% in ozone AMFs at SZA > 90°. To remove this source of error, the top of the atmosphere in models must be at least 80 km.
(c) Errors in the calculation of optical path in individual shells [Eq. (11)] significantly affect ozone AMFs: a systematic underestimation of the geometrical path by x% (1% in this case) decreases the AMF by approximately the same proportion x% at all SZA; taking values of densities at the bottom instead of at the middle of the shells affects ozone AMF by −0.4% at all SZA. As noted by Sarkissian et al,[6] differences between standard models (models similar to the present one) come mainly from the computation of Eq. (11), and differences are significant (spread of results of 2% at 86° SZA and 13% at 94°). A correct calculation must be used.
(d) The intensity-weighted approximation must be avoided.
(e) Background aerosol must be included in the model.
(f) Schemes include double scattering, Raman scattering, and refraction increase the time of computation (double scattering is 400 times longer than single scattering in our model). However, their effects cannot be neglected, but are small enough, that they can be numerically added to the single-scattering calculation, assuming their independence.
(g) Observations from high-altitude increase the ozone AMF and corrections must be made even for 1 km.
(h) Vertical profiles are important parameters in the calculation of AMFs (a well-known conclusion, e.g., Syed and Harrison[14]). Unfortunately, this source of error cannot be removed *a priori*.
(i) Aerosols are difficult to introduce correctly because of their large variation in optical thickness and scattering phase function in time and location. This source of error cannot be removed *a priori*. Note that our computations which explore sensitivity to aerosol include double scattering, although results with only single scattering are similar (largest effects agree within 4% at SZA ⩽ 92°).

The results in Table 2 show that ozone AMF varies with the location and the season, reflecting its dependence on vertical profiles of air and ozone densities. Note that the AMFs from SAOZ standard software (Sarkissian[4]) are close to our default computation.

6. CONCLUSION

Total errors in ozone AMFs at 510 nm increase notably at SZA > 91°, so that SZA ⩾ 92° should not be used for interpretation of ground-based zenith-sky observations of ozone in the visible. Note that this upper limit in SZA also applies to Langley plots for calculation of Y_{ref}. This result, together with the lower limit to SZA from the first term of Eq. (2) gives the interval of 87° to 91° SZA for accurate averaging of vertical columns to produce a daily value. This interval, commonly used in the community, allows measurements in polar regions up to latitude 67° 34′ in winter. Using this interval and supposing five observations during twilight (87°, 88°, 89°, 90° and 91° SZA), errors in vertical ozone due to potential computational errors are ±1.2% (Sarkissian et al[6]), and the sum of systematic errors due to neglecting multiple scattering, refraction, and Raman scattering is −2.2%.

In Table 2, the mean of the values at each angle averged over the range of angles is the equivalent error due to differences in vertical profiles, provided they are correlated at different SZA. Supposing that there are no computational errors, and no approximations, errors in AMFs come only from wrong assumptions about these vertical profiles. Supposing five observations during twilight, the mean of the differences from the default computation is represented in column 5 of Table 2, the annual mean for one location in column 6, and the global mean for all seasons and locations in column 7. The standard deviation (1σ) is also indicated. This would represent the error when using a mean profile for each location, instead of our default profile. Hence the mean error due to using one set of AMFs for all locations and seasons is ±2.4%. The mean error due to using one set of AMF for all seasons and only one location is reduced to ±0.9% at 20° N, ±1.9% at 45° N, 21.% at 60° N and ±0.2% at 60° S.

For events such as the ozone hole, polar stratospheric clouds or volcanic aerosols in the stratosphere, errors increase significantly and special calculations have to be made. Note that this

paper does not attempt to quantify absolute errors in AMFs. The only way to do this is to compare calculations with observations, beyond the scope of this work.

Acknowledgements—This work was supported by the STEP-0013 and SCUVS projects of the CEC. A. Sarkissian is a CEC Research Fellow. D.J. Fish is supported by NERC. We thank J. P. Pommereau for helpful discussions.

REFERENCES

1. J. F. Noxon, E. C. Whipple Jr, and R. S. Hyde, *J. Geophys Res.* **84,** 5047 (1979).
2. J. P. Pommereau and F. Goutail, *Geophys. Res. Lett.* **15,** 891 (1988).
3. J. Topping, *Errors of Observation and Their Treatment*, Chapman and Hall, London (1972).
4. A. Sarkissian, Thèse de Doctorat de l'Université Paris 6, Paris (1992).
5. A. Jones, H. K. Roscoe, A. Sarkissian, J. D. Shanklin, and E. W. Wolf, *JQSRT*, **54,** 481–494.
6. A. Sarkissian, H. K. Roscoe, D. J. Fish, M. Van Roozendael, M. Gil, H. B. Chen, P. Wang, J. P. Pommereau, and J. Lenoble, *Geophys. Res. Lett.*, in press.
7. L. M. Perliski, Ph.D. thesis, Univ. of Colorado, Boulder (1992).
8. A. Dahlback, P. Rairoux, B. Stein, M. Del Guasta, E. Kyrö, L. Stefanutti, N. Larsen, and G. Braathen, *Geophys. Res. Lett* (EASOE special issue), **21,** 1399 (1994).
9. J. Lenoble and H. B. Chen, *Current Problems in Atmospheric Radiation*, S. Keevallik and O. Kärner, eds., p. 481, A. Deepak, Hampton, VA (1993).
10. M. Friedler, H. Franck, T. Gomer, M. Hausmann, K. Pfeilsticker, and U. Platt, *Geophys. Res. Lett.* **20,** 959 (1993).
11. M. Van Roozendael, M. de Mazière, and P. C. Simon, *JQSRT* **52,** 231–240 (1994).
12. S. Solomon, A. L. Schmeltekopf, and R. W. Sanders, *J. Geophys. Res.* **92,** 8311 (1987).
13. *Handbook of Geophysics and Space Environments*, Mc Graw–Hill, New York (1965).
14. M. Q. Syed and A. W. Harrison, *Can. J. Phys.* **58,** 788 (1980).
15. D. R. Bates, *Planet. Space Sci.* **32,** 785 (1984).
16. M. Nicolet, *Planet Space Sci.* **30,** 935 (1982).
17. D. J. Fish, Ph.D. thesis, Cambridge (1994).
18. B. G. Gardiner and J. C. Farman, British Antarctic Survey (1988).
19. W. D. Komhyr, S. J. Oltmans, P.R. Franchois, W. F. J. Evans, and W. A. Matthews, *Ozone in the Atmosphere*, Bojkov and P. Fabian, eds., p. 147, A. Deepak Publ., Hampton, VA (1989).
20. M. P. McCormick, C. R. Trepte, and M. C. Pitts, *J. Geophys. Res.* **94,** 11241 (1989).
21. A. Sarkissian, J. P. Pommereau, and F. Goutail, *Geophys. Res. Lett.* **18,** 779 (1991).
22. A. Sarkissian, J. P. Pommereau, F. Goutail, and E. Kyro, *Geophys. Res. Lett.* EASOE special issue, **21,** 1319 (1994).
23. J. P. Pommereau and J. Picquard, *Geophys. Res. Lett.* EASOE special issue, **21,** 1227 (1994).

APPENDIX 1

The Intensity-weighted Approximation

Equation (5) states the formulation of the AMF:

$$\mathrm{AMF}_Y = \frac{1}{Y_{\mathrm{ver}}\sigma_Y}\left[-\ln\left(\frac{I}{I^*}\right)\right] \tag{5}$$

Assuming an infinitely narrow field of view and replacing the integration in Eq. (4) by a summation,

$$I = \sum_Z I_Z^* \exp[-k_Y(z)] \quad \text{and} \quad I^* = \sum_Z I_Z^*$$

Equation (5) then becomes

$$\mathrm{AMF}_Y = \frac{1}{Y_{\mathrm{ver}}\sigma_Y}\left[-\ln\left\{\frac{\sum_Z I_Z^* \exp[-k_Y(z)]}{\sum_Z I_Z^*}\right\}\right]$$

If $k_Y(z) \ll 1$, then $\exp[-k_Y(z)] \approx 1 - k_Y(z)$. Hence

$$\mathrm{AMF}_Y \approx \frac{1}{Y_{\mathrm{ver}}\sigma_Y}\left[-\ln\left\{\frac{\sum_Z I_Z^*[1-k_Y(z)]}{\sum_Z I_Z^*}\right\}\right]$$

$$= \frac{1}{Y_{\mathrm{ver}}\sigma_Y}\left[-\ln\left[1-\frac{\sum_Z I_Z^* k_Y(z)}{\sum_Z I_Z^*}\right]\right]$$

If $k_Y(z) \ll 1$, then $(\Sigma_Z I_Z^*(z)/\Sigma_Z I_Z^*) \ll 1$, and since $\ln(1+x) \approx x$ when $x \ll 1$

$$\mathrm{AMF}_Y \approx \frac{1}{Y_{\mathrm{ver}}\sigma_Y}\frac{\sum_Z I_Z^* k_Y(z)}{\sum_Z I_Z^*}$$

In the case of weak absorption by Y, then $I_Z \cong I_Z^*$ so that

$$\mathrm{AMF}_Y \approx \frac{1}{Y_{\mathrm{ver}}\sigma_Y}\frac{\sum_Z I_Z k_Y(z)}{\sum_Z I_Z}$$

This equation takes the weighted average of the AMFs of each ray in the calculation, the weights being set sequal to the intensity received by the instrument for each eay. This intensity-weighted approximation has been commonly used (e.g., Solomon et al;[12] Sarkissian[4]) but only agrees with the more exact Eq. (5) in the limit of weak absorption ($k_Y \ll 1$). Since the above derivation includes three successive approximations relying on this condition, the approximation fails at rather weaker absorption than the values 0.1 to 0.2 normally considered adequate when discussing the single weak condition $\exp(-k_Y) \approx 1 - k_Y$.

APPENDIX 2

Double Scattering

When a ray is allowed two scattering events before reaching the instrument (commonly called second-order scattering), the Sun illuminates volumes of air $V2$ with geocentric polar coordinates, r, Θ, Φ as sketched in Fig. 3. $V2$ scatters the radiation in all directions including toward the volume V, which scatters the radiation again toward the ground. Our model makes a numerical integration of this radiation reaching the ground by varying the position of $V2$ over all the atmosphere, and, as in the single-scattering calculation, by varying the altitude of V from the ground to the top of the atmosphere.

Our purpose in designing this double-scattering model was to investigate whether differences between single and middle-scattering events. Hence the scheme of this calculation is the same for single as for double scattering: light beams illuminate atmospheric volumes of finite extent and the fluxes scattered are summed. This important principle makes the originality of this model. Note that it requires calculations of absolute fluxes, not relative. Previous models used analytical functions (Noxon et al,[1] Dahlback et al[8]), with different approximations to integrate single scattering from those to integrate double or multiple scattering. Here, the integration is numerical for both single and double scattering.

The flux $\mathrm{d}I_{V2}$ from double scattering via $V2$ and V to the ground is:

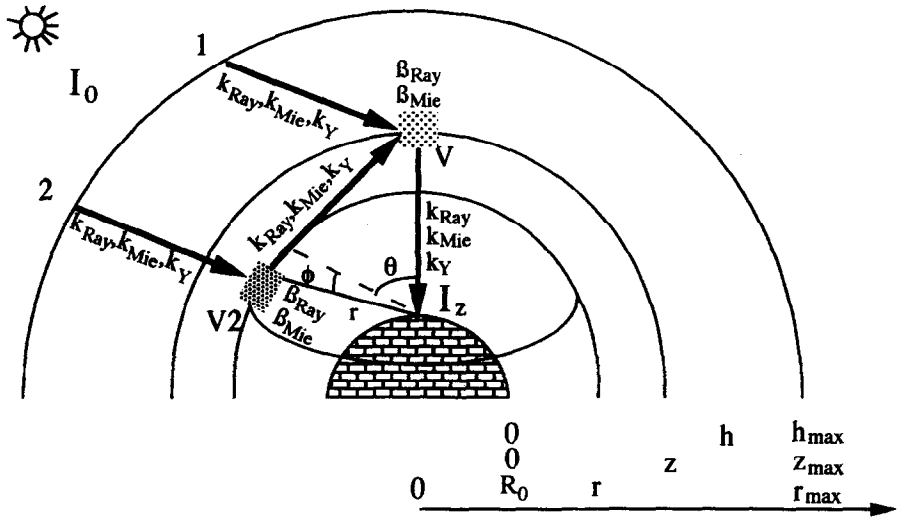

Fig. 3. Our double-scattering scheme involves integrating all of the fluxes singly scattered from V for all locations of V within the field-of-view (a scheme identical to that for single scattering), as well as the integrals of the fluxes doubly scattered from $V2$ then V, for all locations of $V2$ (all z, Θ and Φ) at all locations of V within the field-of-view.

$$\frac{dI_{V2}(z, r, \Theta, \Phi)}{I_0} = \frac{dV}{4\pi r(V)^2} \frac{dV2}{4\pi r(V, V2)^2} \cos[\alpha(V)]$$
$$\times [\beta_{Ray}(V2) + \beta_{Mie}(V2)][\beta_{Ray}(V) + \beta_{Mie}(V)] \exp[-\tau(V2)]$$

where $\tau(V2)$ is calculated using the same scheme as in single-scattering [Eqs. (10) and (11)] and $r(V, V2)$ is the distance between V and $V2$.

The flux received by the detector at the ground is then

$$I = \sum_Z \left[I_V(z) + \sum_r \sum_\Theta \sum_\Phi I_{V2}(z, r, \Theta, \Phi) \right]$$

The resolution of the net for $V2$ is fixed in r and z: $\Delta r = \Delta r = \Delta z = 1$ km, from R_0 (the ground) to $r_{max} = R_0 + 90$ km. Θ varies from 0° to 20° and Φ from 0° to 360° to cover all the atmosphere seen from the highest layer ($z = 90$ km) above the instrument. The default sampling of the net used in the calculations is $\Delta\Theta = 0.1°$ $\Delta\Phi = 5°$. A finer sampling increases the duration of the computation without significant change to the result of the calculations.

Note that this model allows non-homogeneous atmospheres in Θ and Φ, although the results shown here are for a homogeneous atmosphere.

GEOPHYSICAL RESEARCH LETTERS, VOL. 22, NO. 9, PAGES 1113-1116, MAY 1, 1995

Ozone and NO_2 air-mass factors for zenith-sky spectrometers: Intercomparison of calculations with different radiative transfer models

A. Sarkissian[1], H.K. Roscoe[1], D. Fish[2], M. Van Roozendael[3], M. Gil[4], H.B. Chen[5], P. Wang[5], J.-P. Pommereau[6] and J. Lenoble[5]

Abstract. Calculations of air-mass factors (AMFs) for ground-based zenith-sky UV-visible spectrometers are now well developed in laboratories where stratospheric constituents are measured with this technique. An intercomparison between results from the different radiative transfer models used to calculate AMFs at twilight is presented here. The comparison was made for ozone AMFs at 510 nm and for NO_2 AMFs at 440 nm. Vertical profiles were specified. Results are presented firstly for calculations in a pure Rayleigh atmosphere, then including background aerosols. Relative differences between calculated AMFs from different models cause relative errors in vertical columns of ozone and NO_2 measured by zenith-sky spectrometers. For commonly used averages over solar zenith angles, these relative errors are ±2.3% in the vertical column of ozone and ±1.1% in the vertical column of NO_2. Refinements to the calculations, suggested by the intercomparison, should reduce these errors to ±1.0% for ozone and ±0.5% for NO_2.

Introduction

Several stratospheric constituents important in ozone depletion are routinely measured by ground-based zenith-sky UV-visible spectrometers. The line-of-sight amounts observed during twilight by spectrometers are interpreted using air-mass factors (AMFs): the AMF of a constituent is the ratio between the amount of the constituent in the line-of-sight of the observation and the amount in a vertical column. AMFs of ozone and NO_2 in the visible are a maximum at twilight, justifying observation during this time.

AMFs are calculated by radiative transfer models. Although AMFs were calculated in the past [Noxon et al., 1979], the work of Solomon et al. [1987], the recent deployment of UV-visible spectrometers such as SAOZ (Système d'Analyse par Observations Zénithales) [Pommereau and Goutail, 1988] in SCUVS (Stratospheric Climatology Using UV-visible Spectroscopy) and the NDSC (Network for the Detection of Stratospheric Change) have given AMFs and their calculations a high priority. Since 1990, at least 5 laboratories have developed new models, with original schemes of computation. It is important that there are no trends induced in the results of zenith-sky spectrometers because of time- or atmosphere-dependent artefacts in AMFs. Furthermore, computations made by different radiative transfer models should agree as closely as possible to reduce bias between sets of data.

The goal of this paper is to enlarge our knowledge of some of the possible errors in calculated AMFs by making a comparison between existing models. Section 2 presents an overview of existing radiative transfer models developed at several laboratories, using single or multiple scattering schemes. Section 3 presents vertical profiles used for the intercomparison. Section 4 presents the results of the intercomparison which are discussed in section 5.

This paper does not address the question of the absolute accuracy of calculation of AMFs. This can only be done by comparing results of measurements of vertical columns by UV-visible zenith-sky spectrometers with measurements by independent techniques. For the formulation of the AMF and for a wider discussion about sources of errors in calculation (including vertical profiles, absorption and scattering cross-sections), see Sarkissian et al. [1995].

Existing Models and Participants in the Intercomparison

To reproduce zenith-sky observations from the ground, models must make radiative transfer calculations, simulating the source (the Sun) and calculating optical paths in the atmosphere. Sunlight is absorbed and scattered as it traverses the atmosphere. Models have to calculate geometrical paths, absorption, extinction and scattering, and must integrate fluxes coming from different altitudes and directions. Differences between models can arise from (i) the scheme used in the path calculation, (ii) constituents and parameters included in the calcu-lation of optical thickness, and (iii) the scheme used to integrate the field of view if the model is more than two-dimensional.

Although some details differ, the basic scheme used for geometrical path calculation in spherical geometry is the same for all models in the intercomparison, and adopts that of Solomon et al. [1987]. Table 1 lists some laboratories where AMF calculations have been made since 1987 and the computation scheme used by each. Briefly, the different schemes are:

- single scattering model (called standard here) using ray tracing in a spherical 2-D atmosphere [Solomon et al., 1987] ;
- Monte Carlo model, which traces rays backward from a source at the ground and where photons are scattered randomly until they leave the atmosphere or are absorbed;
- Discrete Ordinate, from the radiative transfer equation solved by Chandrasekhar for parallel layers, corrected for a spherical atmosphere;
- Numerical Integration method, which follows the standard

[1] BAS, Madingley Road, Cambridge CB3 0ET, UK
[2] UCAM, Cambridge, UK
[3] IASB, Brussels, Belgium
[4] INTA, Madrid, Spain
[5] LOA, Villeneuve d'Ascq, France
[6] SA, Verrières-le-Buisson, France

Paper number 95GL01032
0094-8534/95/95GL-01032$03.00

Table 1. A summary of more recent radiative transfer models used for calculation of air-mass factor.

Laboratory	Model	References	Orders
NOAA (USA)	Standard	Solomon et al. [1987]	1
SA (France)	Standard (SAOZ)	Sarkissian [1992]	1
INTA (Spain)	Standard	Gil and Cacho [1992]	1
UH (Germany)	Standard	Fiedler et al. [1993]	1
IASB (Belgium)	Standard	Not published	1
UCAM (UK)	Standard	Not published	1
LOA (France)	Standard	Not published	1
NOAA (USA)	Monte Carlo	Perliski [1992]	All
LOA (France)	Monte Carlo	Lenoble and Chen [1993]	All
NILU (Norway)	Discrete Ordinate	Dahlback et al. [1994]	All
BAS (UK)	Numerical Integration	Sarkissian et al. [1995]	2

scheme with an extension to the 3-D atmosphere and the second order of scattering.

When there is no publication for the model, table 1 includes the nearest reference (results of observations, presentation of the instrument). SA results are supplied to SAOZ users for routine analysis. The list is not exhaustive. Note that model BAS is a significant technical and schematic advance on the SA model from which it grew [Sarkissian, 1992].

Vertical Profiles

A first attempt at an intercomparison of ozone AMFs used different vertical profiles of constituents and air density, reflecting the prejudice of each group. The results were not quite as chaotic as we might now expect with hindsight: the spread was 6% between 86° and 91° SZA and increased at higher SZA to reach 35% at 94°. The conclusion was that the identification of differences between calculations was not easy without specification of vertical profiles.

For the intercomparison proper, input profiles of constituents were specified, chosen from some in frequent use by the community. Figure 1 shows the atmospheric density from Handbook of Geophysics [1965] corresponding to subarctic winter, and the Mie extinction coefficient at 450 nm by background aerosol. The Rayleigh scattering cross-section and phase function were not specified. The Mie background aerosol extinction coefficient comes from the Handbook of Geophysics [1965] in the troposphere and from SAGE II (Stratospheric Aerosol and Gas Experiment on Nimbus 7) satellite observations in April 1988 at 65°N for the stratosphere (low content of aerosol after years without volcanic eruption). The Mie scattering coefficient at 90° is

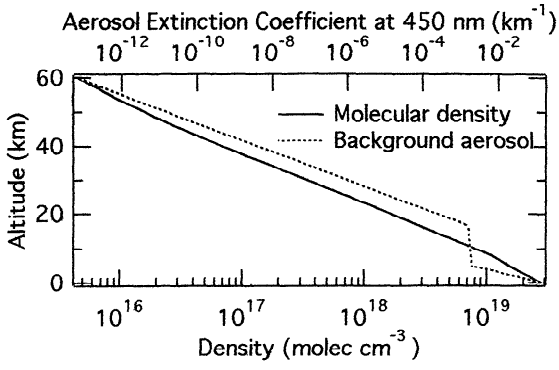

Figure1. Vertical profiles of aerosol (top scale) and density (bottom scale) used for the intercomparison.

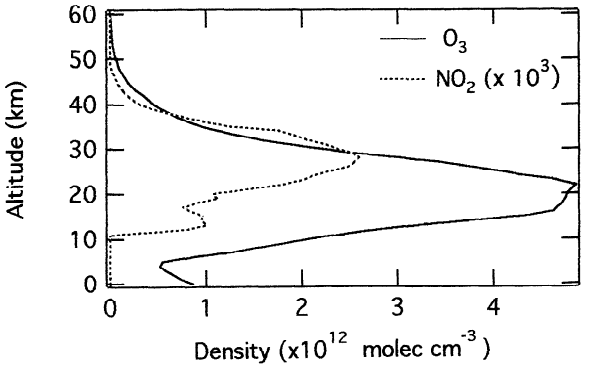

Figure 2. Vertical profiles of O3 and NO2 used for the intercomparison.

specified to be the extinction coefficient divided by 40. This corresponds to a Henyey-Greenstein phase function with an asymmetry factor g = 0.6715. In some models the angular dependence is neglected. The Mie extinction coefficient is specified to be inversely proportional to the wavelength.

Figure 2 shows the specified ozone profile from the Handbook of Geophysics [1965], and specified NO2 profile from balloon-borne solar occultation measurements from 10 to 22 km and from SAGE II above, both at 44° N in September 1986 [Cunnold et al., 1991]. Absorption cross-sections of ozone and NO2 were not specified.

Results of the Intercomparison

Geometrical parameters (thickness of the layers, sphericity of the atmosphere, etc.) were not specified, although all profiles are given from 0 to 60 km at 1 km intervals, limiting the top of the atmosphere to 60 km.

Calculations were requested at solar zenith angles (SZAs) of 86°, 88°, 90°, 92° and 94°, and at single wavelengths of 440

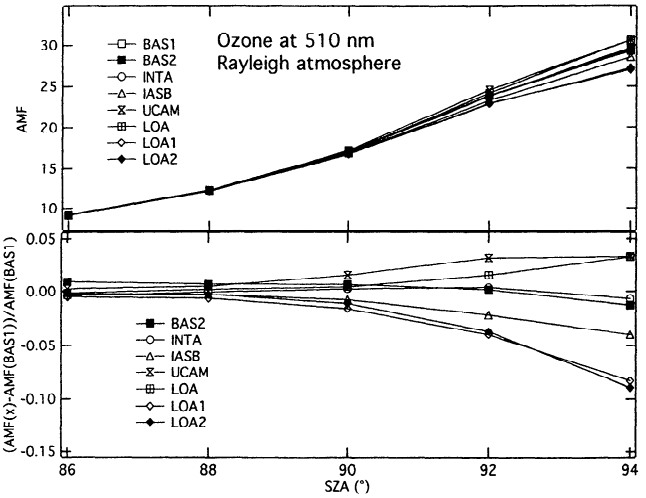

Figure 3. Results of the intercomparison of AMF for O3 at 510 nm in a pure Rayleigh atmosphere with specified profiles of atmospheric, O3 and NO2 densities. Upper figure, the AMFs. Lower figure, their relative differences from BAS1. Calculations with more than one scattering event are shown with full symbols. The numbers at the end of the name of the laboratories indicate that the same model is used for calculations with both a single (1) and more than one (2) scattering event allowed. LOA calculations are made by a standard model. LOA1 calculations are made with Monte-Carlo code but allowing one scattering only.

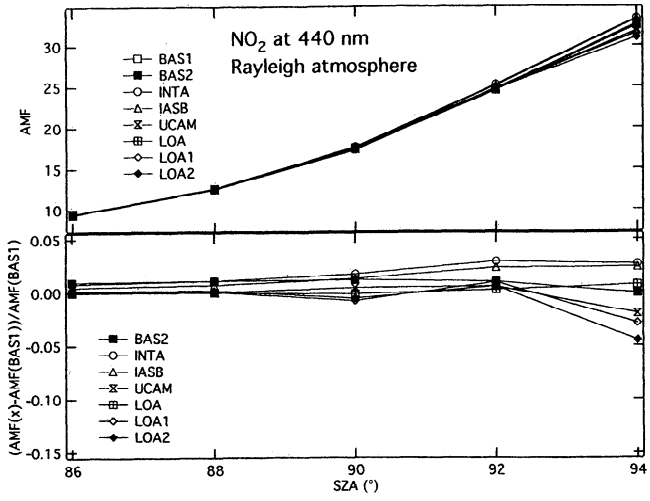

Figure 4. As Fig 3, but for NO2 at 440 nm.

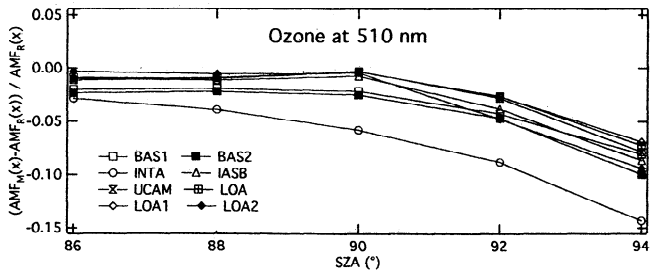

Figure 5. Relative effect of background aerosol on AMF of O3 at 510 nm. The subscript M refers to calculations with both Mie (aerosol) and Rayleigh (molecular) scattering, the subscript R to calculations with Rayleigh scattering only.

nm for NO2 and 510 nm for O3. Separate calculations were requested with a pure Rayleigh atmosphere and with added background aerosol.

AMFs calculated for ozone in an aerosol-free atmosphere are presented in figure 3. The lower panel shows the relative difference from one of the calculations, chosen arbitrarily. The numbers at the end of the name of the laboratories indicate that the same model is used for calculations with both a single (1) and more than one (2) scattering event allowed.

At low SZA (86° to 90°), the maximum spread of the calculations is small, < 4%. At high SZA (92° to 94°), the spread increases to 13%. Differences between BAS1 and BAS2 or between LOA1 and LOA2 are due to including multiple scattering. These differences are small (<1%) for both models. Models IASB, INTA, UCAM, LOA and BAS1 are all standard, with nominally the same scheme, but the spread in the results at 94° is 10%. The difference between LOA1 and BAS1 illustrates the difference between Monte-Carlo and standard schemes, both with single scattering. This difference is small, less than 1% from 86° to 90°, 5% at 92° and 9% at 94° SZA; it is of the same order as the spread between the different standard models.

Figure 4 shows results for NO2, which are similar in character to those for ozone. The spread is 7% at high SZA. From 86° to 92° SZA, the effect of including multiple scattering is small (<1%) rising to 2% for LOA2 versus LOA1 at 94° SZA. At low SZA (86° to 90°), the spread of standard calculations is small (<1°). At high SZA, spread increases to 5%. The difference between Monte-Carlo single scattering and standard schemes is <1% from 86° to 92° SZA rising to 3% at 94°.

Figure 5 shows the relative difference between calculations of ozone AMF made by the same model with and without background aerosol. AMFs decrease upon introducing background aerosol. They differ in the size of the decrease which can reach 15% at 94° SZA. The spread rises from 3% at 86° to 8% at 94° SZA. The spread due to including multiple scattering is <1% at SZA ≤ 90° and rises to 3% at 94° SZA.

Sensitivity of NO2 AMFs to background aerosol are shown in figure 6. No systematic effect due to background aerosol can be observed. The amplitude of the spread is similar to the one previously observed in the aerosol-free atmosphere. At low SZA (86° to 90°), the spread is 1%. At high SZA, some (UCAM, BAS1, IASB and LOA) models are barely affected (less than 2%) by background aerosol, INTA increases by 3% at 92° SZA, and LOA1 decreases by 3% at 94° SZA.

Discussion

In the intercomparison of ozone AMF, the spread of the results decreased from 6% to 1% at 86° SZA and from 35% to 13% at 94° SZA when vertical profiles were specified. This emphasises the well-known conclusion [e.g. Syed and Harrison, 1980] that vertical profiles are some of the dominant parameters in AMF calculations (as well as the less obvious point that research groups will not choose identical profiles even when there are standard profiles in the literature).

However, even after specifying profiles, the remaining differences between models show that other parameters in models cannot be neglected. Sarkissian et al. [1995] evaluate the effects of computational parameters on ozone AMF with the BAS1 model. Amongst other influences on AMF, they show that: (i) the common approximation of calculating AMFs by intensity weighting instead of from the ratio of fluxes with and without absorber decreases AMF by 1% at 90° and 4% at 94° SZA; (ii) optical thickness of each atmospheric shell calculated using the value interpolated to the centre instead of the value at the bottom of the shell increases AMF by 2% at 94° SZA; and (iii) a systematic underestimation by x% of the geometrical path decreases the AMF by the same value at all SZA.

BAS1, INTA, IASB, LOA and UCAM are all standard models. The spread of their results is due to differences in calculation parameters: IASB and LOA use the intensity-weighted approximation; LOA, BAS1 and INTA use values of densities at the bottom of the shells; UCAM makes an analytic integration of the optical thickness inside those shells which are not homogeneous. Hence the spread in AMF of 2% at SZA≤90° between the five standard models arises from systematic differences in geometrical path calculations in individual shells.

Amongst other smaller influences on NO2 AMF, calculations with BAS1 show that: (i) optical thickness of each atmospheric shell calculated using the value interpolated to the centre instead of the value at the bottom of the shell increases AMF by 2% at 94° SZA; and (ii) a systematic

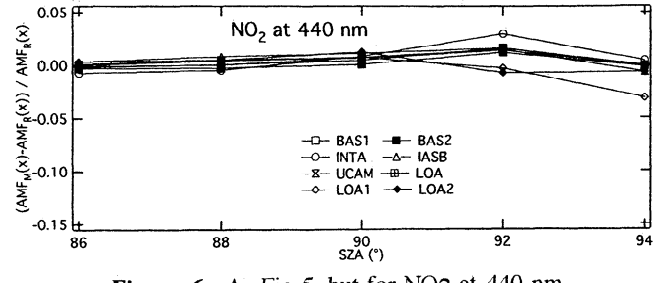

Figure 6. As Fig 5, but for NO2 at 440 nm.

underestimation by x% of the geometrical path decreases the AMF by the same proportion x% at all SZA. Hence the spread of 4% of NO2 AMF at 94° SZA for the standard models arises from differences in optical path calculations; and the spread of 1% at SZA ≤90° arises from systematic differences in geometrical path calculations in individual shells. Note that removing ozone to calculate NO2 AMF as done by INTA (only one absorber at a time in the model) does not affect the results.

Introduction of background aerosol affects all computations by a decrease of the ozone AMF at all SZA. The mean change is a decrease of 2% from 86° to 90° and of 10% at 94° SZA. The spread of the results increases from 4% at 86° to 8% at 94° SZA. This is due to differences in optical path calculation in individual shells, because the scale height of background aerosol is 2 to 3 km, very small compared to that of density (7 to 8 km). A value taken at the centre of the shell, instead of the bottom as in BAS1, increases the AMF by 2% at SZA<90° and by 10% at 94° SZA [Sarkissian et al., 1995]. To achieve better accuracy in future calculations, optical paths in individual shells must be integrated.

The effect of background aerosol on NO2 AMF is small: the mean value is near 0 at all SZA. That is because NO2 is located at higher altitudes where background aerosols have a smaller extinction and smaller scattering. The spread in results is due to differences in computational parameters as in the case of an aerosol-free atmosphere.

The differences between BAS2 and BAS1, or LOA2 and LOA1 are within the spread of models, pointing to a small influence of multiple scattering both for a molecular atmosphere and for background aerosol.

Conclusion

This intercomparison allowed us to identify the sources of differences between calculations by different models of air-mass factors of ozone and NO2. When vertical profiles are specified, the spread of the results is 1% at 86° and 13% at 94° SZA for ozone and 1% at 86° and 8% at 94° SZA for NO2. These differences are due to differences in computational parameters and schemes of radiative transfer model. Some of the lessons for future work are: intensity-weighted AMF and homogeneous shell approximations must be avoided; optical paths have to be integrated in individual shells; background aerosols cannot be neglected ; and including multiple scattering has a small effect on calculations of ozone and NO2 AMFs, as long as there is no volcanic perturbation or polar stratospheric aerosol [Lenoble and Chen, 1993].

Most workers have calculated vertical amounts of ozone and NO2 by averaging observations from 85° to 92° SZA [Noxon et al., 1979; Sarkissian, 1992; Fiedler et al., 1993]. Supposing four observations during twilight (86°, 88°, 90° and 92°), the rms scatter from the mean of the values at each angle averaged over the range of angles is the equivalent error due to differences in models, provided they are correlated at different SZA as the figures show them to be. (If they were uncorrelated, they would be divided by the square roots of the number of angles.). The error due to major differences in the type of model is ±1% for ozone and ±0.3% for NO2. The error due to the computational scheme is ±2% for ozone and ±1% for NO2. We believe that these computational errors would be reduced by making accurate computations of optical thicknesses in individual shells. The uncertainty due to including multiple scattering or not is ±0.2% for ozone and ±0.4% for NO2.

Hence total relative errors are ±2.3% for ozone and ±1.1% for NO2. These errors are comparable with the errors of ±2.4% made when using one set of AMFs for climatological ozone measurements for all seasons and locations varying ozone and air density profiles; these are smaller than the errors due to extreme volcanic aerosol (-14%) or to extreme polar stratospheric clouds (-5.4%) [Sarkissian et al., 1995]. If the problems due to interpolation and other differences in computation scheme can be solved, the remaining relative errors are ±1.0% for ozone and ±0.5% for NO2. These relative errors are determined without discussion of the absolute accuracy of the AMF.

Acknowledgements. The authors wish to thank J. C. Farman for scientific discussions. This work was supported by the CEC STEP-0013 and SCUVS projects. Alain Sarkissian is a CEC Research Fellow.

References

Cunnold D.M., J.M. Zawodny, W.P. Chu, J.P. Pommereau, F. Goutail, J. Lenoble, M.P. McCormick, R.E. Veiga, D. Murcray, N. Iwagami, K. Shibasaki, P.C. Simon and W. Peetermans, Validation of SAGE II NO2 measurements, *J. Geophys. Res.*, 96, 12,913-12,925, 1991.

Dahlback A., P. Rairoux, B. Stein, M. del Guasta, E. Kyrö, L. Stefanutti, N. Larsen and G. Braathen, Effects of stratospheric aerosols from the Mt. Pinatubo eruption on ozone measurements at Sodankylä , Finland in 1991/92, *Geophys. Res. Lett.*, 21, 1399-1402, 1994.

Fiedler M., H. Franck, T. Gomer, M. Hausmann, K. Pfeilsticker and U. Platt, Ground-based spectroscopic measurements of stratospheric NO2 and OClO in Arctic winter 1989/90, *Geophys. Res. Lett.*, 20, 963-966, 1993.

Gil, M. and J. Cacho, NO2 total column evolution during the 1989 spring in Antarctic Peninsula, *J. Atm. Chem.*, 15, 187-200, 1992.

Handbook of Geophysics and Space Environments, McGraw-Hill, NY, 1965.

Lenoble J. and H.B. Chen, Monte-Carlo study of the effects of stratospheric aerosols and clouds on zenith sky spectrometric measurements, in *Current problems in atmospheric radiation*, Edited by S. Keevallik and O. Kärner, A. Deepak Publ., Hampton, p. 481, 1993.

Noxon J.F., E.C. Whipple Jr and R.S. Hyde, Stratospheric NO2, 1. Observational method and behavior at mid-latitude, *J. Geophys. Res.*, 84, 5047-5065, 1979.

Perliski L.M., The role of multiple scattering in twilight zenith sky observations of atmospheric absorbers: diurnal photochemistry and air mass factors,, Ph.D. thesis, Univ. of Colo., Boulder, 1992.

Pommereau J.P. and F. Goutail, O3 and NO2 ground-based measurements by visible spectrometry during arctic winter and spring 1988, *Geophys. Res. Lett.*, 15, 891-894, 1988.

Sarkissian A., Observation depuis le sol des nuages et des poussières dans l'atmosphère: Applications à la stratosphère polaire et à l'atmosphère de Mars, Ph.D. thesis,, Université Paris 6, 1992.

Sarkissian A., H.K. Roscoe and D. Fish, Ozone air-mass factors for zenith sky spectrometers: an evaluation of errors in air-mass factors calculated by radiative transfer models, *JQSRT*, in press, 1995.

Solomon, S., A. L. Schmeltekopf and R.W. Sanders, On the interpretation of zenith sky absorption measurement, *J. Geophys. Res.*, 92, 8311, 1987.

Syed M.Q. and A.W. Harrison, Ground-based observations of stratospheric nitrogen dioxide, *Can. J. Phys.*, 58, 788, 1980.

H.B. Chen, P. Wang and J. Lenoble, LOA, Univ. Lille, France.
D. Fish, Cambridge University, Lensfield Road, Cambridge, UK.
M. Gil, INTA, Madrid, Spain.
J. P. Pommereau, SA du CNRS, 91371 Verrières-le-Buisson, France.
A. Sarkissian and H. K. Roscoe, British Antarctic Survey, Madingley Road, Cambridge CB3 0ET, UK. (e-mail: a.sarkissian@bas.ac.uk)
M. Van Roozendael, IASB, Brussels, Belgium.

(Received May 12, 1994; revised October 10, 1994;
accepted March 17, 1995.)

JOURNAL OF GEOPHYSICAL RESEARCH, VOL. 102, NO. D1, PAGES 1379–1390, JANUARY 20, 1997

Accuracy of measurements of total ozone by a SAOZ ground-based zenith sky visible spectrometer

A. Sarkissian,[1,5] G. Vaughan,[2] H. K. Roscoe,[1] L. M. Bartlett,[2] F. M. O'Connor,[2]
D.G. Drew,[3] P. A. Hughes,[4] and D. M. Moore[4]

Abstract. During a 2-week intercomparison of ground-based zenith sky visible spectrometers in September 1994 at Camborne, United Kingdom (50°N, 5°W), ozone profiles were measured by electrochemical cell (ECC) sondes during 11 twilight periods. We use these profiles and a radiative transfer model to calculate separate air mass factors (AMFs) for each twilight period. We examine ozone data from one of the spectrometers of the Système d'Analyse par Observation Zénithale (SAOZ) design and we show that these separate AMFs give very straight Langley plots, except at solar zenith angles exceeding 90°. Total ozone calculated using these AMFs, by a variety of commonly used procedures, agrees with the total ozone calculated by vertically integrating the sonde profiles, with mean differences of 0 to 7 Dobson units (DU), depending on the method, and standard deviations of 9 to 11 DU (1 σ). Total ozone calculated using the best procedure (i.e., averaging twilight values), which is not sensitive to errors in the gradients of AMFs, gave excellent agreement whether using separate AMFs or fixed climatological AMFs. We analyse the variance of the data set and several sources of systematic error in the measurements. We also illustrate from an example during the campaign that such analyses are pointless in the presence of a strong jet stream, which can give rise to changes in ozone during the course of the day that are large enough to invalidate the Langley plot.

1. Introduction

Stratospheric ozone has been measured since 1988 by ground-based zenith sky spectrometry in the visible Chappuis bands [*Pommereau and Goutail,* 1988]. Twilight geometry enhances the path of the sunlight in the stratosphere allowing more sensitivity to stratospheric absorbers. Line-of-sight amounts of constituents are deduced from spectra by differential absorption spectroscopy. Radiative transfer models calculate the enhancement of the optical path (commonly called the air mass factor, (AMF)) to convert line-of-sight amounts of ozone into vertical columns. Worldwide, at least 30 ground-based zenith sky visible spectrometers have been built since 1988, and at least 10 radiative transfer models have been developed for calculation of AMFs.

Both instruments and radiative transfer models have taken part in validation exercises in the past [*Sarkissian,* 1992; *Goutail et al.,* 1994], either during intercomparison campaigns when several kinds of instruments were operating simultaneously, or during long-term routine measurements when observations by other instruments (Dobson spectrometers or electrochemical cell (ECC) sondes) were available [e.g., *Kyro,* 1993; *Jones,* 1995]. These validation exercises were conducted at high latitudes in winter. As we demonstrate below, radiative transfer models have improved, so that an update of these earlier validation activities is now necessary. As we further demonstrate, the accuracy of ozone from the visible measurements can now be comparable to that from UV measurements.

The instrument used here is a broadband (300-600 nm), medium resolution (1.0 nm) diode array (512 pixel, metal-oxide semiconductor (MOS) detector) spectrometer of the SAOZ design (Système d'Analyse par Observation Zénithale) [*Pommereau and Goutail,* 1988], which normally resides at Aberystwyth, Wales. SAOZ is designed to measure column totals of ozone and NO_2 twice a day at twilight. Spectra are recorded throughout the day: every 5 min during twilight up to 94° solar zenith angle (SZA); and every hour at SZA < 85°. Spectra are analysed by differential absorption spectroscopy relatively to a reference spectrum taken at low SZA. Absorptions by O_3, NO_2, H_2O, and O_4 are derived by an iterative technique, as presented by *Sarkissian* [1992] but with updated cross sections and improved wavelength calibration (J.-P. Pommereau, private communication). Ozone is derived from a 100-nm wide band centred at 510 nm. Errors in ozone quoted by SAOZ are the standard error in the slope of a least squares linear fit of the plot of differential cross section versus differential optical thickness, each point on the plot being the values corresponding to each pixel in the selected bandwidth of 100 nm. These errors are due to residuals, and this formulation assumes they are uncorrelated with atmospheric phenomena (a possibly dangerous assumption, particularly for an undersampled spectrometer).

The results presented here were obtained during the intercomparison of ground-based UV-visible spectrometers conducted at Camborne (50° N, 5° W) from 12 to 24 September 1994 [*Vaughan et al.,* this issue], on behalf of the Second European Stratospheric Arctic and Midlatitude Expedition (SESAME). During this campaign, which involved 11 UV-visible instruments, a total of 11 ECC ozonesondes were launched during twilight periods to measure the temperature and ozone profiles immediately above the station. Special procedures were adopted:

[1]British Antarctic Survey, National Environment Research Council, Cambridge , England.
[2]Department of Physics, University of Wales, Aberystwyth, Wales.
[3]Meteorological Office- Radiosonde, Kehelland, Camborne, Cornwall , England.
[4]Meteorological Office, Bracknell, Berks, England.
[5]Currently at Service d'Aéronomie du CNRS, Verrières-le-Buisson, France.

Paper number 95JD03836.
0148-0227/97/95JD-03836$09.00

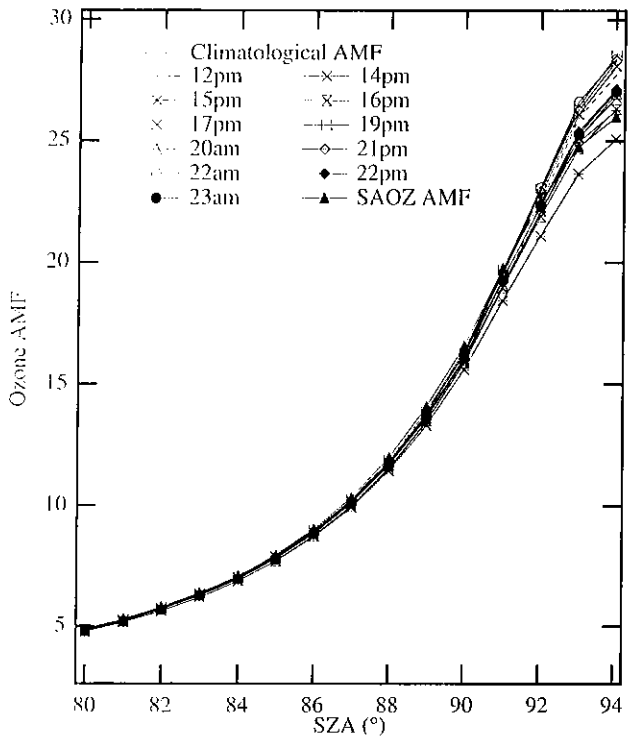

Figure 1. Ozone AMFs calculated using the ozone and density profiles measured by each ozonesonde flown in September 1994 at Camborne, U.K. (50° N, 5° W), together with the SAOZ AMF (see text).

each spectrum was analysed (1) by using as a reference the noon spectrum on the same day; (2) by using as a reference the noon spectrum on September 15 (a relatively cloud-free day). Despite the very humid atmosphere (and so the prominent H_2O absorption features in the spectra), residual features in the differential spectra corresponded to optical depths < 0.001 after the contributions of O_3, NO_2, ring effect, O_4, and H_2O were removed.

Vertical ozone columns V, are normally obtained from the line-of-sight columns S, derived from the differential spectra, by using the following relationship:

$$V = \frac{S + R}{AMF} \tag{1}$$

where R is the amount of absorber in the reference spectrum and AMF is the air mass factor. Normally, vertical columns from this equation are averaged over a suitable range of SZA. *Pommereau et al.* [1991] and *Van Roozendael et al.* [1994] have made a convincing case that using only twilight values minimises errors, and that is the procedure we use here:

$$\overline{V} = \frac{1}{N} \sum_{SZA=85^\circ}^{91^\circ} \frac{S_{SZA} + R}{AMF_{SZA}} \tag{2}$$

where N is the number of spectra measured between 85° and 91° SZA.

2. Radiative Transfer Model

A set of AMFs as a function of SZA was calculated for a high-latitude winter atmosphere by *Sarkissian* [1992] and are used routinely by the SAOZ software in operational use; they are referred to here as the "SAOZ AMFs". For the Camborne measurements, however, separate AMFs were calculated for each half-day period which contained an ozonesonde ascent, using the new radiative transfer model described by *Sarkissian et al.* [1995b].

The single-scattering part of the model, which is a technical and schematic advance on the model used by *Sarkissian* [1992] to calculate the SAOZ AMFs, uses the flux calculation scheme of *Solomon et al.* [1987]. Particularly new in the model is the double-scattering part, which uses a flux calculation scheme over the whole atmosphere, and individual contributions are numerically integrated. Calculations presented here are for single-scattering with no albedo and no refraction, except where stated. Also new is the intercomparison to which this model has been subjected, and the detailed analysis of possible errors. For ozone measured at 510 nm from 85° to 91° SZA, the relative accuracy deduced by intercomparison between different models (single-scattering, Monte-Carlo, numerical integration) is ± 1% [*Sarkissian et al.*, 1995a]. The sensitivity of the ozone AMF to vertical profiles of constituents, air temperature (hence air density) and particles (background aerosol, tropospheric cloud, volcanic aerosol, and polar stratospheric cloud) is studied by *Sarkissian et al.* [1995b]. For measurements averaged between 87° and 91° SZA, the variability of the ozone AMF over all seasons and latitudes is shown to be 2.4 % rms, and the difference between AMF for 60° N in January (the profiles used to compute the SAOZ AMFs) and the mean of all latitudes and seasons is 1.2%.

Profiles of ozone and temperature (and hence density) from the sondes launched during the campaign were used to calculate AMFs for the corresponding half day. The results of these calculations are plotted as a function of SZA in Figure 1. Also shown are climatological AMFs from *Sarkissian et al.* [1995b], interpolated from their northern midlatitude values to mid-September. The results are plotted as differences from the climatological values in Figure 2.

Figure 2 also shows that between 85° and 91° SZA, the climatological AMFs for the campaign differed from the SAOZ

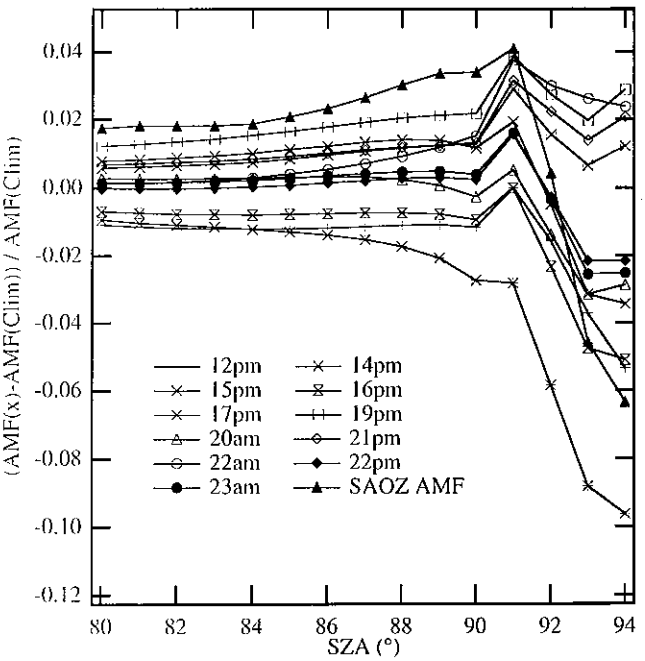

Figure 2. Relative difference of the AMFs of Figure 1 from the SAOZ AMF. These differences in AMF lead to identical differences in total columns.

AMFs by 2 to 4 %. An accurate calculation of the mean over this range of SZA gives 2.3 %. This would introduce a difference in the derived vertical column of ozone of -2.3 %, the SAOZ AMF result being smaller.

3. Langley plots

Equation 1 may be rearranged

$$S = V \times AMF - R \quad (3)$$

A plot of S as a function of AMF for a half day period, commonly called a Langley plot, should therefore be a straight line. The line will only be straight if: (1) the AMFs calculated are correct; (2) V does not change during the period; and (3) the ozone is horizontally uniform (slant paths at large zenith angles may lead to a measurement 200 km away from the instrument). If these conditions are satisfied, the slope V_{LP} should give V directly, while the intercept $-R_{LP}$ should correspond to V(Reference) x AMF(Reference), but see section 6 for discussion. Least squares straight line fits, weighted by the inverse square of their standard error, are used to determine R_{LP} and V_{LP} by means of standard formulae.

Although V_{LP} and $\overline{V}$ (2) are equivalent when the line is straight, they are not the same in practice because the statistics of the weights in real data are applied differently in the two formulations.

4. Results From the Procedure Using Daily Noon Reference Spectra

Examples of Langley plots, together with the corresponding ozone profiles, are shown in Figure 3a to 3k. (Here and after, numbers indicate the day in September, am and pm are respectively morning and evening measurements). Also shown is the variation of $\overline{V}$ with SZA. (The part from noon to 80° SZA is not shown because of the large scatter of the values close to noon: large relative errors in measurements arise from the small amount of absorption). All the SAOZ measurements in these panels use as a reference the spectrum at noon on the same day. A total ozone value for the sonde, V_{sonde}, (horizontal lines in the right-hand panels) was obtained by integrating the ozonesonde profile, and assuming a constant mixing ratio above the burst altitude. This is a reliable procedure for sondes which reach 28 km or above. (The software used to integrate sonde profiles was issued by the Norsk Institutt for Luftforskning data centre, Lillestrøm, Norway). The amount of ozone in the daily noon reference spectrum, R_{sonde}, was calculated as

$$R_{sonde} = V_{sonde} \times AMF_{noon} \quad (4)$$

All the plots are straight with little scatter, but there is a systematic deviation from linearity at large zenith angle (SZA>90°). In the absence of systematic errors, both the slope and the intercept of the Langley plots should be consistent with the independent measurement of total ozone by the sondes. These conjectures are examined in Table 1 and Table 2, respectively. Two ranges of angles were used for the calculations: 80° to 90° and 85° to 91°. The choice of 85° to 91° is based on the criteria for minimising errors, as described in section 1 above. In the tables, 17 pm has been rejected from averaging. This is because the plots in Figure 3 are very poor on this day, which is explained by the strong north-south jet stream which arose, giving rise to significant spatial and temporal gradients in ozone. Such temporal gradients will greatly increase the scatter of the Langley plot, as observed. Furthermore, the whole concept of AMFs will be invalidated when there are strong spatial gradients, a concept which assumes a homogeneous slant path.

The last two rows of the tables show the mean difference between the values in that column and the values in the last column. The standard error in the mean and the standard deviation of the values are calculated using well-known formulae [e.g., pp. 53 and 10, *Barlow*, 1989].

4.1. Total Ozone

As shown in Table 1, all methods give similar standard deviations of 9 to 12 Dobson unit (DU) (1 DU = 2.69 x 10^{16} mol cm^{-2}), to be expected as the number of spectra used is similar in all cases. The method which gives rise to the best result has marginally the smallest standard deviation, as might be expected.

Both calculations of the slopes of Langley plots give an underestimate with respect to the sonde. This agrees with the systematic tendency for the vertical columns to decrease with SZA in Figure 3, right-hand panels. This tendency increases at larger SZA, hence slopes determined from 85° to 91° have larger difference from the sonde (-7 DU) than slopes determined from 80° to 90° (-3 DU).

Of various methods of evaluating $\overline{V}$ in Table 1, the best agreement is seen using the amount in reference spectrum derived from R_{sonde}, that is, using integrated profiles of sondes and the AMF at noon. Indeed, the agreement is now excellent (no offset and a standard deviation of 9 DU), especially on days when the total ozone remained especially constant (September 12, 14, 15, and 19), where the standard deviation is only 4 DU. This agreement is better than V_{LP}, which confirms that (2) represents the best method for deriving total ozone from zenith sky spectra, provided R is known.

Instead of using R_{sonde} from (4) to derive total ozone, some laboratories [e.g., *Fiedler et al.*, 1993] calculate R_{amf} as

$$R_{amf} = V_{LP\,85\text{-}91} \times AMF_{noon} \quad (5)$$

$\overline{V}_{amf}$ (Table 1) can then be derived from (2) between 85° and 91° SZA using R_{amf}. The agreement between sondes and SAOZ is then also very good with a mean offset of -1 ± 3 DU and a standard deviation of 11 DU.

In Table 1, the column ($\overline{V}$ using climate AMF) is calculated in the same way as using R_{sonde} but with the fixed climatological AMFs from *Sarkissian et al.* [1995b] for mid-September. The agreement with mean of zero would be expected from the symmetrical points in Figure 1; but the lack of any significant increase in standard deviation is striking.

4.2. Ozone in Reference Spectra

Table 2 compares the results from the various methods of deriving the amounts of ozone in the reference spectra. Although there are possible systematic errors which may correlate with ozone (see section 5), their ability to give rise to an offset between twilight and noon on the same day, without affecting the twilight averages, is very questionable. Hence we would expect these results to agree with R_{sonde} from (4).

In Table 2, R_{amf} (5) gives the best result; a mean offset of -12 DU with a standard deviation of 16 DU. The work in section 4.1 suggests that the agreement would be even better if the range 80° to 90° were used to determine V_{LP} in this method.

As expected from the systematic tendency to underestimate ozone at larger SZA in Figure 3, right-hand panel, the agreement of Langley plot intercepts is worse using the SZA range of 85° to

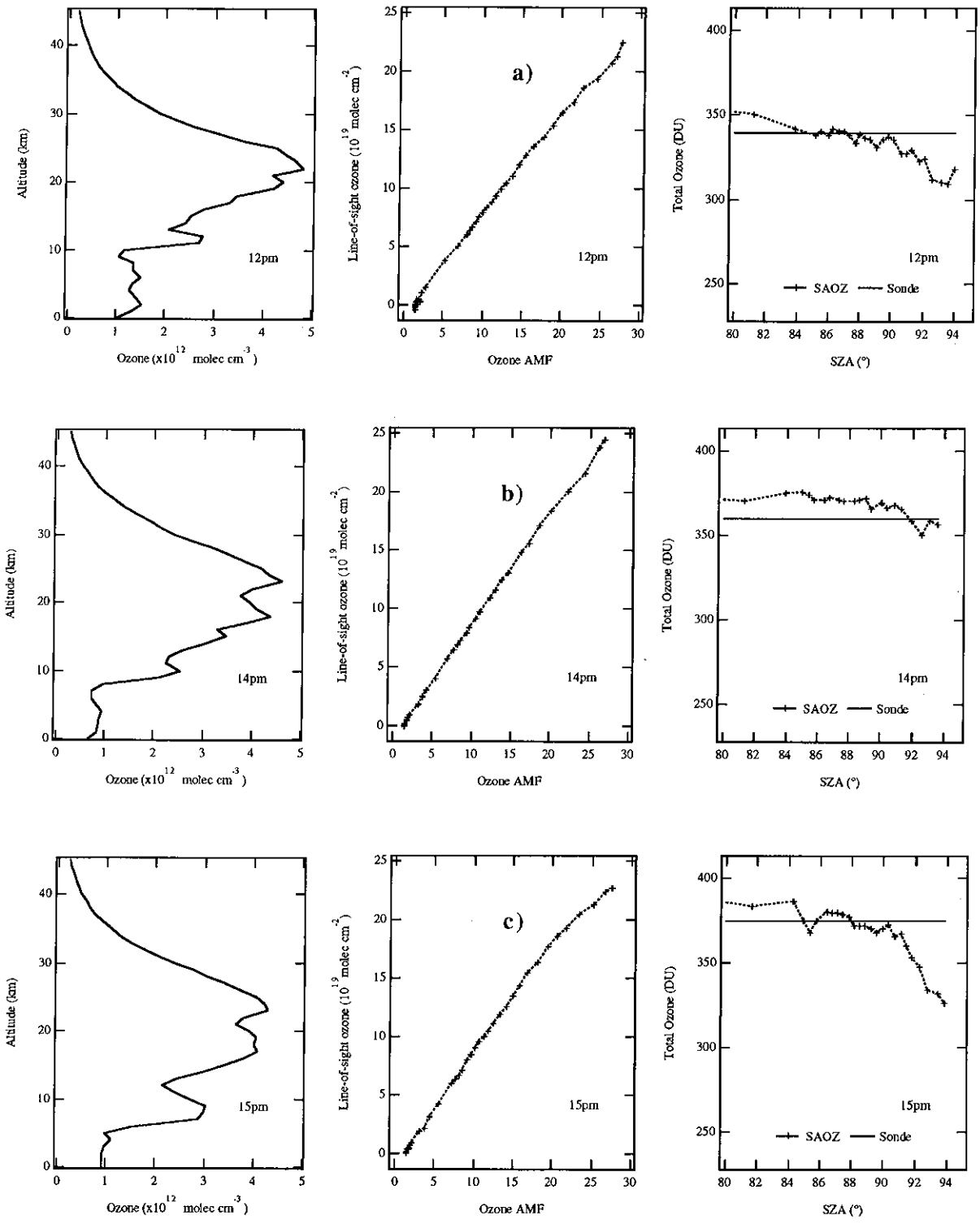

Figure 3. (a) - (k) Ozone measurements in September 1994 at Camborne, UK (50°N, 5°W). Left-hand panels: The ozone profiles from ECC ozonesondes. Values above the highest altitude of the sonde are calculated assuming a constant mixing ratio up to 90 km. Middle panels: The Langley plot for half-day periods when a sonde was flown. Measurements are from the SAOZ spectrometer which is normally stationed at Aberystwyth, UK. AMFs are calculated using measured ozone and temperature (hence density) profiles. The reference spectrum used in these SAOZ analyses is taken at noon on each day. Right-hand panels: Vertical ozone from SAOZ (crosses) using daily AMF and R_{sonde}, and from integrated sonde profiles (horizontal line). SAOZ values at SZA<80° are not shown because of their large scatter.

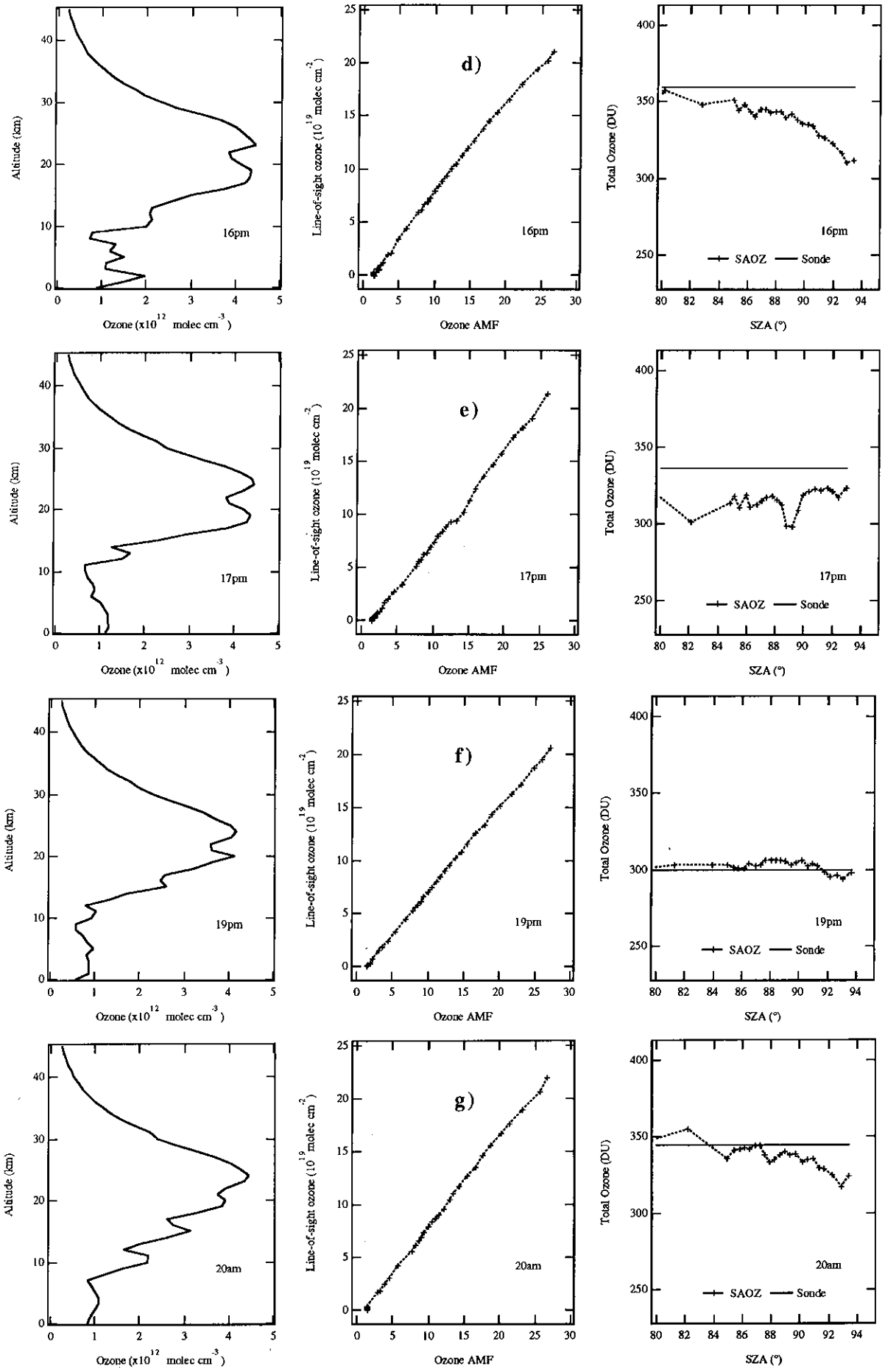

Figure 3. (a) - (k) (continued).

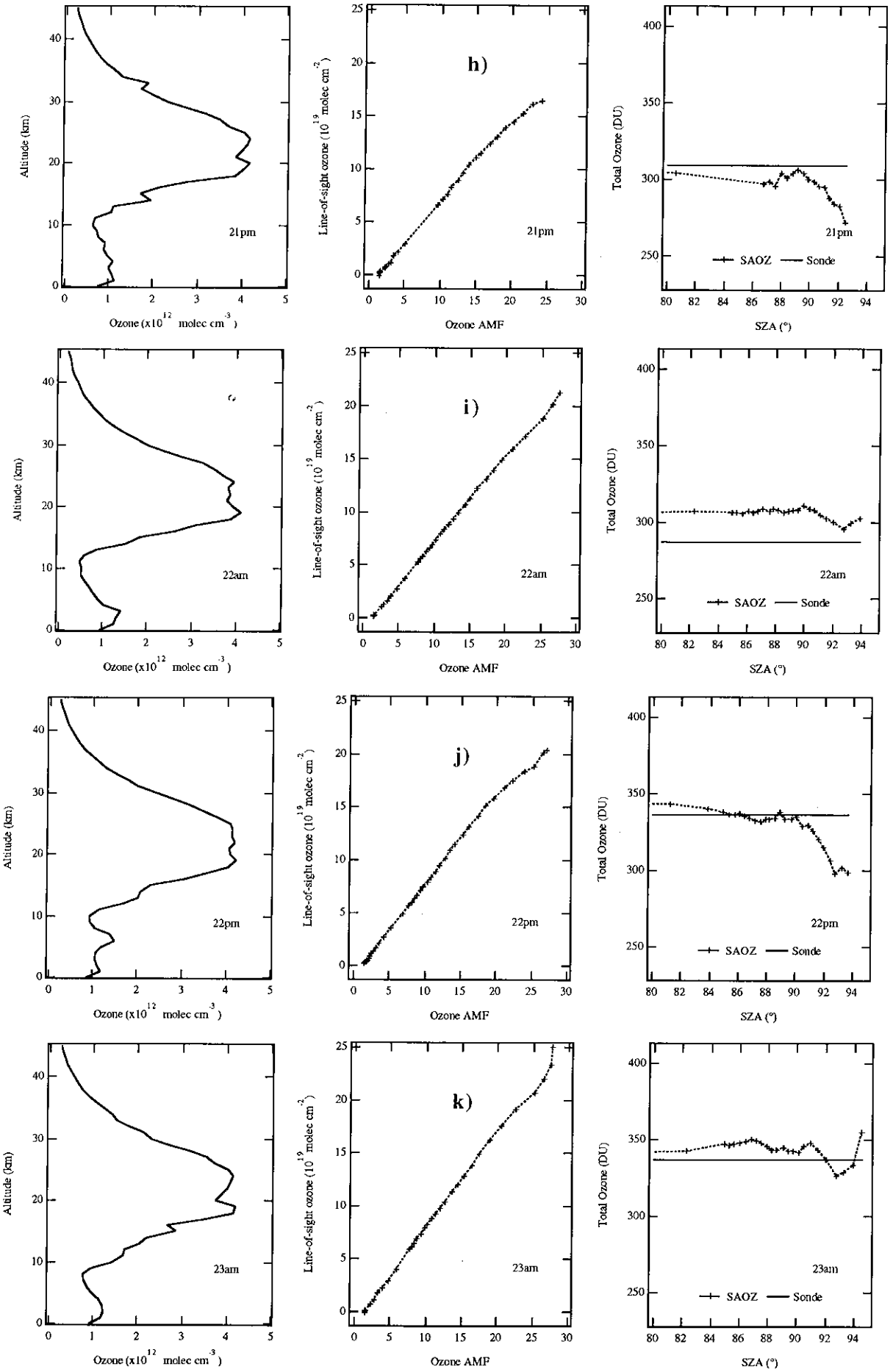

Figure 3. (a) - (k) (continued).

Table 1. Vertical Column Amounts of Ozone (DU) Calculated Using Different Procedures and Instruments, for Each Half Day Period When an Ozonesonde was Flown

Period	Slope of Langley plot, V_{LP}		$\overline{V}$ using R_{sonde}	$\overline{V}_{amf}$	$\overline{V}$ using Climate AMF	$\overline{V}_{15pm}$ using R_m	Dobson	V_{sonde}
	85° to 91°	80° to 90°	85° to 91°	85° to 91°	85° to 91°	85° to 91°		
12 pm	324	333	340	338	336	324		339
14 pm	358	362	367	366	370	361		360
15 pm	378	376	381	382	373	382	381	375
16 pm	325	335	344	339	341	343		359
17 pm	(312)	(303)	(311)	(308)	(314)	(313)	(339)	(336)
19 pm	297	300	298	297	304	293		300
20 am	334	333	339	337	338	327		345
21 pm	286	298	296	293	300	292	313	309
22 am	299	305	304	306	307	307	321	287
22 pm	324	329	334	332	334	328	321	336
23 am	337	343	345	345	346	332		337
Mean Difference from V_{sonde} ± standard error	-7 ± 3	-3 ± 3	0 ± 3	-1 ± 3	0 ± 3	-6 ± 4		
Standard deviation	11	11	9	11	10	12		

$\overline{V}$ and V_{LP} are calculated using equation 2 and the Langley plot respectively, and using the listed SZA intervals. $\overline{V}_{amf}$ is calculated using R_{amf} from equation 5. ($\overline{V}$ using R_{sonde}) is calculated with daily AMFs and equation 2. ($\overline{V}$ using climate AMF) is calculated in the same way as ($\overline{V}$ using R_{sonde}), except that the climatological AMFs are used for the whole data set. ($\overline{V}_{15pm}$ using R_m) is calculated using results from the procedure using the noon spectrum of September 15 as a reference. Note that R_m was calculated from Langley plots from 80° to 90° SZA. The last two rows show the mean difference (DU) between the values in that column and the values in the last column. Note that 17 pm is excluded from the averages (see text).

91° (-99 DU) than the range 80° to 90° (-49 DU). The likely reason for the large standard deviations (60 DU and 41 DU) is the extrapolation necessary to derive the intercept; a point further examined in section 5. Note that these differences should be divided by 12.8 to find their effect on $\overline{V}$; which are then -8 DU with a standard deviation of 5 DU (85° to 91° SZA) and -4 DU with a standard deviation of 1 DU (80° to 90°). These values are very similar to the differences of V_{LP} in Table 1: -7 DU and -3 DU, although the standard deviations are much smaller.

5. Results From the Procedure Using the Noon Spectrum of September 15 as a Reference

In order to examine the internal consistency of the SAOZ data set, all the spectra were re-analysed using as a reference the spectrum for noon on September 15 1994. As before, Langley plots were drawn for the twilight periods when ozonesondes were launched, using the separate air mass factors for each twilight period. Because R in (3) is a property of the reference spectrum, the intercepts of all the plots should (if the analysis programs and

Table 2. Slant Column Amounts of Ozone in the Daily Reference Spectra (DU) Calculated by Three Different Procedures, for Each Half Day Period When an Ozonesonde was Flown

Period	Intercept of Langley Plot, R_{LP}		R_{amf}	R_{sonde}
	85° to 91°	80° to 90°	(=$V_{LP\ 85\text{-}91}$ X AMF_{noon})	(=V_{sonde} X AMF_{noon})
12 pm	297	378	454	478
14 pm	416	457	512	516
15 pm	493	467	545	539
16 pm	309	404	466	520
17 pm	(514)	(435)	(460)	(491)
19 pm	433	460	437	446
20 am	468	450	496	515
21 pm	325	452	424	465
22 am	374	427	450	435
22 pm	406	445	491	509
23 am	428	505	514	514
Mean difference from R_{sonde} ± Standard error	-99 ± 20	-49 ± 13	-12 ± 5	
Standard deviation	60	41	16	

The SZA interval is listed when using Langley plots, as well as the equation used to derived R_{amf} and R_{sonde}. The last two rows show the mean difference (DU) between the values in that column and the values in the last column.

Table 3. The Amounts in the Reference Spectrum of September 15, 1994 (R) and Their Standard Errors (σ_R) Determined From the Intercept of the Langley Plot of Each Half Day's Data Together With the Values of χ^2 for Each Plot

Period	R, DU	σ_R, DU	χ^2 for linear fit	χ^2 for quadratic fit
12 pm	546	26	15.2	13.5
14 pm	596	19	5.6	4.4
15 pm	461	26	26.8	25.6
16 pm	498	19	16.6	16.3
17 pm	(509)	(71)	(121.7)	(113.4)
19 pm	703	19	5.1	5.0
20 am	595	44	52.0	39.3
21 pm	610	39	11.1	9.3
22 am	535	7	2.9	2.6
22 pm	587	15	4.8	2.9
23 am	736	22	11.5	5.5

the radiative transfer model were perfect) be the same.

Both straight lines and quadratic lines were fitted to the Langley plots between zenith angles 80° and 90°, with points weighted according to their standard errors. The intercepts of both lines were calculated, with the results shown in Table 3. As earlier, these limits on zenith angle were chosen because of the obvious departure of the data from linearity at SZA>90°, and the large relative errors on measurements at SZA<80°. A further advantage of this choice of limits is that these zenith angles were about 40 min apart in time; close enough for total ozone to be considered constant. (Langley plots beginning at noon are more susceptible to error due to geophysical changes in total ozone during the course of the day). For eight plots (12pm, 14pm, 15pm, 16pm, 17pm, 19pm, 21pm and 22am) the linear and quadratic regressions resulted in similar values of χ^2, which suggests no systematic deviations from linearity. Except for 17 pm (see below), the values of χ^2 were consistent with the theoretical expectation: $\chi^2/(N-2)$ had a mean value of 1.0 and a standard deviation of 0.7. This shows that the precision errors quoted for the SAOZ slant columns are reliable, thus proving that the residuals in the spectra are not markedly correlated.

The resulting intercept values, together with standard errors from the regression analysis, are shown in Figure 4. The standard deviation of the sample is about 3 times greater than the individual standard errors. However, it is clear that there are systematic errors which change the effective amount in the reference spectrum (which must necessarily be the intercept of the Langley plot). One such error, described by *Roscoe et al.* [1994], resulted from wavelength changes in the spectrometer. If such errors correlate with atmospheric or instrumental factors (e.g., cloudiness or ambient temperature), then the result will be an enhanced standard deviation such as we observe. Proper account of these systematic errors must be taken when we compile an error table.

The weighted mean of the intercepts in Figure 4, denoted R_m, yields a value of 550 DU, in excellent agreement with 539 DU, the value obtained for September 15 with the product V_{sonde} x AMF_{noon} in Table 2. For an AMF of 1.438 at noon, this corresponds to a vertical column of 382 DU: in excellent agreement with the Dobson value in Table 1 (381 DU), and with the slope of Langley plot (378 DU). This means that the systematic errors discussed above are approximatively randomly distributed, and with a mean close to zero.

Given that the spread of intercepts is so much greater than the individual standard errors in Figure 4, the uncertainty in R_m is best estimated as the standard deviation of the sample, that is, 75 DU. This corresponds to an uncertainty in vertical column ozone of 6 DU.

If R_m is used to calculate $\overline{V}$, the result, listed in Table 1 as $\overline{V}_{15pm}$, appears to be in good agreement with sondes. However, the difference of -6 DU is in fact disappointing compared with the result for $\overline{V}$ using R_{sonde}: use of a daily reference is better than a single reference for the whole data set. However, this is only necessarily true when using daily AMFs. The standard deviation between $\overline{V}_{15pm}$ and $\overline{V}$ using R_{sonde} (not shown in Table 1) is only 6 DU.

6. Discussion and Error Analysis

SAOZ measurements of total ozone calculated with the various methods of sections 4 and 5 are compared with integrated ozonesondes in Figure 5. $\overline{V}$ using R_{sonde} is what we consider to be the best method of calculating total ozone. Some Dobson spectrophotometer direct sun measurements were obtained during the campaign, and are also shown in Figure 5. Daily average Dobson values were, on average, 6 DU higher than V_{sonde} (with a standard deviation of 16 DU), but because of differences in the times of measurements and the small number of Dobson direct sun measurements, detailed conclusions cannot be drawn, and hence our choice of vertical integration of ozonesonde columns as a standard with which to compared SAOZ measurements during this campaign. Nevertheless, the SAOZ measurements using daily AMFs certainly agree with the Dobson measurements within 10 DU. The generally good agreement between Dobson and sonde

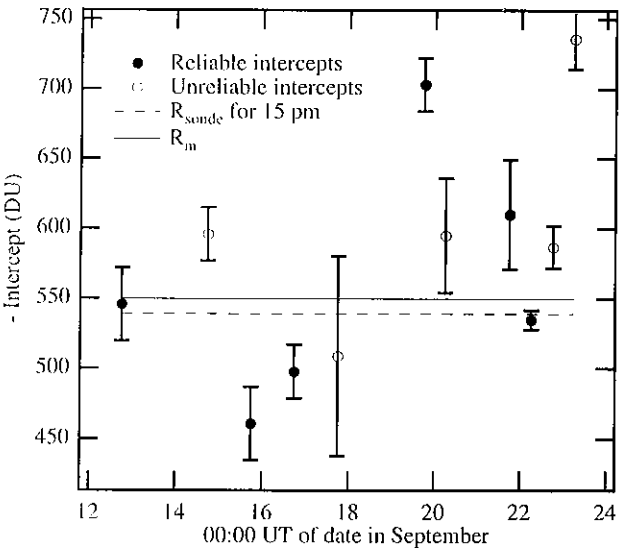

Figure 4. Intercepts calculated from the Langley plots of data with a single reference spectrum on September 15, by a least squares fit from 80° to 90° SZA. In the fits, weights were the inverse squares of the errors calculated from the residuals during the spectral analyses. Langley plots identified by solid circles (open circles) are reliable (unreliable) because linear and quadratic fits agree (disagree). Note the excessively large error bar on 17 pm, because of the large jet stream then and its associated changes in ozone during the day. The dashed line shows R_{sonde} for September 15 (=V_{sonde} x AMF_{noon} for September 15, and the solid line is R_m, the mean of the reliable points.

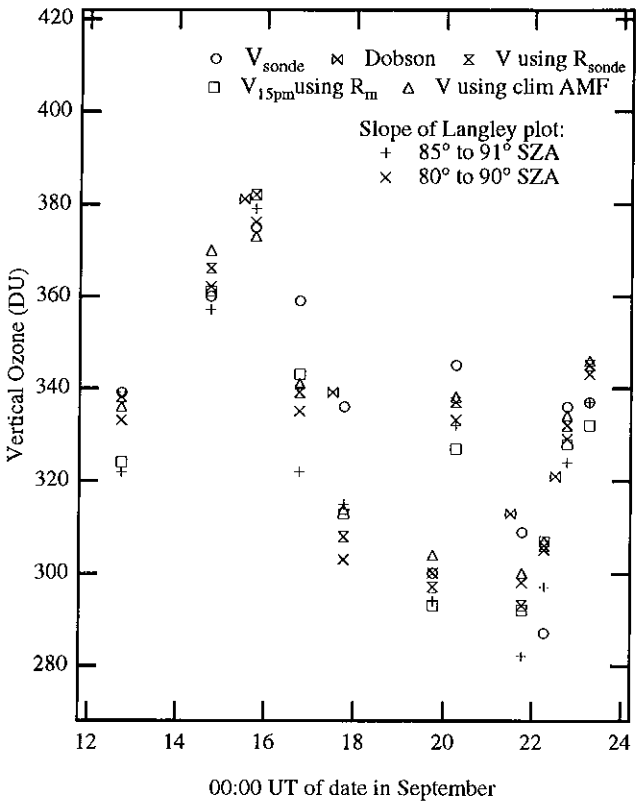

Figure 5. Total ozone measured with SAOZ by various analysis methods (see text), compared with total ozone from the Dobson and from integrated ozonesondes profiles. This figure illustrates the spread of the methods to derive total ozone.

(except on 22 am) supports the method of integration of ozonesondes columns used in this work.

There are several possible sources of systematic errors, which could be responsible for the scatter shown in Figure 5 between SAOZ and sondes. We have summarised these in Table 4, and they are evaluated in detail below.

6.1. Changes and Gradients in Ozone

Changes in ozone affect our results because sondes and SAOZ are not measuring ozone at the same location. A simple geometric calculation shows that in the morning (evening), the light rays reaching SAOZ traverse the atmosphere from about 200 km east (west) of the instrument to its zenith (see *Fiedler et al.* [1993], Figure 1, for a schematic description). Sondes were launched at 05 00 (or at 17 00) to reach the lower stratosphere 45 min after launch, when the SZA is 85° (90°), and 30 km at 90° (85°) after 90 min. Figure 6 shows the air masses observed by SAOZ for mornings and evenings, and the trajectory of the sondes using radar data (not available for 20 am and 21 pm). Note the important changes in wind direction during the 12-day campaign. Also note the large difference on 17 pm, when a jet stream was established as discussed earlier.

Because changes in total ozone at midlatitudes are often dominated by changes in tropopause height, we cannot use stratospheric winds multiplied by temporal gradients to estimate spatial gradients; total ozone does not follow the wind field. But we can estimate spatial gradients, at least in the east-west direction, from the SAOZ data itself, because its morning and evening locations are separated as shown in Figure 6. Figure 7 shows all data from the campaign, not just the values on sonde days discussed so far (necessarily, these are evaluated using SAOZ standard procedure and fixed AMFs, and so differ in detail from the values in Table 1). If we interpolate between the means of adjacent am-pm and pm-am pairs (i.e., between each "noon" and "midnight" value), we can derive the expected total ozone overhead (i.e., at the centre of the circle in Figure 6) at the time of each morning or evening measurement. Hence we can deduce the east-west spatial gradient for each sonde period. Ignoring 17 pm, we find a mean spatial difference between each sonde and the SAOZ twilight of 0 DU, with a standard deviation of 6 DU.

Note that we cannot evaluate north-south spatial gradients. Fortunately, the north-south distances in Figure 6 are much less than the East-West distances when we exclude 17 pm. The mean north-south distance is then 12 km with a standard deviation of 16 km.

6.2. Clouds

Blue sky was reported for the whole of only one twilight period during the campaign, 22 pm. Cirrus was reported at some point during all other twilight periods, except when the sky was obscured by 8/8 low cloud. The model used to calculate AMFs for the results in section 4 did not include clouds because the cloud parameters were not known, and the uncertainty which results is as great as the error resulting from omitting clouds in the first

Table 4. Estimates of the Size of Systematic Errors and of Their Contribution to the Standard Deviations in Table 1 Together With the Random Error From Residuals

Source of Error	Section	Probable Mean Error, DU	Standard Deviation Due to Error, DU
EW spatial gradients in ozone	6.1	0	6
Cirrus clouds	6.2	1	3
Lower-tropospheric clouds	6.2	0	0
Multiple scattering	6.3	-4	0
Background aerosol	6.4	0	0
Miscellaneous	6.5	3	0
Total		0	7
$\overline{V}$ using R_{sonde} - V_{sonde}	Table 1	0	9

The Root-Sum-Square Total of These Terms Agrees Well With the Differences of ($\overline{V}$ Using R_{sonde}) in Table 1.

place. To give an order of magnitude of the effect of clouds, a cirrus cloud of 0.1 optical depth at 8 km (very thick cirrus) was included in the double-scattering model. This reduced the AMF at 86° by 6.8% and at 90° by 1%, a mean of 4% (14 DU) from 85° to 91° SZA and a change in slope of 1.5%/degree (5 DU/degree). Its effect would therefore be to exacerbate rather than alleviate the slight curvature at large SZA of the Langley plots evident in Figure 3, right-hand panels. We therefore believe that cirrus was less than 1/10 of this amount on average, but we must allow the possibility of up to 1/5 this amount as a contribution to the standard deviation.

Low-altitude cloud has very little effect on AMFs in the absence of photochemical pollution (not a problem at Camborne): a cloud near the ground with optical depth 1 decreases the AMFs by 0.2% from 82° to 86° SZA [*Sarkissian et al.* 1995b].

Experimental verification that clouds do not appear to affect the zenith sky measurements is provided by the data for September 22. A cloudy sky at 06 00 (91.5° SZA) progressively gave way to a clear sky at 07 00 (80° SZA) while the evening twilight was clear. The Langley plots from both periods look very similar (Figure 3), as do the total columns, where the values remain largely constant from 85° to 90°, before decreasing sharply up to 92°. Furthermore, there is no systematic deviation of the vertical columns from the sonde values on half days when total cloud cover was observed (14 pm, 19 pm, 20 am and 21 pm). This lack of correlation suggests that this method of measuring stratospheric ozone is not sensitive to the type of clouds commonly seen in midlatitudes in September. (Note that, in the presence of tropospheric ozone even at comparatively unpolluted northern hemisphere values, a correlation is found when the tropospheric scattering is very strongly enhanced, as in a snow shower [*Van Roozendael et al.*, 1994]).

6.3. Multiple Scattering

The mean slope of the vertical column values shown in Figure 3 (a) to (k) is -1.1 ± 0.9 DU/degree from 85° to 91° SZA. We have rerun the radiative transfer model for the conditions of 12pm but including double scattering. With double scattering, the AMFs are changed such that ozone values decrease by 2.8% at 60° SZA, by 1.6% at 80° and by 1.0% at 90° SZA. If these changes were repeated on all days, the above mean slope would reduce to -0.8 ± 0.8 DU/degree, but the mean difference from sondes would change from -3 DU to -7 DU. Thus multiple scattering does correct the curvature of the Langley plots at high zenith angle, but gives smaller values of total ozone. This sensitivity test shows a potential systematic error of 4 DU, and illustrates possible compensating errors, hence worse agreement with the more accurate calculation. Note that in the absence of clouds, errors in AMFs due to not including multiple scattering cannot contribute significantly to the standard deviation of the measurement of total ozone.

6.4. Background Aerosol

Numerical tests have been conducted to evaluate the effects due to an incorrect aerosol profile in the radiative transfer model as the aerosol loading in September 1994 was still greater than the pre-Pinatubo background aerosol assumed in the model. Extinction profiles measured in April 1988 at 65° N (the background aerosol profile in the model), in September 1990, and in September 1994 (during the campaign) at midlatitudes by the Stratospheric Aerosol and Gas Experiment (SAGE II) on Nimbus 7 satellite [*WMO*, 1994] differ by around 10% in the stratosphere. However, these

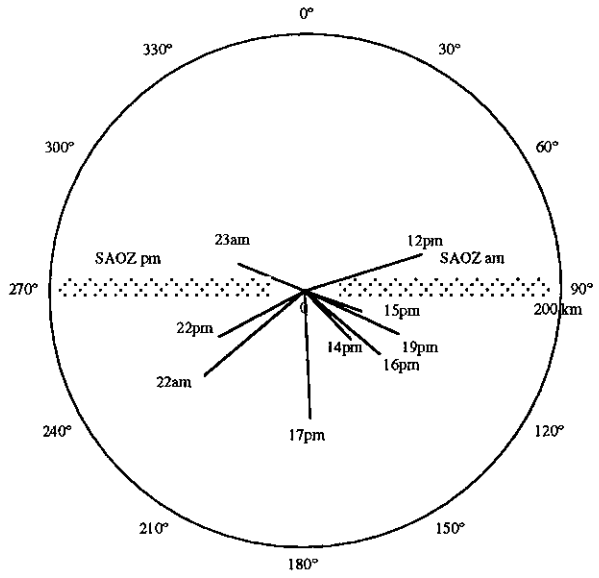

Figure 6. Trajectories (lines) of the sondes from the station (except for 20 am and 21 pm when there were no radar measurements), compared to air masses observed at twilight by zenith sky spectrometers such as SAOZ (rectangles). The radius of the circle is 200 km. Note the important changes of the wind direction during the 12-day campaign.

profiles affect the AMFs at 85° to 91° SZA by ± 0.1%. Such changes are too small to be significant in the present work.

6.5. Miscellaneous

Numerical tests have been conducted to evaluate the effects on AMFs due to (1) an incorrect field of view of the instrument in the radiative transfer model, (2) the width of the wavelength interval

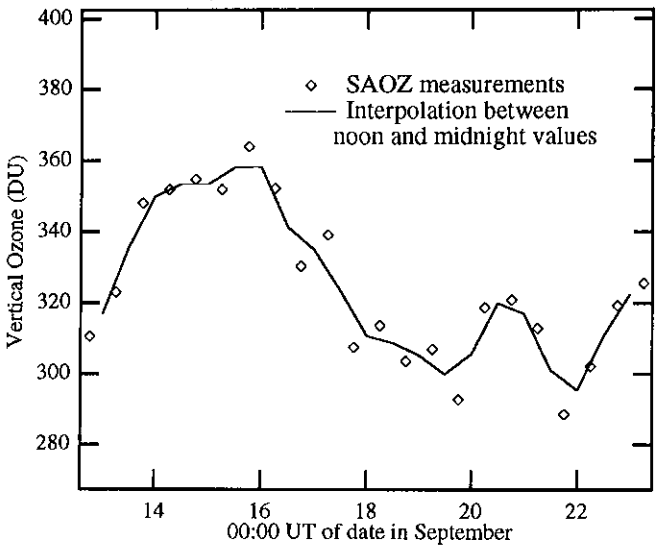

Figure 7. SAOZ measurements of ozone at all twilight periods during the campaign, (points), and the line joining the noon and midnight means (solid line). Differences between the SAOZ measurement when there was a simultaneous sonde, and the line at the same time, were used as estimates of the spatial gradient between the air mass overhead and that sampled by SAOZ. These SAOZ values must use fixed SAOZ AMFs, so they differ from those of Figure 5.

used in the SAOZ analysis, and (3) the integration time of the measurement with the result that it averages in time over a changing nonlinear AMF. They are evaluated at 90° SZA with our model to be, respectively, +0.1%, -0.5%, and -0.6% for plausible values of each parameter. As such errors will be consistent from one day to the next, they will not contribute to the standard deviation of differences found in this campaign.

6.6. Analysis of Variance

The various estimates of systematic error in Table 4 can now be combined. The probable mean errors sum to 1 DU, equal to the difference between $\overline{V}$ using R_{sonde} and V_{sonde}. This suggests that there are no unaccounted systematic errors with a nonzero mean.

However, the root-sum-square of the standard deviations due to these systematic errors is 7 DU, less than the 9 DU in Table 1 using our preferred method ($\overline{V}$ using R_{sonde}). This suggests that there are unaccounted random errors, or systematic errors of zero mean, with a standard deviation of about 6 DU. The random error due to residuals in the spectral fitting is not responsible, as it is usually less than 1 DU when averaged over SZA 85° to 91°. There remain north-south spatial gradients in ozone during the campaign, and errors in vertical integration of ozonesonde profiles, each of which is plausible. Hence we need not appeal to unknown sources of error.

In the Langley plots, the scatter of points exceed the errors from the residuals. This suggest that there are other source of systematic error during the course of the day with apparently random character. These sources of error can be any of those in Table 4, except distance from sonde and/or change in ozone itself.

7. Conclusions

During a campaign when 11 ozonesondes were launched close to twilight, SAOZ measurements of total ozone in the visible have been compared to values from integrating ozonesonde profiles, using AMFs calculated from each sonde profile. The mean difference of our preferred method for calculating vertical ozone from the SAOZ was 0 ± 3 DU and the standard deviation was 9 DU (1σ). Such good agreement was not observed before, and it has now allowed us to investigate other sources of error and to make recommendations for analysis procedures. For example, even with these AMFs, the Langley plots show clear curvature at SZA>90°. Combined with arguments about possible changes in ozone during the course of the day, this leads us to recommend that Langley plots use the range 80° to 90° for determinations of both slope and intercept.

Using this range for the slope of the Langley plots still gives a slightly worse result than the best method for determining total ozone by averaging values in the twilight period, by 3 ± 4 DU. This leads us to recommend the use of twilight averages for current conversion of slant to vertical columns.

Currently, all the various methods for calculating total ozone from SAOZ measurements agree with those from vertical integration of ozonesondes within 7 ± 3 DU. However, if AMFs at SZA>90° were improved, it is probable that all methods would give equal results; the choice of method would then depend on considerations of random errors (S/N ratio) rather than systematic errors. Measurements at these large SZAs are also those which contain most profile information at visible wavelengths, so that improvements in AMFs at SZA>90° is essential before profiles can be inverted from ground-based data. Although we have shown that profiles at midlatitudes in September are not important for accuracy of total ozone to a standard deviation of 10 DU, they will be important for good accuracy at high latitudes and improvements to this standard deviation are sought at midlatitudes.

When there are no simultaneous ozonesondes, it is not possible to use daily AMFs. In this case one can either use a daily reference spectrum and find the slope of the Langley plot, or a single reference spectrum and average the vertical amounts during twilight. The former method gives slightly better accuracy, but only when the range 80° to 90° SZA is available.

At high latitudes, this SZA range will not be available for a significant part of the year, so that a single reference must be used. The effective amount in this reference is the intercepts of Langley plots, which show greater scatter in our midlatitude data than the errors from the straight line fits. This suggests other sources of error in the Langley plot, correlated with atmospheric phenomena of a random appearance. The excellent agreement between the mean of the intercepts and the actual amount in the single reference spectrum suggests that these errors have a mean of zero.

The major source of systematic error in total ozone was the distance between air masses sampled by the sonde and the spectrometer, together with spatial gradients in ozone. Such changes in ozone are common in September at midlatitudes, so any future intercomparison should take place at a time and place where spatial and temporal gradients are expected to be much smaller. Careful analysis of this error during this campaign showed that it had a mean value of 0 DU but a standard deviation of 6 DU. Other estimates of systematic errors sum to 0 DU but do not significantly increase the standard deviation, nor does the random error due to residuals in the spectral fitting. As the observed standard deviation was 9 DU, there were unexplained systematic errors whose mean is close to zero but whose standard deviation is 6 DU.

More significant errors are introduced if Langley plots are used on days of large temporal and spatial gradients in total ozone. At midlatitudes these are usually caused by strong jet streams leading to disturbances in tropospheric height as occurred once during the campaign, or by tropospheric folds. At high latitudes these are usually caused by overhead passage of a vortex boundary. On such a day, use of the slope of a Langley plot or its intercept will lead to large errors.

Acknowledgments. Thanks to J.-P. Pommereau and F. Goutail for useful discussions. This work was supported by the STEP-0013, SCUVS, and SESAME projects of the CEC, and by the U.K. Natural Environment Research Council. A. Sarkissian is a CEC Research Fellow.

References

Barlow, R.J., Statistics, John Wiley, New York, 1989.

Fiedler, M., H. Frank, T. Gomer, M. Haussmann, K. Pfeilsticker and U. Platt, The "Minihole" event on 6 FEB. 1990: Influence of Mie-scattering on the evaluation of spectroscopic measurements, *Geophys. Res. Lett.*, *20*, 959-962, 1993.

Goutail, F., J.-P. Pommereau and A. Sarkissian, Four years of ground-based total ozone measurements by visible spectrometry in Antarctica, *Proc. 1992 Quad. Ozone Symp. 602*, 1994.

Jones, A. E., H.K. Roscoe, A. Sarkissian, J.D. Shanklin, and E.W. Wolff, Year-round column ozone observations at 65° S: Validation and polar winter data, *J. Quant. Spectrosc. Radiat. Trans.*, *54*, 481-494, 1995.

Kyro, E., Intercomparison of total ozone data from NIMBUS 7 TOMS, the Brewer UV spectrophotometer and SAOZ UV-visible spectrometer at high latitudes observatory, Sodankylä, *Geophys. Res. Lett.* , *20*, 571-574, 1993.

Pommereau, J.-P., and F. Goutail, O_3 and NO_2 ground-based measurements by visible spectrometry during arctic winter and spring 1988, *Geophys. Res. Lett.* , *15*, 891-894, 1988.

Pommereau, J.-P., F. Goutail, M. Pinharanda, J. Piquard, and A. Sarkissian, Ground-based total ozone measurements in the visible Chapuis bands, *First European Workshop on Polar Stratospheric Ozone Research*, edited by Pyle J. and Harris N., Cambridge, pp. 41-44, 1991.

Roscoe, H.K., J.A.C Squires, D.J. Oldham, A. Sarkissian, J-P. Pommereau & F. Goutail, Improvements to the accuracy of zenith sky measurements of total ozone by visible spectrometers, *J. Quant. Spectrosc. Radiat. Trans.*, *52*, 639-648, 1994.

Sarkissian, A., Observation depuis le sol des nuages et des poussières dans l'atmosphère: Applications à la stratosphère polaire et à l'atmosphère de Mars, Thèse de Doctorat de l'Université Paris 6, 1992.

Sarkissian, A., D. Fish, M. Van Roozendael, M. Gil, H.B. Chen, P. Wang, J.P. Pommereau, and J. Lenoble, Ozone and NO_2 air-mass factors for zenith sky spectrometers: Intercomparison of calculations with different radiative transfer models, *Geophys. Res. Lett.*, *22*, 1113-1116, 1995a.

Sarkissian, A., H.K. Roscoe, and D. Fish, Ozone measurements by zenith sky spectrometers: An evaluation of errors in air-mass factors calculated by radiative transfer models, *J. Quant. Spectrosc. Radiat. Trans.*, *54*, pp. 471-480, 1995b.

Solomon, S., A. L. Shmeltekopf and R.W. Sanders, On the interpretation of zenith sky absorption measurement, *J. Geophys. Res.*, *92*, 8311, 1987.

Van Roozendael, M., M. de Mazière, and P. C. Simon, Ground-based visible measurements at the Jungfraujoch station since 1990, *J. Quant. Spectrosc. Radiat. Trans.*, *52*, 231-240, 1994.

Vauhan G., et al., An intercomparison of ground-based UV-visible sensors of ozone and NO_2, *J. Geophys. Res.*, this issue.

World Meteorological Organization (WMO), Scientific assesment of ozone depletion: 1994, *WMO Global Ozone Res. and Monitoring Project, Rep. N° 37*, World Meterorol. org., Geneva, 1994.

L.M. Bartlett, F.M. O'Connor, G Vaughan, Department of Physics, University of Wales, Aberystwyth SY23 3BZ, UK. (e-mail: gxv@aber.ac.uk)

D. G. Drew, Meteorological Office, Radiosonde, Kehelland, Camborne, Cornwall TR14 0DZ, UK.

P. A. Hughes and D. M. Moore, Meteorological Office, Bracknell, Berks, RG12 2SZ, UK.

A. Sarkissian, H.K. Roscoe, British Antarctic Survey, NERC, Cambridge CB3 0ET, UK. (e-mail: alain.sarkissian@aerov.jussieu.fr; hkro@bas.ac.uk)

(Received August 8, 1995; revised November 21, 1995;
accepted November 21, 1995.)

Atmos. Meas. Tech., 2, 319–326, 2009
www.atmos-meas-tech.net/2/319/2009/

Atmospheric Measurement Techniques

Water vapor total column measurements using the Elodie Archive at Observatoire de Haute Provence from 1994 to 2004

A. Sarkissian[1] **and J. Slusser**[2,*]

[1]LATMOS, CNRS UMR 8190, Université Versailles Saint-Quentin, Université Pierre et Marie Curie, Institut Pierre-Simon Laplace, 91371 Verrières-le-Buisson, France
[2]USDA, UV-B Radiation Monitoring Program, NREL, Colorado State University, Fort Collins, CO 80521, USA
[*]now retired

Received: 28 January 2009 – Published in Atmos. Meas. Tech. Discuss.: 15 April 2009
Revised: 23 June 2009 – Accepted: 25 June 2009 – Published: 7 July 2009

Abstract. Water vapor total column measurements at Observatoire de Haute Provence (5°42′ E, +43°55′ N), south of France, were obtained using observations of astronomical objects made between July 1994 and December 2004 on the 193-cm telescope with the high-resolution spectrometer Elodie. Spectra of stars, nebulae, and other astronomical objects were taken regularly during 10 years. More than 18 000 spectra from 400 nm to 680 nm are available on-line in the Elodie Archive. This archive, usually explored by astronomers, contains information to study the atmosphere of the Earth. Water vapor absorption lines appear in the visible in delimited bands that astronomers often avoid for their spectral analysis. We used the Elodie Archive with two objectives: firstly, to retrieve seasonal variability and long-term trend of atmospheric water vapor, and secondly, to remove signatures in spectra for further astronomical or geophysical use. The tools presented here (the workflow, the interoperable Elodie Archive and the web service Tellodie) are developed following, when possible, formats and standards recommended by the International Virtual Observatory Alliance.

1 Introduction

The Elodie archive is a database of high-resolution spectra of astronomical objects (spectral domain: 385 nm to 680 nm; sampling 0.005 nm; resolution: 0.0065 nm) obtained with the Elodie spectrograph on a 193-cm diameter telescope at Observatoire de Haute Provence (5°42′ E, +43°55′ N, altitude 681 m) from July 1994 to December 2004 (Moultaka et al., 2004). Note that Sophie spectrograph replaced the Elodie Spectrograph in July 2005 but the Sophie archive was not open when we started this work. More than 18 000 spectra of stars, galaxies, and other astrophysical objects are available in the Elodie archive (the ELODIE archive presently contains 34 992 spectra, among which 18 318 were public when we started this work), accessible using an online web service or php protocol. This database is updated regularly, when spectra with restricted access are opened to the community, or after updating the pipeline of the processing. The archive allows wider use of existing data sets, and this paper applies Virtual Observatory (VO) concepts of the workflow (Appendix A), see the International Virtual Observatory Alliance (IVOA, 2007) web site at http://www.ivoa.net/ and references therein for details. Initially developed for presentation to students using the "hot" theme of exoplanet search (Sarkissian, 2007), this tool is used here in geophysical application of the atmospheric water vapor budget.

The composition of the Earth's atmosphere is of great interest not only to atmospheric scientists but also to astronomers for whom the atmosphere is an annoyance to be removed in order to interpret astronomical observations without interference from terrestrial gases and aerosol. Intensive astronomical stellar spectroscopic observations began in the early 20th century. Fowle (1912) pioneered the determination of atmospheric water vapor from infrared absorption lines in the solar spectrum. Challonge and Divan (1952) pioneered the determination of atmospheric ozone from UV astronomical stellar spectral observations. We present a study of terrestrial atmospheric water vapor derived from astrophysical observations in the visible. Water vapor in the atmosphere has become increasingly important due to its strong feedback to global warming by man-made greenhouse gas

Correspondence to: A. Sarkissian
(alain.sarkissian@latmos.ipsl.fr)

emission. The involvement of water vapor in the stratospheric ozone equilibrium is related to tropospheric water vapor convection and troposphere-stratosphere exchanges. Water vapor in the atmosphere plays a crucial role since water vapor absorbs the longwave radiation of the Earth's surface. The amount of water vapor is expected to increase with temperature (Clausius-Clapeyron equation) so that a water vapor feedback can amplify global warming by anthropogenous greenhouse gas emissions. Long-term monitoring of atmospheric water vapor is mandatory for a better understanding and prediction of climate change (Held and Soden, 2000).

The current paper makes available water vapor column measurements from both recent and long term astrophysical observations. Common techniques to retrieve water vapor on site for astrophysical observations have always been without telescope dependent instruments, for instance: surface humidity sensors or precipitable water vapor sensor. Spectrometric observational methods are difficult, however, because line or band intensity and broadening depend on ambient temperature and pressure, requiring vertical profile rather than altitude on the line of sight, see Angione (1987), and references therein. We believe that this difficulty is now partly solved by improvement of spectral analysis techniques.

Measurements of water vapor by UV-visible spectrometers from the ground on direct sun, zenith sky, or from space on nadir sky has been demonstrated by Wagner et al. (2003). The most common method to measure atmospheric absorbants by UV-visible spectrometry is the Differential Optical Analysis Spectroscopy (DOAS), (Perner and Platt, 1979; Vaughan et al., 1997; Fayt and Van Roozendael, 2001; Sarkissian, 1992, 2000). Using Global Positioning System (GPS) and its signal time delay due to the atmosphere, one can make use of the satellite network of detectors and readily available handheld units to measure column water vapor (Bastin et al., 2005; Champolion et al., 2004). Infrared atmospheric sensors (Schneider et al., 2006), lidar (Hoareau et al., 2009), passive microwave radiometry (Westwater et al., 2005) and radio techniques also provide measurements of water vapor, vertical profiles or total amount. The existing network of these instruments, developed at the end of the last century for long term studies, will probably not grow to include more sites. The water vapor measurement presented here would continue to be available on-line at Tellodie web service (http://bdap.ipsl.fr/tellodie/, 2009) with regular updates (the Elodie full Archive, the Sophie Archive, etc.) to the scientific community.

The following section presents an overview of the spectral analysis. Section 3 presents the spectrum of the water vapor absorption cross-section. Section 4 describes in more details the spectral analysis, and Sect. 5 presents the results on 18 318 spectra. Description of a workflow in the VO is given in Appendix A.

2 Spectral analysis: overview

The spectral analysis has been specially developed for water vapor removal for future astrophysical use of the spectra. The authors' initial objective was to develop a spectral analysis to search water vapor signatures in external sources like exoplanets and bodies of the solar system. First analysis shows that water vapor signature in the visible in exoplanets is so tiny (optical thickness of 10^{-9} at most) that its detection is not possible with existing techniques, but in the infrared, water vapor, ozone and carbon dioxide absorption can reach a significant percentage, justifying development of this technique.

In atmospheric research, most spectrometric instruments use solar light as the source. The differential optical absorption spectroscopy (DOAS) method is used commonly for tiny absorptions because scattered light from zenith sky at twilight has path lengths up to 20 air masses (Sarkissian et al., 1995). Here, because the source is not always the same, the DOAS method cannot be applied and an absolute method had to be developed for Elodie. An example of a spectrum of the Elodie archive is presented in Fig. 2. The spectral range around 592 nm is displayed in Fig. 3. Not all astronomical spectra have as many visible absorption lines that are proper to solar type stars, here 51 Peg of spectral type G2. Some astronomical objects have only broad or a few lines visible, like hot O stars, or sometimes emission lines like nebulas. The wide range of sources make the spectral analysis more difficult, as we will discuss in the Sect. 5. If I_0 is the spectrum of the astronomical object outside the atmosphere, and taking into account the absorption by water vapor only, the Beer-Lambert law gives

$$I_{\text{observed}} = I_0 \times e^{-\tau_{H_2O}}, \quad (1)$$

where I_{observed} is the intensity of the observed spectrum and τ_{H_2O} the water vapor optical thickness in the observed spectrum. We called here our analysis an absolute method compared to the DOAS one because we compensate water vapor signature in the observed spectra adding a negative absorption (i.e. equivalent to an emission) at intensity levels instead of doing it at differential intensity level,

$$I_{0,\text{calculated}} = I_{\text{Elodie}} \times e^{+\tau_{H_2O}}, \quad (2)$$

where I_{Elodie} is the intensity (in counts) of the spectrum observed by the Elodie spectrometer, $I_{0,\text{calculated}}$ the spectrum calculated without water vapor signature and $+\tau_{H_2O}$, the measured water vapor optical thickness in the observed spectrum. Absolute methods are often used when signal-to-noise ratio of observation is so low that differentiation will generate too much noise for use. Because of the very high quality of spectra needed in astronomy, most spectra (up to 96.5%) were used in the analysis. Then, the amount of water vapor molecules in the line-of-sight of the observation, n_{H_2O}, is

obtained by

$$\tau_{H_2O} = \sigma_{H_2O} \times n_{H_2O}, \quad (3)$$

where σ_{H_2O} is the water vapor absorption cross-section, derivable by means of a line list (Fally et al., 2003) under consideration of instrumental and observational characteristics, as presented below.

3 Water vapor absorption cross-section

Building the spectrum of the water vapor absorption cross-section from the line list was made in two steps: first, building a very high resolution and over-sampled set of cross-sections that can be adapted, as a second step, to each Elodie spectra when making spectral analysis. The high resolution cross-section is then kept as an input for the spectral analysis. This approach is time consuming, but guarantees the accuracy of the final resolution reached. In our case, a water vapor absorption cross-section is calculated from the on-line list at http://www.ulb.ac.be/cpm (2007), of water vapor line parameters, from 26 000 to 13 000 cm^{-1} (respectively, 770 nm to 385 nm) measured at 291.3 K (Coheur et al., 2002; Fally et al., 2003), with a portable high-resolution (0.06 cm^{-1}) Fourier Transform spectrometer within a 602-m long absorption cell. Table 1 summarizes modifications applied to the original list to build water vapor cross-section for Elodie spectra. Water vapor lines have a Voigt profile dominated by self-broadening and air-broadening modulated by air temperature and pressure variability on the line-of-sight of the telescope. We used a Gaussian weighting function when building the water vapor cross-section, because during analysis, an empirical Gaussian fit had a lower residual compared to other simple convolutions (see Sect. 5 for explanation on residuals). We also noted that vertical retrieval of atmospheric pressure and temperature seems to be possible using the water vapor line shape at these wavelengths, something to be explored in the future (Liu et al., 2006). Also, wavelength shift is calculated during spectral analysis, and no corrections were made compared to vacuum values when building the cross-section. Fig. 1 shows atmospheric water vapor lines convoluted with a Gaussian of 0.2 cm^{-1} width sampled at 0.01 cm^{-1}. Markers indicate the spectral position and the intensity in the original list. This set, converted into wavelength scale, was used as the starting point for the analysis of all spectra. This high resolution cross-section is convoluted by a Gaussian of R_{H_2O} nm Half Width Half Maximum (HWHM), resampled at Elodie spectral sampling, i.e., at 0.005 nm (0.13 cm^{-1} at 590 nm) for each spectrum individually. R_{H_2O} varies during the spectral analysis in order to cover all possible resolutions for Elodie spectra, i.e., from approximatively 0.08 to 0.12 nm, see Table 2.

The wavelength range chosen for the analysis is 591.5 to 593 nm because it includes two water vapor triplets (see Figs. 3 and 4) and is easy to identify visually as well as through dedicated software. The choice of a narrow (few

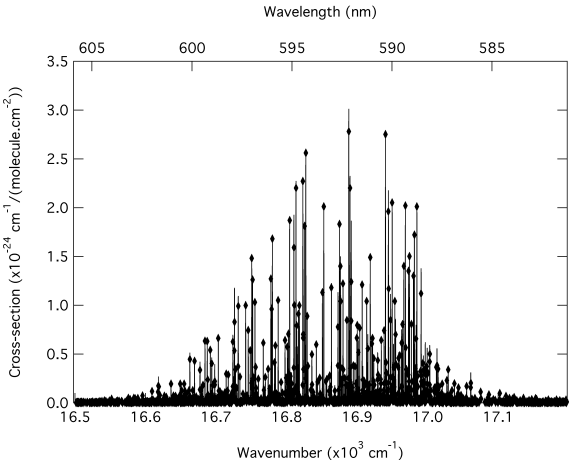

Fig. 1. H_2O absorption cross-section between 585 and 605 nm. The line list presented as markers is provided by Coheur et al. (2002) and Fally et al. (2003). The cross-section is calculated by convolution of the line list using a 0.17 cm^{-1} (0.0065 nm) HFWM Gaussian.

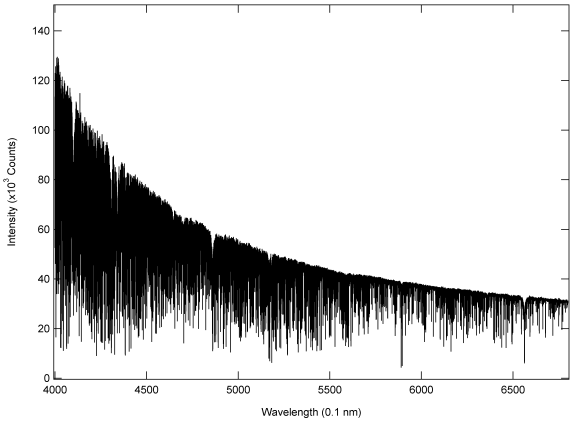

Fig. 2. Example of Elodie spectra: 51 Peg of spectral type G2 taken by Mayor and Queloz on 6 November 1995.

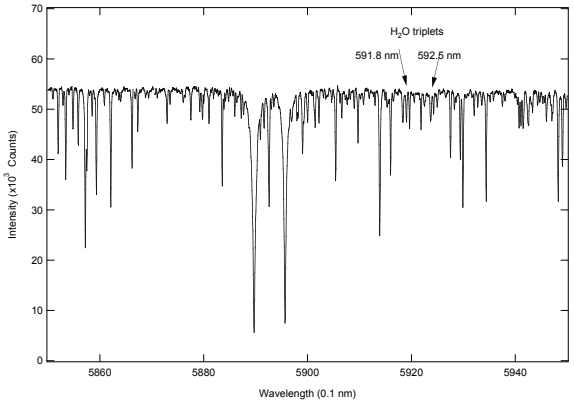

Fig. 3. Example of Elodie spectra (see Fig. 2), but focused on the water vapor absorption region at around 590 nm. Note the triplet at 591.8 nm, followed by the triplet at 592.5 nm.

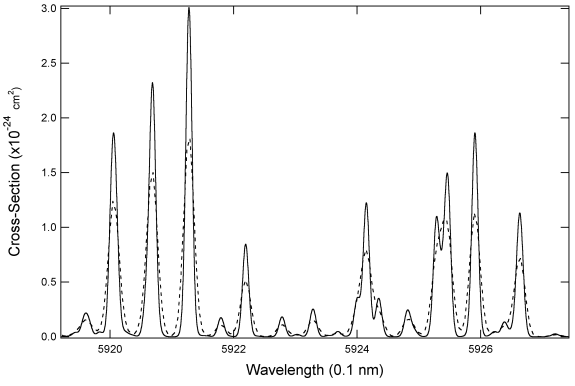

Fig. 4. H_2O cross-section (dotted line) resampled to Elodie HWHM (calculated from spectrum 199511060011 of 51 Peg) from initial cross-section (full line). Broadening and shift are calculated by minimizing the residual after substraction (see text).

Table 1. Resolution, sampling, and spectral shift of H_2O at 592 nm.

Source	Sampling	HWHM	Shift
Reims, provided (cm^{-1})	list	0.096	−0.03
Reims, convolved (cm^{-1})	0.01	0.17	0
Elodie, theoretical (cm^{-1})	0.14	0.18	−4.93
Reims, convolved (nm)	0.00035	0.0065	0
Elodie, theoretical (nm)	0.005	0.0065	−0.163
This analysis (nm)	0.005	0.0090	−0.164
Equivalent ($m \times s^{-1}$)	2532	3544	−83 050

Table 2. Results of spectral analysis on Elodie Archive, 18 318 spectra.

Value unit	Line-of-Sight amount 10^{22} molecule$\times cm^{-2}$	HWHM nm	Spectral Shift nm
Mean	6.00	0.00912	−0.163750
Minimum	0.00	0.00824	−0.16200
Maximum	20.00	0.01000	−0.16600
Step	0.02	0.00003	0.00002

nanometers wide) wavelength spectral range is due to the low probability of interference with similar intensity stellar spectral lines, as indicated by several runs made during analysis improvements. Also, the compromise between fast spectral analysis and the accuracy needed justifies such a narrow spectral range.

Saturation problems are common with strong water vapor absorption lines in the visible, and are usually corrected by a coefficient applied on the final result: a modified Langley technique (Michalsky et al., 1995; Wagner et al., 2003). Because the lines at 592 nm are so weak, our water vapor cross section are not corrected, and therefore do not take into account this effect. Discussion on this non-linearity of water vapor cross-section is in Sect. 6.

4 Observations

Observation of astronomical objects with Elodie, on the 193-cm telescope at Observatoire de Haute Provence at the south of France, started in July 1994 and ended in July 2005 when the Sophie spectrometer replaced Elodie (Moultaka et al., 2004). We analyzed the spectra available when we began writing this paper in December 2006. Spectra of stars, galaxies, and other astronomical objects were taken regularly each night when the sky was clear enough, over a 10-year period, and more than 18 000 spectra are available on-line for intensive use of the Elodie archive (which contains 34 992 spectra). The on-line data reduction procedure removes scattered light and makes spectral wavelength and relative flux calibrations. Spectra are stored in Elodie archive in FITS (Flexible Image Transport System) format, a standard data format used in astronomy, endorsed by NASA and the International Astronomical Union (2007, http://fits.gsfc.nasa.gov/). Observations have been made by numerous astronomers, but most necessary information has been stored in the archive (like the time of the observation needed for astronomers for variable processes, the air-mass factor of the line-of-sight needed for information of the amplitude of atmospheric absorption lines, etc.). Unfortunately, some parameters such as atmospheric pressure around the observation site and humidity were not recorded or measured during observations. However, the astronomical data are so well referenced and the procedures identified so that the homogeneity of the data set is conserved. This paper is a demonstration of such homogeneity because no normalization factors have been applied from one result to another, or from one period to another. An example of a spectrum of the Elodie archive is presented in Fig. 2. The spectral range around 592 nm is displayed in Fig. 3. Not all astronomical spectra have as many visible absorption lines that are proper to solar type stars, here 51 Peg of spectral type G2. Some astronomical objects have only broad or a few lines visible, like hot O stars, or sometimes emission lines like nebulas. The wide range of sources make the spectral analysis more difficult, as we will discuss in the next section.

5 Spectral analysis

Our spectral analysis is composed of cyclic procedures, varying spectral resolution of water vapor cross-section, spectral shift of water vapor cross-section and n_{H_2O}, the total column of water vapor molecules per surface area in line-of-sight for each individual spectra. One cycle is calculated for one set

of these three parameters only. Note that there is no convergence procedure, and all possible cycles were evaluated in sequence. At the end of the analysis of each spectrum, the water vapor calculated is removed from the spectrum, i.e., its spectral signature substracted from the initial spectrum. The quality of the spectral analysis can be evaluated by the presence of water vapor signatures in the obtained spectrum: an efficient spectral analysis should remove any water vapor signature.

A spectral shift of $\Delta\lambda_{H_2O}$ is also applied to convert vacuum wavelength into air wavelength. The Shannon scheme (Shannon, 1949) is built for interpolation of cross-sections, and the water vapor optical thickness τ_{H_2O} measured with the Beer-Lambert law for the observation allows us to deduce water vapor line-of-sight amount of water vapor,

$$n_{H_2O} = \frac{\tau_{H_2O}}{\sigma_{H_2O}}. \quad (4)$$

The best values of n_{H_2O} are obtained by minimizing residuals, i.e. minimizing the standard deviation of $\ln(I_{0,\text{calculated}})$ after removing water vapor from spectra. A high quality residual reaches 0.005 while a low quality spectrum, or a spectrum with a dominant non-water vapor absorption or emission line in the spectral domain, increases residual up to 0.3. Values higher than 0.1, representing 0.1% of the data, are rejected in this analysis.

Figure 4 (dotted line) shows a water vapor cross-section calculated for spectrum of 51 Peg (Fig. 5) taken on November 1995. Applied spectral shift is not visible at this scale. The amount n_{H_2O} calculated is 7×10^{21} molecule$\times$cm^{-2}, giving an optical thickness represented by the upper dotted line on Fig. 5. The lower dotted line shows the spectrum before subtraction of water vapor signature, i.e., before analysis. The full line shows the spectrum after subtraction of water vapor signature, i.e., after analysis. Water vapor total column, N_{H_2O} is obtained by:

$$N_{H_2O} = \frac{n_{H_2O}}{\text{AMF}}. \quad (5)$$

AMF is the air-mass factor of the observation, i.e., the ratio between line-of-sight air column and vertical column above the observational point, a value provided in the Elodie archive and equivalent to $1\div$ cosine of the source zenith angle for elevations larger than 20°. Note that for astronomers, objects are observed close to the meridian when possible, i.e. when the zenith angle is minimum. In present data set, less than 1.5% of observations are made at zenith angle higher than 70°.

6 Results and discussion

Results of the spectral analysis of all the spectra are summarized in Table 2, and values of N_{H_2O} are presented in Fig. 6. Mean value of the spectral shift measured during the analysis corresponds to the theoretical one presented in

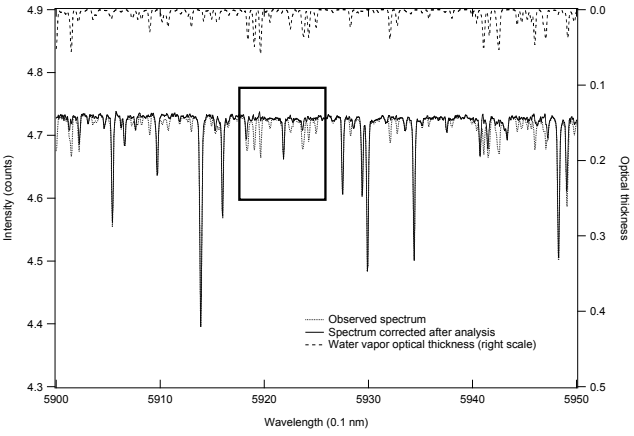

Fig. 5. Optical thickness of H_2O in Elodie spectrum 199511010018 (right scale, dotted upper line). Respectively, dotted and full lines, spectrum and spectrum corrected from H_2O absorption.

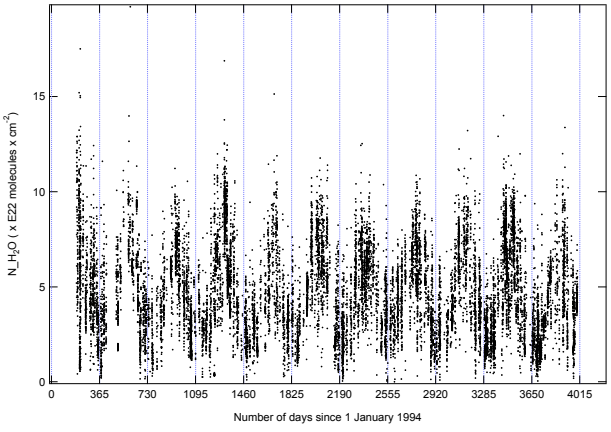

Fig. 6. Result of spectral analysis on 18 318 spectra of Elodie.

Table 1. Mean value of the HWHM measured during the analysis do not correspond to the theoretical one presented in Table 1 because atmospheric turbulences and effects on integration time and integration on the line-of-sight, i.e., with variable properties difficult to evaluate. The seasonal variation can be easily seen with higher values in summer and lower values in winter, an effect due to the variability of the dew point with atmospheric temperature. Sometimes, in winter, extremely low values are reached indicating the dryness of the atmosphere above Observatoire de Haute-Provence. For further interpretation, daily (nightly), weekly, and monthly means have been calculated from these results, as well as a simple sine curve fit (Fig. 7). A negative slope of $-0.44\pm0.24\times10^{22}$ molecule$\times$cm^{-2} per 10 years (i.e. -9.6% per decade) is obtained after removing the sine fit, indicating a not significant trend because it is not larger than two times its error. This is in agreement with the review of measured trends over Europe made by Morland et al. (2009). This negative slope might be introduced by the

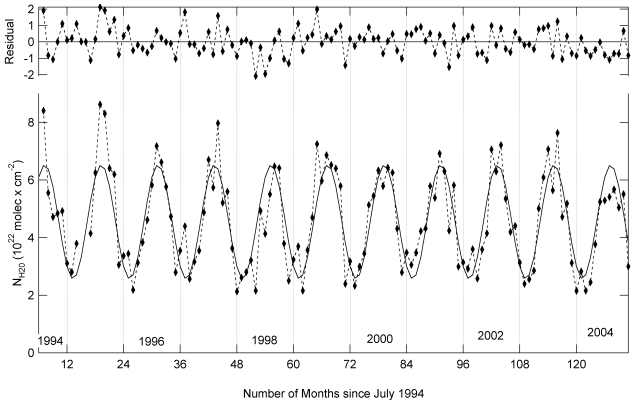

Fig. 7. H_2O monthly mean at OHP from 1994 to 2004 and a sine fit curve (dotted line) to show seasonal variation. The residual after subtraction of the sine fit, shown at the top of the graph, has a negative slope of $-0.44\pm0.24\times10^{22}$ molecule$\times$cm^{-2} per 10 years.

high summer values in 1994 and 1995. We believe that more detailled trend calculation, including seasonal trends calculations, could be made after we extend this analysis to the full Elodie Archive and to the Sophie Archive.

The first point for the discussion concerns the improvement of the building of water vapor cross-section, and its effect on error budget. Then, because most of the atmospheric parameters are not known, the retrieval process can be made using climatological atmospheric variability.

Secondly, saturation effects on strong absorption lines in the polyad 5ν range at 592 nm are not negligible and can reach up to 5% (Wagner et al., 2003). Such effects can be corrected by applying a linear correction factor depending on the quantity of water vapor, but we did not apply it at this stage. Our observations are made at low air-mass reducing enhancements of column amounts. Multiple scattering effects are reduced because astronomers make observations during clear skies. The spectral range chosen needs a lower correction factor than spectral ranges at higher wavelength. The very high spectral resolution of Elodie makes correction factor even lower than for low resolution instruments because individual lines are resolved. The amount of water vapor in the line-of-sight measured without correction is always lower than 30×10^{22} molecule$\times$cm^{-2}, and then saturation affects the linearity of Langley relation by less than 3% on less than 1% of all measurements, rending correction negligible when making monthly averages.

And thirdly, all observations are made at night during clear sky and it is possible that the water vapor trend estimation is biased.

In order to perform a validation of our measurements, they were used to calibrate lidar water vapor profiles obtained from May 1999 until December 2000 (Hoareau et al., 2009, as well as using radiosondes from Nîmes (the distance between OHP and Nîmes is less than 100 km). The calibration procedure uses the variance between radiosonde profiles and lidar profiles between 2 and 8 km calibrated with our total column values on available days of lidar observation. This variance (0.4 at 2 km, nearly 1 at 5 km, decreasing to $0.6\,g^2\,kg^{-2}$ at 8 km) is due to the natural time variability of atmospheric water vapor at these altitudes. The decrease of this variance by few (5 to 10) percent observed when using Elodie water vapor data gives information on the sufficient validity of our measurements, but we need more co-located and simultaneous observations for better validation.

Our workflow is developed in the frame of the Astronomical Virtual Observatory and is available online as a web service, with results in VOtable format ready for interoperability (http://bdap.ipsl.fr/tellodie/, 2009). The concept of interoperability is already difficult to develop for astronomy and is even more complicated in interdisciplinary research, but this study is a demonstration that science-driven application can be developed more easily when using tools and standards of the Virtual Observatory.

7 Conclusions

We have presented water vapor total column measured at Observatoire de Haute-Provence between 1994 and 2004 using the Elodie archive: 18 318 spectra obtained by the Elodie high-resolution spectrometer on the 193-cm telescope. Seasonal variability of water vapor as well as a preliminary study of its trend above the observatory was possible because of the high quality of the available data. Astronomy can provide valuable past and present observations useful for atmospheric science, and this should be explored further. The large number of spectral databases in astronomy and their covering time periods, starting at the beginning of the previous century gives perspectives for extension of this workflow to ozone in the visible and for NO_2 at around 430 nm. The next step is to explore water vapor line shape sensitivity to air temperature and pressure and to extend this analysis to the full Elodie Archive and to the Sophie Archive.

Appendix A

Workflow in the Virtual Observatory

The Virtual Observatory is comprised of a workflow consisting of a group of tasks involving one or more sources, which may include data banks, web services, etc. The simplest workflow for an instrument in modern astrophysics is a series of tasks, usually called a pipeline. A pipeline has its own local and fixed input and output parameters, fixed by instrument conditions, and does not interfere with or depend upon external programs, parameters, or data. This is the main difference from the workflow. Pipelines are needed because data sources are permanently in evolution (new observations,

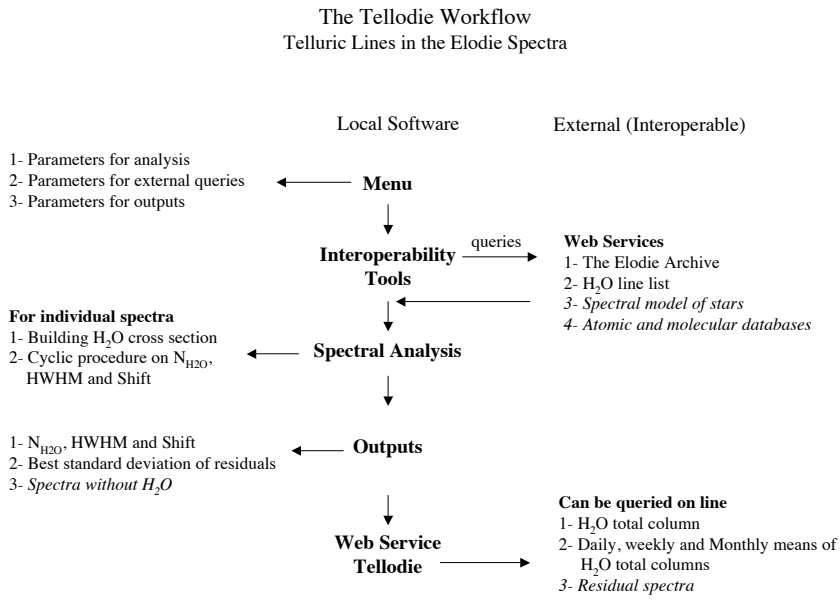

Fig. 8. Workflow diagram for derivation of water vapor from spectra. Options not used for this work are in italics.

improvement of a pipeline, update of available resources), whereas a workflow must integrate a complex approach of data treatment, including interactivity with other centers. Then, the interoperability between data centers, which is the basis of the Virtual Observatory, is the only way to make a reliable workflow. Not all the conditions of a workflow as defined by the Virtual Observatory, are present in our workflow, but we consider this a first step towards the minimum requirement.

The main goal of the workflow presented herein uses spectral analysis to retrieve amounts of trace gases. Although we focus on atmospheric water vapor, we can retrieve other gases such as NO_2 and ozone (Michalsky et al., 1995).

Our workflow is composed of four parts (Fig. 8): the menu, the search for sources (spectra, cross-sections, information on sources etc.), the spectral analysis, and the output. The menu is a user interface where one can select the type of workflow needed: some parameters like a selection of sources in time or high and low resolution analysis, and of course, the output format. Then, depending of selected parameters, the workflow searches for available components in an interoperable way. The search for sources is limited to the Elodie archive, but can easily be extended to other spectral archives. For example, a search for radial velocity variation studies is also plugged as an option, and this was the original objective during the initial development of this workflow. Today with limited options, our workflow will be extended and available as beta version to both astronomical and atmospheric communities. The main subject of this paper is the water vapor total column measurement whereas the spectral analysis contains several other outputs as well as a menu for input parameters. These are not presented in this study.

Acknowledgements. Thanks to IPSL for funding this study. Thanks to VO-France and VO-Paris Data Centre for support and advice in workflow development using interoperability concepts, useful for this paper. Thanks to Philippe Prugniel and Sergio Ilovaiski for their help in the use of Elodie Archive and to Manuel Pinaranda for his help in building a water vapor cross-section. Thanks to Philippe Keckhut and Albert Herzog for their usefull discussions about this work. Thanks to OHP and to all anonymous astronomers for their observations. And finally, thanks to the anonymous referees for their usefull comments.

Edited by: J. Staehelin

References

Angione, R. J.: Precipitable Water Vapor at Mount-Laguna Observatory, Publications of the Astronomical Society of the Pacific, 99(August), 895 pp., 1987.

Bastin, S., Champollion, C., Bock, O., Drobinski, P., and Masson, F.: On the Use of GPS Tomography to Investigate Water Vapor Variability During a Mistral/Sea Breeze Event in Southeastern France, Geophys. Res. Lett., 32, L05808, doi:10.1029/2004GL021907, 2005.

Challonge, D. and Divan, L.: Recherche sur les spectres continus stellaires, Ann. Astrophys., 15, 201–236, 1952.

Champollion, C., Masson, F., Van Baelen, J., Walpersdorf, A., Chery, J., and Doerflinger, E.: GPS monitoring of the tropospheric water vapor distribution and variation during the 9 September 2002 torrential precipitation episode in the Cevennes (southern France), J. Geophys. Res., 109, D24102, doi:10.1029/2004JD004897, 2004.

Coheur, P.-F., Fally, S., Carleer, M., Clerbaux, C., Colin, R., Jenouvrier, A., Mérienne, M.-F., Hermans, C., and Vandaele,

A. C.: New water vapor line parameters in the 26 000–13 000 cm^{-1} region, J. Quant. Spectrosc. Ra., 74, 493–510, 2002.

Coheur, P.-F., Clerbaux, C., Carleer, M., et al.: Retrieval of atmospheric water vapor columns from FT visible solar absorption spectra and evaluation of spectroscopic databases, J. Quant. Spectrosc. Ra., 82, 133–150, 2003.

Fally, S., Coheur, P.-F., Carleer, M., Clerbaux, C., Colin, R., Jenouvrier, A., Mérienne, M.-F., Hermans, C., and Vandaele, A. C.: Water vapor line broadening and shifting by air in the 26 000–13 000 cm^{-1} region, J. Quant. Spectrosc. Ra., 82, 119–131, 2003.

Fayt, C. and Van Roozendael, M.: WinDOAS 2.1 Software User Manual, BIRA-IASB, Brussels, Belgium, http://www.oma.be/BIRA-IASB/Molecules/BrO/WinDOAS-SUM-210b.pdf, 2001.

Fowle, F. E.: The Spectroscopic Determination of Aqueous Vapor, Astrophys. J., 35, 149–162, 1912.

Held, I. M. and Soden, B. J.: Water Vapor Feedback and Global Warming, Annu. Rev. Energ. Env., 25, 441–475, 2000.

Hoareau, C., Keckhut, P., Sarkissian, A., Baray, J.-L., and Durry, G.: Methodology for Water monitoring in Upper Troposphere with Raman Lidar at Observatory of Haute-Provence, J. Atmos. Ocean. Tech., in press, doi:10.1175/2009JTECHA1287.1, 2009.

Liu, X., Chance, K., Sioris, C. E., Newchurch, M. J., and Kurosu, T. P.: Tropospheric ozone profiles from a ground-based ultraviolet spectrometer: a new retrieval method, Appl. Optics., 45, 2352–2359, 2006.

Morland, J., Collaud Coen, M., Hocke, K., Jeannet, P., and Mätzler, C.: Tropospheric water vapour above Switzerland over the last 12 years, Atmos. Chem. Phys. Discuss., 9, 7239–7271, 2009, http://www.atmos-chem-phys-discuss.net/9/7239/2009/.

Michalsky, J., Liljegren, J., and Harrison, L.: A comparison of sun photometer derivations of total column water vapor and ozone to standard measures of same at the Southern Great Plains Atmospheric Radiation Measurement site, J. Geophys. Res., 100(D12), 25 995–26 003, 1995.

Moultaka, J., Ilovaisky, S. A., Prugniel, P., and Soubiran, C.: The ELODIE Archive, Publications of the Astronomical Society of the Pacific, 116, 693–698, 2004.

Perner, D. and Platt, U.: Detection of nitrous acid in the atmosphere by differential optical absorption, Geophys. Res. Lett., 6, 917–920, 1979.

Sarkissian, A.: Observation depuis le sol des nuages et poussières dans l'atmosphère: Applications à la stratosphère polaire et à l'atmosphère de Mars, Ph.D. thesis, 1992.

Sarkissian, A., Fish, D., Van Roozendael, M., Gil, M., Chen, H. B., Wang, P., Pommereau, J. P., and Lenoble, J.: Ozone and NO−2 air-mass factors for zenith-sky spectrometers: Intercomparison of calculations with different radiative transfer models, Geophys. Res. Lett., 22(9), 1113–1116, 1995.

Sarkissian, A.: Monitoring Stratospheric Constituents by Ground-based UV-visible Dobson and SAOZ spectrometers, European Research Courses on Atmosphere, edited by: Boutron, C., Volumn 4, Chapter X, 179–194, 2000.

Sarkissian, A.: Workflow for fast and simple analysis of Elodie spectra, invited paper at EPSC 1, Berlin, Germany, 18–22 September, 2006.

Sarkissian, A.: Détection de planètes extrasolaires par la méthode des vitesses radiales, in: Les Cahiers Clairaut, n 117, edited by: Paturel, G., Printemps, 2007.

Schneider, M., Hase, F., and Blumenstock, T.: Water vapour profiles by ground-based FTIR spectroscopy: study for an optimised retrieval and its validation, Atmos. Chem. Phys., 6, 811–830, 2006, http://www.atmos-chem-phys.net/6/811/2006/.

Shannon, C. E.: Communication in the presence of noise, Proc. Institute of Radio Engineers, 37(1), 10–21, 1949.

Tellodie: Telluric lines in the Elodie archive, Sarkissian, http://bdap.ipsl.fr/tellodie/, 2009.

Universite Libre de Belgique: Service de Chimie Quantique et Photophysique, http://www.ulb.ac.be/cpm/, 2007.

Vaughan, G., Roscoe, H. K., Bartlett, L., O'Connors, F. M., Sarkissian, A., Van Roozendael, M., Lambert, J.-C., Simon, P. C., Karlsen, K., Kastad Hoskar, B. A., Fish, D. J., Jones, R.L., Freshwater, R., Pommereau, J.-P., Goutail, F., Andersen, S. B., Drew, D. G., Hughes, P. A., Moore, D., Mellqvist, J., Hegels, E., Klupfel, T., Erle, F., Pfeilsticker, K., and Platt, U.: An intercomparison of ground-based UV-visible sensors of ozone and NO_2, J. Geophys. Res., 102, 1411–1422, 1997.

Wagner, T., Heland, J., Zöger, M., and Platt, U.: A fast H_2O total column density product from GOME -Validation with in-situ aircraft measurements, Atmos. Chem. Phys., 3, 651–663, 2003, http://www.atmos-chem-phys.net/3/651/2003/.

Westwater, E. R., Crewell, S., and Mätzler, C.: Surface-Based Microwave and Millimeter Wave Radiometric Remote Sensing of the Troposphere: a Tutorial, IEEE Geoscience and Remote Sensing Society Newsletter, 134, 16–33, 2005.

Infrared Physics & Technology xxx (2009) xxx–xxx

Contents lists available at ScienceDirect

Infrared Physics & Technology

journal homepage: www.elsevier.com/locate/infrared

Brightness temperature of synchronic exoplanets measured by infrared photometry from the ground: Method and perspective

Alain Sarkissian *

Université Versailles St-Quentin, UPMC Univ. Paris 06, CNRS/INSU, LATMOS-IPSL UMR 8190, Route des Gâtines, 91371 Verrières-le-Buisson, France

ARTICLE INFO

Article history:
Received 23 June 2009
Available online xxxx

PACS:
97.82.−j
42.68.−w
95.85.−e

Keywords:
Exoplanet
Mid-infrared
Earth's atmosphere
Differential photometry

ABSTRACT

We explore a method to measure the temperature at the surface of "hot Jupiter" type exoplanets by relative photometry in the infrared at around 10 μm in N spectral band. The method is described and validated by numerical simulations. Thermal radiation from an exoplanet and its parent star are analysed. Geometrical configurations of extra-solar planet rotating synchronously around parent star are explored for a feasibility study of the detection. A Jupiter size planet in orbit at 0.025 astronomical unit from Sun-like parent star should have a harmonic signature of up to 0.2% in amplitude with a period of the planets orbital duration. Such a signature is difficult to detect when making absolute measurements, but by differential methods of analyses, and using a radiative transfer model to take into account background sky contribution of the Earth's atmosphere, this relative accuracy can be reached. Some results of simulations of observation are also presented.

1. Introduction

Discovery of extra-solar planet around main sequence star 51 Pegasus in 1995 by Mayor and Queloz [1] intensified developments of new studies in this new field of astronomy because of the obvious links to planetary system formation, atmospheric and geophysical sciences, and detection of extraterrestrial life [2]. State of the art observational techniques such as interferometry and adaptative optics are now intensively used from the ground and will soon be used from space to improve direct detection of extra-solar planetary systems (see for example reviews [3 or 4]). Also, detection of water and oxygen outside our solar system became a priority recently because of their role as chemical basis of extra-solar life [5]. Finally, the topic of this paper, determination of physical properties of exoplanets is a challenging issue because we need constraints for our planetary models to understand formation and evolution mechanisms, and we need information on the atmosphere and surface of planets to evaluate the possibility of life.

Observation in the infrared is in intensive development for observations of interstellar and interplanetary mediums. Planets in our solar system have surface temperatures from 60 K to 700 K and the maximum black body emission for these temperatures falls in the mid-infrared region. Observation in this spectral range is more suitable than in the visible [6], but the brightness of the parent star remain a problem as well as the low accuracy of absolute measurements in this spectral range. Developments of observational tools in the infrared should be completed with improvement of detection method adapted to extra-solar planets observation to achieve measurements of the surface brightness temperature of extra-solar planets.

Observation in the middle infrared allows brightness temperature measurements of a planet, which is an important parameter because it provides information on life feasibility at the surface of the planet and indicates the possibility of an atmosphere, depending of orbital conditions. Observation of astronomical bodies in the infrared is planned and already operational within European and international projects like TIMMI2 and VISIR at ESO, La Silla, Chile, and also more recently with HARPS [7,8]. Mostly oriented toward planet formation purposes, these experiments are open for proposal and the availability of these large telescopes provide access to detection of exoplanets with techniques that are complementary to the radial velocity method, such as the one presented here. The main goal of this paper is to show that the mid-infrared spectral range is suitable for extra-solar planet detection, as well as for determination of their physical parameters. I will describe our proposed method of detection of exoplanets and retrieval of thermal surface properties of exoplanets, assuming orbital parameters are known from the radial velocity method. The objective of this paper is not to compete with existing detection methods, but to open a new area for determination of their properties, not explored extensively until now, in order to

* Tel.: +33 (0)1 64 47 43 02; fax: +33 (0)1 69 20 29 99.
E-mail address: alain.sarkissian@latmos.ipsl.fr.

1350-4495/$ - see front matter © 2009 Elsevier B.V. All rights reserved.
doi:10.1016/j.infrared.2009.11.005

increase the number of physical parameters of planets we can observe.

After a presentation of the method, I will present the general conditions taken into account in the simulations, followed by computation of observational parameters concerning the brightness of the extra-solar planet and parent star system. Then I will make a sensitivity study to identify atmospheric parameters important for ground-based observations in the infrared, followed by a feasibility study of infrared observation from the ground. The conclusion of this work will indicate the perspectives of the presented method.

The surface of an exoplanet indicates here the dominant emissive layer of the exoplanet in the infrared, being gaseous, liquid or solid: formation and possibility issues are not the topic of this paper and are not determinant in the simulations and are almost unknown for "hot Jupiter" like exoplanets.

2. General approach

Seen from the Earth in an orbital plane parallel to the line-of-sight, a planet rotating around its parent star shows alternatively its day and night faces. For extra-solar planets detected recently, most of them are so close to the parent star that they are thought to be dynamically locked because of tidal forces [9] and should have synchronic rotation around the parent star. This will produce a large gradient of temperature between night and day sides because the main source of heat for the planet is its parent star irradiance (see Fig. 1).

The surface temperature of the planet depends mainly on its surface and atmospheric thermal properties: thermal emission, thermal conduction. Transport in the atmosphere or ocean also affect thermal budget and therefore temperature. An atmosphere modifies the net thermal budget because of absorption and reflectivity, and because of dynamic transport from cold to warm sides, reducing the thermal gradient [10–13]. The goal is to enhance the measurement possibilities using the thermal differences between day and night sides seen alternately from the Earth because of the orientation of the line-of-sight, with a period corresponding to the period of the planet rotation around the parent star (see Fig. 1). Similar techniques but using transiting exoplanets during secondary eclipse have been proved efficient to measure thermal emission from space, but restricted by the low probability of such event [14,15].

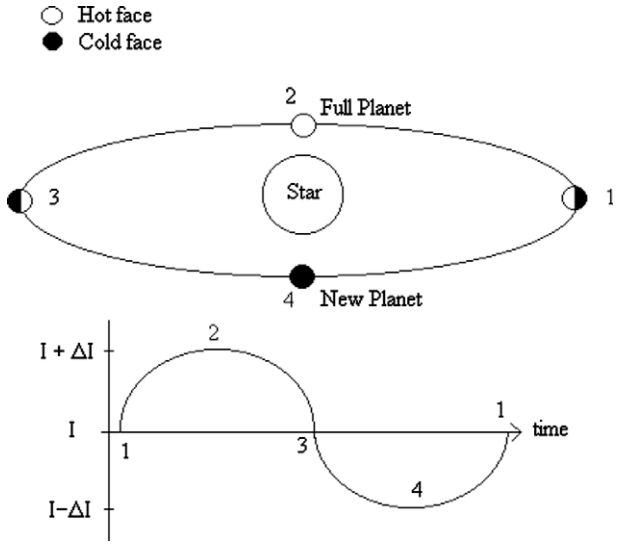

Fig. 1. Extra-solar synchronic planet and its parent star seen in the infrared from the Earth.

Another important point for the proposed method is based on data analysis using relative methods and multi-parameters analysis. For infrared observations from the ground, absolute measurements are difficult because (i) the Earth's atmosphere itself is a dominant source at these wavelengths, (ii) the optical thickness of the atmosphere is varying rapidly at these wavelengths due to aerosol and water vapour, CO_2 and ozone content in the gas phase, and (iii) the need for a reference star or source (which are infrequent, see catalogue at La Silla Observatory web site for example, www.ls.eso.org) which makes observational conditions even more difficult. We propose to study the relative variation in time, of several mid-infrared windows, one more sensitive to relatively high temperatures (i.e. shorter wavelength) and the other more sensitive to cooler temperatures (i.e. longer wavelength). Clearly, if we have the possibility to separate individual contributions: atmospheric radiance and transmission, telescope radiance, and source radiances in term of individual measurements at different wavelengths, then, our experience in statistical analysis indicates that the relative accuracy can be improved significantly [16,17]. For example, trend analysis in ozone or atmospheric temperature uses efficiently such techniques to detect harmonic signatures even on top of a very high constant signal even when measured with large uncertainties [18–20].

The general approach of our proposed method is composed of four points:

(1) To make measurements in a spectral range where planets thermal emission is maximum.
(2) To have enough sensitivity for detection from the ground.
(3) To use relative and differential measurements to be freed from absolute calibrations.
(4) To search for harmonic variation in the signal seen from the Earth during planets (known) rotation around parent star.

These four points determine partly the general conditions chosen in the next paragraph and for the observational technique presented in this paper.

3. Brightness temperature of synchronous exoplanets

In this paper, calculations are made assuming a Jupiter size planet rotating synchronously around a parent star with similar spectral type G4 at emission temperature of 5700 K and Sun-like size. Also, we will assume that all bodies presented here are black or grey and follow the Planck emission relationship. Surface thermal properties of the exoplanets are assumed homogeneous with a visible albedo of 0.07 and an emissivity of 0.9 in the infrared. These values are in agreement with ISO-SWS observations of cloud free Jupiter at 10 μm [21] chosen because these parameters are not measured yet for "hot Jupiter" like exoplanets. Heating internal sources are neglected and internal heat flow from the core to the surface, which is negligible on Earth (few mW/m^2) compared to solar irradiance (1367 W/m^2), will also be neglected [22]. Discussion on the age of the observed planetary system is then excluded at this stage.

The temperature at the surface of a planet is determined by its parent star irradiance on the day side and on thermal cooling properties on the dark side. On bodies without atmosphere or oceans, these effects are straightforward, not being perturbed by thermal convection and transport. Synchronic planets have the local star zenith angle always the same at the same location and therefore constant irradiance, leading to nearly stationary thermal state unless large eccentricity of the orbit. On the dark side of the body the temperature of the surface depends of its radiative cooling and thermal conductive properties. On the day side of the planet, the parent star permanent irradiance will determine surface temperature, limited by radiative cooling and at lower level internal ther-

Please cite this article in press as: A. Sarkissian, Brightness temperature of synchronic exoplanets measured by infrared photometry from the ground: Method and perspective, Infrared Phys. Technol. (2009), doi:10.1016/j.infrared.2009.11.005

mal conductivity. Also, diurnal variation is fast enough for the thermal wave to propagate to few meters or less from the surface only. Note that taking into account model calculations using high resolution thermal conductivity for Mercury does not modify significantly our results because surface day side temperature is dominated by surface layer thermal radiance [23]. Another point re-enforcing the temperature difference between hot and cold faces, thermal conductivity at the sub-surface should not play a determinant role due to the existence of a gas phase instead of solid phase, because for the same reason as for the atmosphere, the distances are so large that there is not enough time for mass transfer unless unrealistic dynamical consideration are assumed [24,25]. The planetary orbital plane is assumed to be in our line-of-sight except when indicated. Dark sky (3 K) and zodiacal light (280 K, $\tau = 3e^{-8}$ [26]) in the visible radiation is neglected because they can be assumed to be constant in (relatively short) time on the line-of-sight, removed when using a relative method. Reflections and radiation from hypothetical nearby cold bodies (satellites, other planets, other bodies) are neglected because of the weakness of the signature. The length of the orbit of the planet around the parent star is usually small (less than one astronomical unit) compared to the distance of the system to the Earth (several parsecs) and variation of radiance due to distance variation is also neglected. The scintillation limit has no significant effect for such calculations because angular resolution is not needed for the method. Reflected light from the star on the planet is not taken into account because the dilution factor acts twice. Even so, because the effect is similar to the thermal variation in term of period and phases of the planet, it enhances the detection possibility having the same sign and amplitude complicating only the interpretation of observations.

The calculated temperatures for selected distances to the parent stars are 1605 K at 0.025 a.u., 1135 K at 0.05 a.u., 803 K at 0.1 a.u., 508 K at 0.25 a.u., 359 K at 0.5 a.u. and 254 K at 1 a.u. Using theses results, we assume for the rest of this paper a temperature of 1500 K for the exoplanet. Then radiation is computed using Planck's black body formula. Results are shown in Fig. 2 for simulations at 5, 10 and 18 μm, selected because they are atmospheric windows for observation. The relative radiance enhancement shown during the orbital period of the planet indicates clearly what performance we need to achieve for planet detection using photometry in the mid-infrared region. Here, the sky background and the telescope contributions are not included in calculations for clarity. The signal (exoplanet) to be detected from the photometric observation at 5, 10 and 18 μm is at 0.14%, 0.2% and 0.25% respectively. This is the amplitude of an oscillation to be detected on top of a large signal (exoplanet + star). Our objective is to study the possibility of detecting such low amplitude harmonic variation in the infrared or to find some analytical technique to highlight such a signature. Using channels at larger wavelengths increases the detection possibility. For this reason, study of ground-based observations in atmospheric windows at wavelengths 5 μm is not pursued in this paper and enhanced study will be made for windows at 10 and 18 μm.

4. Sky radiance and transmission at Observatoire de Haute-Provence

Simulations of the zenith sky radiance $Rad_{ModTran3}$ and transmission $Trans_{ModTran3}$ at ground-level in the spectral band from 6 to 30 μm have been made using ModTran3 online software of the University of Chicago, Department of the Geophysical Sciences, courtesy of David Archer. Density, temperature, ozone, carbon dioxide, water vapour and atmospheric background aerosol profiles are taken from Handbook of Geophysics [27] for mid-latitude in winter, here and after called the reference "REF" simulation for observations above Observatoire de Haute-Provence (OHP, South of France). Note that well known recent evaluations of trends at mid-latitude for carbon dioxide (330 ppm in the simulation, nearly 370 ppm now), methane (increase from 1700 ppt in the model to 1745 now), ozone (decrease of stratospheric ozone, increase of ozone in the troposphere) and temperature are not included in simulations at this stage (see [28] and references therein for review).

Sensitivity to atmospheric changes has been made applying 10% variation from each reference profile independently and assuming the linearity of the effects in considered intervals. Effects on radiances are dominant (from −20% to +30%) compared to the effects on transmission (−4% to +3%) . Small changes of ground-level temperature and high altitude cloud's optical thickness have dominant effects, followed by H_2O.

Sensitivity to atmospheric changes of temperature and water vapour has been made applying variations from the reference profiles independently and assuming the linearity of the effects in considered intervals. The effects of temperature variations from −10 K to +10 K compared to the reference profile indicate that radiances increase with temperature at all wavelengths and on linear way with coefficients depending of the spectral range selected (see Fig. 3). Note that we found a linear fit of 1.3% per Kelvin demonstrating the linearity of this dependance with high accuracy, with a χ^2 of 3×10^{-5}.

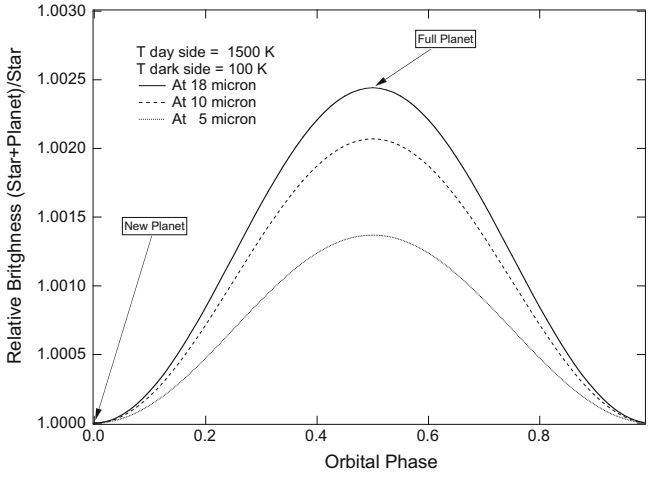

Fig. 2. Relative variation of the brightness of the system Sun-like parent star and Jupiter size planet at 1500 K on daily side and 100 K on night side, at 5, 10 and 18 μm during planet rotation around parent star. Zero phase correspond to the planet been between the star and the Earth, point 4 of Fig. 1.

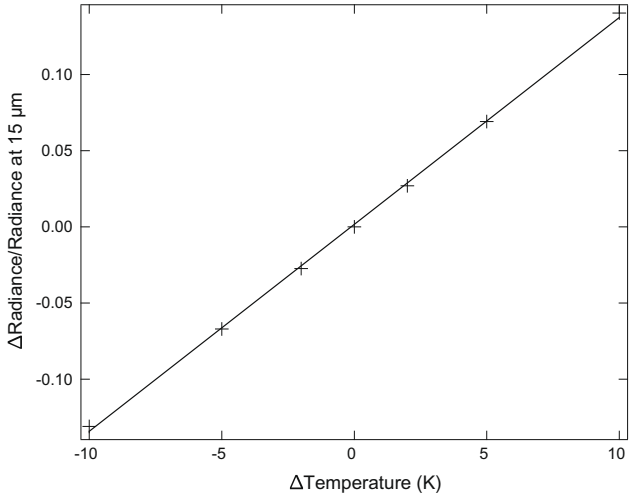

Fig. 3. Linearity of the relative radiance variation at 15 μm with changes of ground-level temperature (crosses) and its linear fit (line).

Please cite this article in press as: A. Sarkissian, Brightness temperature of synchronic exoplanets measured by infrared photometry from the ground: Method and perspective, Infrared Phys. Technol. (2009), doi:10.1016/j.infrared.2009.11.005

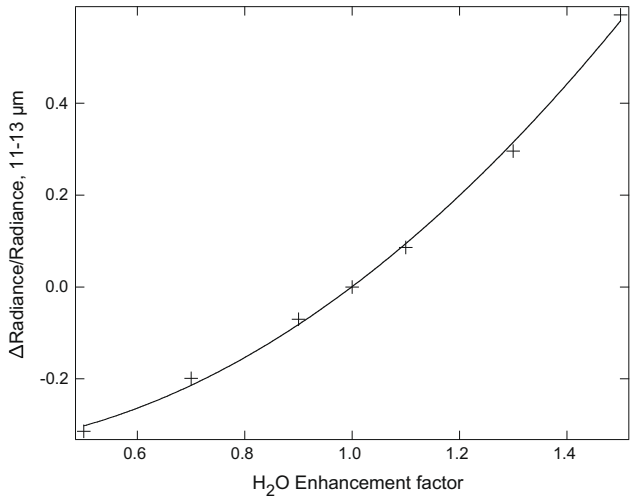

Fig. 4. Relative effect of the water vapour scaling factor from standard dry profile on zenith sky relative radiance from 11 to 13 μm (crosses) and its polynomial fit (line).

We also studied the sensitivity of the radiances to water vapour changes by a scaling factor on the total column. Values of the scaling factor are taken arbitrarily from 0.5 to 1.5 compared to the reference profile. The 15 μm channel is not affected by these variations, but 8 μm, 12 μm and 18 μm channels are affected on a linear scale with H_2O amount. Also, the channel near ozone band at 9.5 μm is less affected than the previous channel, by one order of magnitude.

Fig. 4 shows the relation between the change in water vapour enhancement factor and relative effect on radiance in the 11–13 μm window. A change of 10% of the water vapour mixing ratio around REF (dry) profile provides a relative change of 8.6% of the radiance in this spectral range. Similar effects are obtained in the 8–9.5 μm and 17.5–21 μm windows (not shown). The χ^2 of 1×10^{-3} of the polynomial fit shown in the figure indicates the reliability of the relationship, and of course the possibility to use simultaneously the previously indicated channels for multi-correlative study of atmospheric water vapour variability, and therefore for a better evaluation of atmospheric radiance and transmission at these wavelengths. Then clearly, a first approach of the relative method should be to test the possibility to reduce temperature and aerosol effects from measurements at 15 μm, to deduce water vapour variation using a channel at say 19.0 μm and to search for the thermal signature of the exoplanet in the 8–9 μm and 10.2–13 μm channels. Note that the signature of the parent star, assumed constant in time, should be removed by differential analysis, leading to the exoplanet's signature only. A validation of this technique can be made only with simultaneous observations in the indicated channels and using multi-correlation analysis. Note that such a differential method is commonly used for satellite measurements of tropospheric CO_2, aerosol and water vapour in the infrared (Chédin, personal communication), as well as for stratospheric ozone and aerosol retrieval (TOVS, TOMS, etc...). Also, using simultaneous atmospheric measurements should be necessary to validate such technique as well as to evaluate atmospheric variability during measurements. These are presented in the next section.

5. Facilities at Observatoire de Haute-Provence

Observatoire de Haute-Provence (OHP) is located at 650 m altitude, 44° Latitude North and 5.7° Longitude East. This is an ideal site to develop or to improve a method to reduce astronomical observations using geophysical data because both stations are on the same location. We dispose of several lidars (light detection and ranging) at the geophysical station able to retrieve vertical profile of constituents from the ground to 100 km [29]. The lidar is an active remote sensing instrument similar in principle to the radar but operating in the optical range: backscattered light is recorded with high temporal resolution, allowing ranging, i.e. vertical profiling with altitude equivalent to half the path of the light (h = c.t/2). Depending on the desired measurement, lidar systems use various light-matter interactions such as Rayleigh, Mie and Raman scattering or fluorescence. Measurements of atmospheric ozone are made using the differential absorption laser technique (DIAL) at two wavelengths; temperature measurements can be made using the Rayleigh and Raman processes at one of several wavelengths; and aerosol (including cirrus and sub-visible cirrus clouds) can be retrieved from Mie scattering. Experimental extension provides H_2O, NO_2 and CO_2 and all these measurements are made for long term study with state of the art techniques and analysis procedures in the frame of the Network for the Detection of Atmospheric Composition Change (NDACC), the international network of high quality remote-sounding research stations. Lidars are providing vertical profiles of constituents at very high vertical (from 0.2 to 1 km) and temporal resolution (one profile every 2–20 s) during the night. Profiles can be summed for longer integration time or for statistical studies. Complementary measurements of ground-level ozone, temperature, humidity, water vapour, and pressure are made permanently at the station [17,30].

The need for geophysical parameters is justified by two reasons: first, we need to identify a perfectly stable night in term of IR sky radiance, and a satellite cloud-less instant map, taken usually every 30 mn, is definitively not enough for our study. Sub-cirrus clouds for example, frequent at OHP but also all around the world so seriously affect the radiance that a selection of cloud-less nights would reduce observation possibility to few nights a year [31]. Sub-cirrus clouds are highly variable and appear nearly every night with duration of few minutes to few hours. For a wind of 30 m/s at 10 km (tropopause level and jet stream [27]), this will suppose an extension of 60° at zenith i.e. 40° from the horizon for 10 mn, indicating the time interval needed for non-perturbed observations. Obviously we would select sub-cirrus free periods of a few minutes during the night. Secondly, the vertical profiles provided by the lidars can be used to simulate infrared radiances from the sky and therefore to reduce observation. In that case, we have calculated the impact of variations of atmospheric components to sky radiance using a ModTran3 utility. Table 1 provides results of simulations using available literature or direct observations on OHP real-time lidar profiles (courtesy of Philippe Keckhut) for 10 mn exposure or integration time. For CO_2, we found that a variability of 0.1% during a unpolluted period is large enough to be in agreement with calculated daily changes <0.5% observed in similar condition [32]. Development of a CO_2 channel on OHP lidar in the near future

Table 1
Relative uncertainties of the zenith sky infrared irradiance and transmission calculated for OHP, and the net effect evaluated using common relative variability on total columns. Values are all in %. Calculations are made using ModTran3 radiative transfer model (courtesy of David Archer from University of Chicago) and vertical profiles from the Handbook of Geophysics [27].

Constituent	H_2O	CO_2	O_3 T	O_3 S	Sub-cirrus	T	Total
Variation (%)	+1	+0.1	+1	+1	+1	+0.1	
Radiance	+0.35	+0.047	+0.02	+0.02	−0.87	+0.63	1.13
Transmission	−0.06	−0.014	−0.0056	−0.017	+0.095	−0.085	0.14
Net	+0.29	+0.33	+0.0146	+0.003	−0.775	+0.545	**1.04**

Please cite this article in press as: A. Sarkissian, Brightness temperature of synchronic exoplanets measured by infrared photometry from the ground: Method and perspective, Infrared Phys. Technol. (2009), doi:10.1016/j.infrared.2009.11.005

will help to demonstrate locally such variability. For tropospheric and stratospheric ozone lidars and ground-level sensor, the absolute accuracy is 4% and the relative accuracy of the profiles is <1% because most of the sources of errors are systematic (error in cross-sections, laser beam and collecting mirror parallelism, standard background aerosol in lidar equation). The H_2O lidar is still in an experimental phase at OHP [17], but we believe that when available, the relative accuracy of the tropospheric profile combined with the meteorological station humidity information (due point sensor) will provide a 1% relative accuracy for dry winter cold, cloud free nights. For temperature and aerosol profiles, the expertise at the OHP station has been a determinant for the selection of the observatory and value of 0.1% for temperature (i.e. 0.273 K) and 1% for sub-cirrus optical thickness relative uncertainties are realistic for durations of 10 mn. Note these results are for zenith sky observations and a coefficient of 1/cos(RA) must be applied, where RA is the right ascension of the line-of-sight affecting the results by 10% at 25° solar zenith angle (SZA) and by 30% at 45°*SZA*. Also, background aerosols are included in the calculations but not their variations within 10 mn. This effect depends of the temperature at the altitude of the aerosol variation, but within 10 mn of a clear dry, cloud free winter night, it should be less than 1%.

6. Feasibility study for high accuracy IR photometry on 1.2 m telescope at OHP

In this part, the objective is not to demonstrate the feasibility of exoplanet detection, but to study the feasibility of accurate measurements in the IR with dedicated instrumentation. At this stage, absolute simulations are made without assumption on the efficiency of relative and multi-parameters methods. Conditions to make measurements on a bright star with the 120 cm telescope at OHP will be presented and evaluated to prepare exoplanet detection presented in next section.

Measurements from 7 to 21 μm are planned to be made using a HgCdTe Judson commercial detector with an area of 250 μm × 250 μm (S_{Det}), a field of view of 10° (Ω_{Det}), cooled with liquid nitrogen at 77 K. The electric noise of such detector for the higher shutter frequency of 1000 Hz is 1.26×10^{-9} V/Hz$^{1/2}$, the responsivity 1.5×10^4 V/W, validated in our laboratory, and the sensitivity curve versus wavelength (around 90 in our spectral range) are provided by the commercial.

The OHP telescope used for simulation here and for measurements in the future, has a diameter of 120 cm and a Newton focal plane at 7.2 m. The field of view on the detector, with a scale of 35 μm per ″ corresponds to 7″ × 7″. The impulse response of the telescope or Airy function at 10 μm is 3.3″ . Calculation are made here integrating the field of view on this surface. The secondary mirror is supposed to radiate at 273 K (0 °C) at OHP and at −20 °C at 4000 m in winter, to have a very low infrared emissivity as newly alumined, and to fill into the field of view of the detector, occulting the telescope's walls. The reflectivity of the mirror is assumed to be 1 in the infrared.

Fig. 5 (upper panel) shows results of our calculations for an integration time of 10 mn on the star Alpha Bootis. Calculations have been made using black body radiation at 4030 K (temperature of Alpha Bootis from visible spectrum) normalised to its radiance at 10 μm, i.e. 550 Jansky observed with Short Wavelength Spectrometer (SWS) onboard the Infrared Space Observatory. We selected normalised black body radiation to compute star irradiance in the infrared, here and in the following part, because of the low quality of spectra at larger wavelengths, perturbing our simulations. At around 10 μm and except on the O_3 absorption band at 9.5 μm, Alpha Bootis signature is five times higher then the atmospheric 1% variation and is even much larger than photon and detector noises. In 8–13 μm spectral range and for 10 mn integration, absolute photometry on Alpha Bootis should be possible with a *S*/*N* ratio better than 3. This indicates that improvements are still possible in this field of detection because detector noise and photon noise limits are not approached. The lower panel shows the ratio between Alpha Bootis and total signal. Maximum values (spikes) reach 15% at around 8.5 μm but are not very useful when using large spectral band photometry. The spectral range between 8 and 13 μm without the ozone band is indicated to validate the absolute accuracy using dedicated instrumentation. The spectral range between 16 and 21 μm is less favorable to detect Alpha

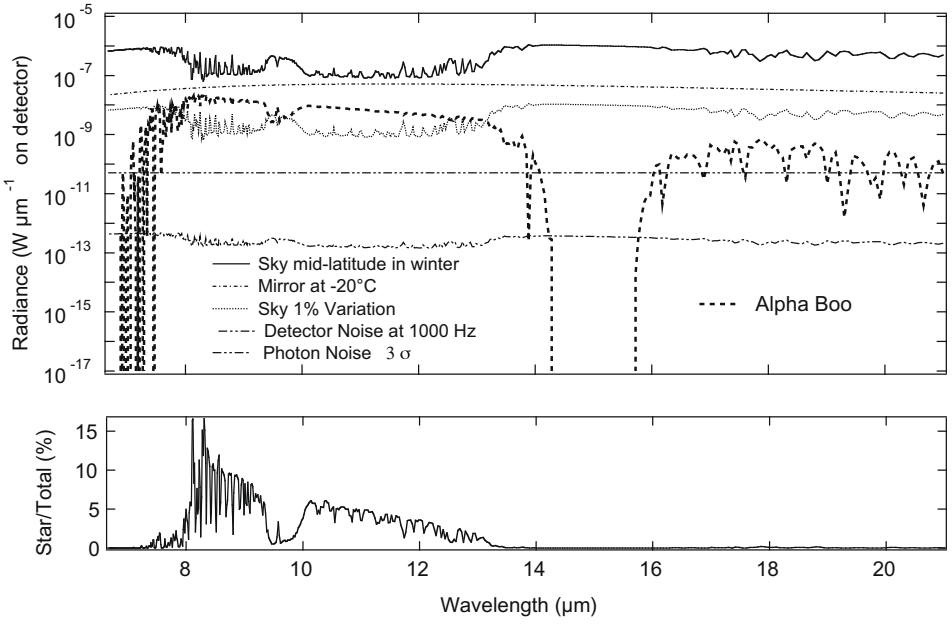

Fig. 5. Upper panel: comparison between detection limit of star Alpha Bootis with the 120 cm telescope and the infrared sensor at OHP and the effect of selected variations of atmospheric parameters. Lower panel: the ratio between star and total irradiances. Note that exoplanets are not the target at this stage.

Please cite this article in press as: A. Sarkissian, Brightness temperature of synchronic exoplanets measured by infrared photometry from the ground: Method and perspective, Infrared Phys. Technol. (2009), doi:10.1016/j.infrared.2009.11.005

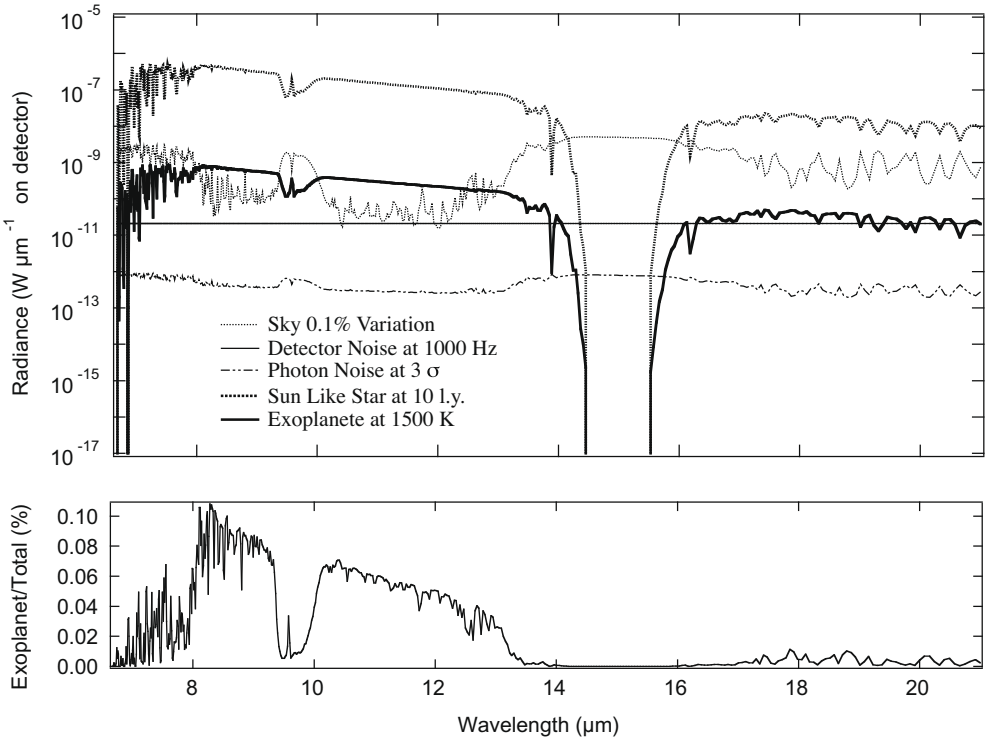

Fig. 6. Radiances of observational parameters for exoplanet detection with high altitude (4000 m) 400 cm diameter telescope.

Bootis in the infrared from the ground because the total irradiance is then more than 4000 times larger than the star irradiance, needing much more accurate photometry. Using a combination of measurements at 8–9.5 µm, 10.5–13 µm, 14.5–15.5 µm and 16.5–21 µm, we should be able to increase the accuracy of relative photometry instead of using an absolute method. Radiative transfer calculations (not shown) indicate that weighting (or contribution) functions for zenith sky viewing atmospheric radiance in this spectral range is dominated by tropospheric layers: the first 2 km of the atmosphere above OHP provides 80% of the total zenith sky radiance. Similar remarks can be made on the variability of the atmospheric constituents: night-time variability of the zenith sky IR radiance is dominated by lower layers. Significant improvements can be made using larger telescope at higher altitude, as it is presented in the next section.

7. Feasibility study for a 400 cm telescope at altitude 4000 m

Here the feasibility study concerns detection of exoplanets and their emission temperature determination. We used the same approach for feasibility study as in previous chapter, however, some changes have been made in simulations: the diameter of the telescope has been set up to 400 cm and the altitude of the station to 4000 m. Spectral irradiance from the full exoplanet outside Earth's atmosphere is calculated using Planck function for the mean temperature of the exoplanet integrated previously taking into account geometrical and line-of-sight effects, and affected by the dilution factor of the observation. Then the exoplanet's spectral irradiance on the detector is calculated using transmission computed for altitude 4000 m at mid-latitude in cold winter [27].

The first direct effect of increasing the diameter of the telescope gives the possibility to reduce the exposure time. The second effect concerns the size of the Airy function of the telescope as the size of the star on the detector is reduced and the sky contribution as well, which, as indicated previously, is one of the most important parameters for the experiment. Observations at higher altitudes reduces the lower atmospheric layer contribution. These lower layers are the most variable ones. We expect that in these conditions, and with refined method for correction of atmospheric variability presented previously, a relative accuracy of 0.1% can be obtained. Fig. 6 shows results of simulations in these conditions for a Jupiter size exoplanet and a Sun-like parent star located at 10 l.y. of our solar system. Note that the 100 closest stars are at less than 20 l.y. indicating the significance of this result.

Note also that the dominant sources, the secondary mirror and the background sky are not shown in the upper figure for clarity. Increasing the integration time increases the detection possibility of the exoplanet's signature, relative to the instrumental noise and compared to the photon noise detection limit (upper panel). The ratio of the signal from the full exoplanet versus the total signal (lower panel, includes mirror and background sky) is not increased by longer exposures because radiances of exoplanet, background sky, star and mirror are all increasing with the integration time. The 0.1% relative accuracy necessary to detect the exoplanet's signature is then in agreement with the same order of relative accuracy expected with this method. Also, another way to increase the feasibility of this experiment: cooling the secondary mirror of the telescope to 77 K would increase the ratio between exoplanet signature and total radiance to 0.15% (not shown), a not negligible improvement to be explored in the future.

8. Detection limit

The detection limit is calculated here taking infrared brightness of Tau Bootis measured by SWS on ISO, available on the web, courtesy of G.C. Sloan and others. Radiative transfer calculations have been made for an exoplanet with surface temperature varying from 600 K to 1500 K, orbiting around a Tau Bootis like star at 1–15 par-

Please cite this article in press as: A. Sarkissian, Brightness temperature of synchronic exoplanets measured by infrared photometry from the ground: Method and perspective, Infrared Phys. Technol. (2009), doi:10.1016/j.infrared.2009.11.005

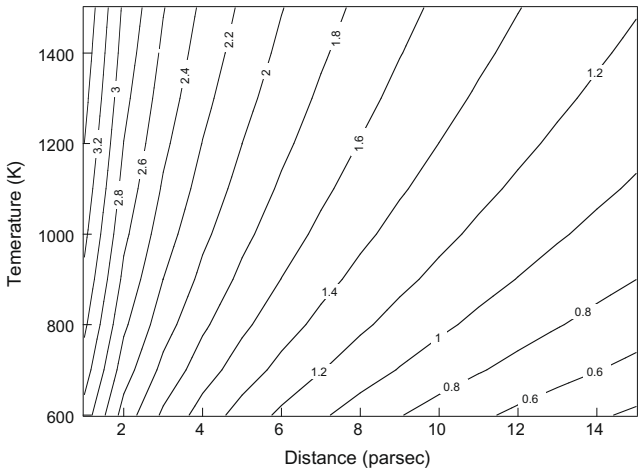

Fig. 7. Detectability of exoplanets depending of their temperature and distance. Values on isolines indicate the ratio between exoplanet radiance and detector noise for 1 h integration on 400 cm telescope. Values larger than 1 indicate that exoplanet, if any, could be detected in theory with this method.

secs from our solar system. Results are presented in Fig. 7. Integration time is 1 h. Isolines indicates the ratio between full exoplanet's signature and detector noise. This ratio has been calculated without atmospheric and star brightness considerations, assumed to be significantly reduced in the differential approach. Values larger than 1 indicates that exoplanets are detectable in this domain, if any. These values can be considered as our theoretical S/N ratio from space or from the ground if proposed relative differential method is able to take out atmospheric and star compounds. The domain covered by the detection method is limited to few parsecs only and can not compete with other, well established powerful methods, but the determination of exoplanet's temperature is a challenging issue that is within the theoretical detection limit of the proposed method.

9. Conclusion and perspective

In this paper, numerical simulations show that photometric detection in the spectral range 5–18 μm of a planet at surface temperature from 600 K to 1500 K is possible in solar neighbourhood. Existing projects of observation from the ground or from space will soon provide a very good opportunity to demonstrate the validity of the method in order to enlarge our ability to detect extra-solar planets and to enhance the number of observed parameters of extra-solar planetary system. Today, several telescopes are announcing detections limits and accuracy very close to exoplanet's detection limit without use of differential methods. We are developing dedicated instrumentation to validate our approach. Observations are planned to be made in near future at OHP to demonstrate the feasibility of high quality relative photometry with the collaboration of the geophysical station at OHP. This will be the first stage for more developments and for future validation of the method. Because of the proximity of H_2O and O_3 absorption bands in the mid-infrared, this spectral range should be also indicated for life search outside our solar system and extensive studies of observational techniques in this spectral range remains our objective in fine.

Acknowledgements

Thanks to Conseil Scientifique of Institut Pierre-Simon Laplace and to Service d'Aéronomie (LATMOS since January 2009) for funding this study. Thanks to LMD at Ecole Polytechnique for its contribution to develop the instrumentation and to finalise sensitivity studies. Thanks to Alain Chédin for useful comments for the experiment and to David Archer for providing ModTran3. Thanks to the Editor for the valuable assistance.

References

[1] M. Mayor, D. Queloz, A Jupiter-mass companion to a solar type star, Nature 378 (1995) 355.
[2] R.N. Bracewell, R.H. MacPhie, Searching for nonsolar planets, Icarus 38 (1979) 136.
[3] J. Schneider, The study of extrasolar planets: methods of detection first discoveries and future perspectives, C.R. Acad. Sci. Paris Ser. IIb 327 (6) (1999) 62.
[4] M. Perryman, Extra-solar planets, Reports Progr. Phys. 63 (2000) 1209–1272.
[5] P. Ehrenfreund, H. Fraser, J. Blum, J.H.E. Cartwright, J.M. Garcia-Ruiz, E. Hadamcik, A.C. Levasseur-Regourd, S. Price, F. Prodi, A. Sarkissian, Physics and chemistry of icy particles in the universe: answers from microgravity, Planet. Space Sci. 51 (2003) 473.
[6] F. Rosenblatt, A two-color photometric method for detection of extra solar planetary systems, Icarus 14 (1971) 71.
[7] TIMMI2, Advanced Instrument Control and Data Reduction Software for TIMMI2, The New Midinfrared Camera for the ESO 3.6-m Telescope, 2004.
[8] N.C. Santos, F. Bouchy, M. Mayor, et al., The HARPS survey for southern extra-solar planets II. A 14 Earth-masses exoplanet around mu Arae, Astrophys. Astron. Lett. 426 (2004) L19.
[9] D.N.C. Lin et al., Orbital evolution and planet–star tidal interaction, Protostars Planets IV (2000) 1111–1134.
[10] T. Guillot, A. Burrows, W.B. Hubbard, J.I. Lunine, D. Saumon, Giant planets at small orbital distance, Astrophys. J. 459 (1996) L35.
[11] T. Guillot, Interiors of giant planets inside and outside the solar system, Science 286 (1999) 72.
[12] A. Burkert, D.N.C. Lin, P. Bodenheimer, C. Jones, H. Yorke, On the surface heating of synchronously-spinning short-period jovian planets, Astrophys. J. 618 (2005) 512–523.
[13] J. Burrows, A theoretical look at the direct detection of giant planets outside the solar system, Nature 433 (2005) 261–268.
[14] D. Charbonneau et al., Detection of thermal emission from an extrasolar planet, Astrophys. J. 626 (2005) 523.
[15] D. Deming et al., Infrared radiation from an extrasolar planet, Nature 434 (2005) 740.
[16] A. Sarkissian, Brightness temperature of synchronic exoplanets measured by infrared photometry: method and perspective, Not. Pole Planét. l'IPSL 9 (2005) 1–15.
[17] C. Hoareau, P. Keckhut, A. Sarkissian, J.-L. Baray, G. Durry, Methodology for water monitoring in upper troposphere with Raman Lidar at observatory of Haute-Provence, J. Atmos. Ocean. Technol. 26 (2009) 2149–2160.
[18] A. Hauchecorne, M.-L. Chanin, P. Keckhut, Climatology and trends of the middle atmospheric temperature (33–87 km) as seen by Rayleigh lidar over the south of France, Geophys. Res. 96 (1991) 15297.
[19] P. Keckhut, A. Hauchecorne, M.-L. Chanin, Midlatitude long-term variability of the middle atmosphere: trends and cyclic and episodic changes, J. Geophys. Res. 100 (1995) 18887.
[20] A. Sarkissian, F. Goutail, P. Keckhut, J.-P. Pommereau, H.K. Roscoe, J. Slusser, Long series of total ozone measured by SAOZ network at polar circle, mid-latitude and tropics, in: Proc. SPARC Meeting, 2000.
[21] T. Encrenaz et al., First results of ISO-SWS observations of Jupiter, Astron. Astrophys. 315 (1996) L397.
[22] H.S. Carlslaw, J.C. Jaeger, Conduction of Heat in Solids, second ed., Clarenton press, Oxford (U.K.), 1959. p. 510.
[23] N. Yan, E. Chassefière, A. Sarkissian, F. Leblanc, Thermal model of Mercury's surface and subsurface: impact of subsurface physical heterogeneities on the surface temperature, Advan. Space Res. 38 (2006) 583–588.
[24] T. Guillot, Atmospheric circulation of hot Jupiters, IAU 202, in: A. Penny et al. (Ed.), Planetary Systems in the Universe: Observation, Formation and Evolution, ASP Conf. Series, 2001.
[25] S. Seager, D.D. Sasselov, Extrasolar giant planets under strong stellar irradiation, Astrophys. J. 502 (1998) L157.
[26] C. Leinert et al., The 1997 reference of diffuse night sky brightness, Astron. Astrophys. Suppl. Ser. 127 (1998) 1.
[27] Handbook of Geophysics, The Geomagnetic Field, The Handbook of Geophysics and the Space Environment, Air Force Geophysics Laboratory, Hanscom AFB, MA, 1985.
[28] Sparc Review, in: C. Michaut (Ed.), Stratospheric Processes and their Role in Climate, 2001.
[29] G. Mégie, G. Ancellet, J. Pelon, Lidar measurements of ozone vertical profiles, Appl. Opt. 24 (1985) 3454–3463.
[30] A. Sarkissian, J. Slusser, Water vapor total column measurements using the elodie archive at Observatoire de Haute Provence from 1994 to 2004, Atmos. Meas. Tech. 2 (2009) 319–326.
[31] L. Goldfarb, P. Keckhut, M.-L. Chanin, A. Hauchecorne, Cirrus climatological results from lidar measurements at OHP (44°N, 6°E), Geophys. Res. Lett. 28 (2001) 9.
[32] A. Chédin, R. Saunders, A. Hollingworth, N. Scott, M. Matricardi, J. Etcheto, C. Clerbaux, T.R. Armante, The feasibility of monitoring CO_2 from high resolution infrared sounders, J. Geophys. Res. 108 (D2) (2004) 4064.

Please cite this article in press as: A. Sarkissian, Brightness temperature of synchronic exoplanets measured by infrared photometry from the ground: Method and perspective, Infrared Phys. Technol. (2009), doi:10.1016/j.infrared.2009.11.005